ENERGY CONVERSION IN LAMINAR MAGNETOHYDRODYNAMIC

CHANNEL FLOW

by

John Paul Penhune

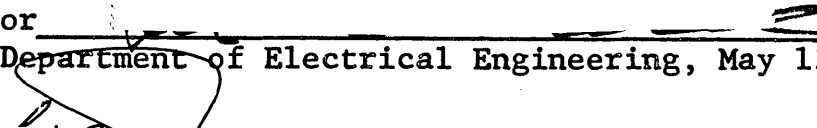S.B. Massachusetts Institute of Technology 1957

Submitted in Partial Fulfillment

of the Requirements for the Degree of

Doctor of Philosophy
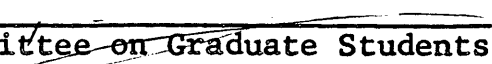
at the

MASSACHUSETTS INSTITUTE OF TECHNOLOGY

June, 1961

Signature of Author_____

Department of Electrical Engineering, May 13, 1961

Certified by_____

Thesis Supervisor

Accepted by_____

Chairman, Departmental Committee on Graduate Students

ENERGY CONVERSION IN LAMINAR MAGNETOHYDRODYNAMIC CHANNEL FLOW

by

John Paul Penhune

Submitted to the Department of Electrical Engineering on May 13, 1961 in partial fulfillment of the requirements for the degree of Doctor of Philosophy.

ABSTRACT

This thesis presents a detailed theoretical analysis of two types (d-c conduction-driven and a-c induction-driven) of laminar, incompressible, viscous magnetohydrodynamic flow in a high-aspect-ratio channel, and of the operation of these flows as various forms of energy converters. The introduction indicates that laminar flow may be of practical importance in magnetohydrodynamic channel flow devices, because the strong magnetic fields that are necessary for efficient energy conversion have been found to suppress turbulence. The treatment is unified by obtaining all of the basic solutions from a single set of fundamental equations in dimensionless form, and by presenting the results in terms of characteristic dimensionless parameters.

First, the basic solutions for d-c conduction-driven (Hartmann) flow are obtained, and a variational principle for this problem is presented. Although the square of the Hartmann number is commonly interpreted as a measure of the ratio of ohmic to viscous dissipation, exact analysis of both the $I = 0$ and the $E = 0$ flow dampers shows that this interpretation is often considerably in error. The operation of this flow as a motor (pump) and a generator is analyzed in detail, and universal efficiency curves are presented. Contrary to some opinion, efficiencies greater than one-half are possible, at the expense of less-than-maximum power conversion.

Second, the non-linear differential equations are derived, which govern a-c induction-driven flow with either even or odd excitation, if the fluid velocity is independent of time. These non-linear equations are converted to an infinite set of linear differential equations with variable coefficients that is

uncoupled from below, by making a perturbation expansion in the
magnetic Reynolds number. This set of equations is solved by
an analytical-numerical technique, and velocity and magnetic
field profiles are presented for various values of the parameters.
These basic profiles are used to form further results such as
flow rate and efficiency curves, and sample plots are presented.
The relative a-c to d-c response in parallel flow is found to be
quite small in common fluids at typical frequencies; and under
this assumption, the equation that governs the second-harmonic
time variations in the fluid velocity is derived.

Thesis Supervisor: William D. Jackson
Title: Assistant Professor of Electrical Engineering

Acknowledgement

During the three years in which the author has been interested in magnetohydrodynamics and plasma physics, he has benefited from associations with many teachers and colleagues. Professors H. H. Woodson and W. D. Jackson aroused the author's interest in magnetohydrodynamics and its energy conversion possibilities, and provided him with the academic freedom that was essential to this research. Professor W. P. Allis introduced the author to plasma physics, and was instrumental in his attending the Summer School in Theoretical Physics of the University of Grenoble, France in 1959.

Throughout the preparation of the thesis, Professor Jackson, who served as supervisor, offered encouragement, criticism and valuable suggestions during discussions of much of the material. Mr. J. W. Poduska discussed parts of the material with the author in detail, and provided many helpful suggestions, particularly concerning mathematical and numerical methods, and digital computer techniques. Finally, the author would like to thank Miss Marguerite Daly who typed the entire manuscript.

Table of Contents

List of Figures

Chapter I

INTRODUCTION

1.1 Historical Background

The first use of a magnetohydrodynamic channel flow as an
energy converter was probably the direct-current electromagnetic
pump for mercury that was designed by Hartmann[*,1] in 1918 for
use with the so-called jet-wave rectifier. Previously, there
had been some simple experiments designed to demonstrate the
interactions between a magnetic field and a flowing, elec-
trically conducting fluid, notably the attempt of Faraday[2] to
measure the voltage induced in the river Thames by its motion
through the earth's magnetic field (the $\bar{v} \times \bar{B}$ electric field),
and the demonstration by Northrup[3] of the deformation of the
surface of a pool of mercury caused by a current passed through
its bulk (the $\bar{J} \times \bar{B}$ body force).

The first detailed theoretical investigation of a magneto-
hydrodynamic channel flow was also made by Hartmann,[1] in 1937.
He obtained the velocity profile and the fluid resistance law
for the laminar flow in a high-aspect-ratio channel of a con-
ducting fluid in the presence of a uniform transverse magnetic
field; and discussed some of the consequences of this analysis
in the design of electromagnetic pumps. In the same year,
Hartmann and Lazarus[4] reported some experimental results that

---

[*]The superscript numerals refer to the Bibliography that begins
on p.171.

were partially explained by Hartmann's theoretical work. The work of Hartmann prompted the author to investigate in detail the properties of this flow when it is employed as various types of energy converters.[5]

The principal energy conversion application of incompressible magnetohydrodynamic channel flows has been to electromagnetic pumps (both conduction and induction) for circulating liquid metal coolants through the heat exchangers of atomic reactors.[*] There has been considerable practical design analysis of such pumps, but invariably slug flow (flow in which the fluid velocity is constant across the channel) is assumed and terminal properties are emphasized.[**] A notable theoretical exception is the work of Harris,[***] in which he shows that under certain circumstances laminar induction driven flow resembles Hartmann flow. This work aroused the author's interest in formulating a general theory of laminar induction driven flows in which non-linear effects are considered.

Recently there has been considerable interest in magneto-hydrodynamic channel flow devices in which the working fluid is a conducting gas or plasma. A large part of this effort centers around the direct-current magnetohydrodynamic power generator,[****]

---

[*] For reviews of the various types of electromagnetic pumps and their applications, see Cage,[6] Barnes,[7] and Watt.[8]

[**] Prominent among such analyses are those of Blake[9,10] and Watt.[11]

[***] See Ch. 8 of Harris.[12]

[****] For design studies, see Sporn and Kantrowitz,[13] and Steg and Sutton.[14] Some experimental results are presented by Way et al.,[15] and Rosa.[16]

which its proponents hope will become a large-scale source of electric power. There has also been continuing interest in the acceleration of a plasma by a traveling magnetic field.[17,18,19] Most of the theoretical analyses of these plasma devices are based on one-dimensional, compressible, magnetofluid dynamics.

1.2 The Object and Scope of This Investigation

The object of this investigation is to provide a unified and detailed description of two types of magnetohydrodynamic channel flow (direct-current conduction-driven, and alternating-current induction-driven), and of their operation as various types of energy converters. The treatment is unified because the derivation of all flow and field properties begins with a general and fundamental set of equations of motion in dimensionless form (see Chapter II); and because the results are presented in terms of characteristic dimensionless groups, so that the effect on the solutions of changes in various physical parameters is clearly evident, and different results are easily compared. The treatment is detailed because its emphasis is on first obtaining the detailed properties of the flow, such as the velocity profile and the magnetic field distribution, and then on deducing from these detailed properties the terminal properties of the flow operating as an energy conversion device. A further objective of the chapters dealing with induction-driven flow is to obtain the solution to a non-linear magnetohydrodynamic problem. All too often, such problems are either linearized or abandoned. However, in energy conversion non-linearity is the rule; not the exception. Finally, the object of this investigation is not primarily to discuss the practical design of better magnetohydrodynamic energy converters, but to provide better understanding

of the detailed nature of two classes of magnetohydrodynamic channel
flows and the energy conversion processes that take place within
them.

The scope of this investigation is restricted to the laminar,
viscous, incompressible[*] magnetohydrodynamic channel flow of a
homogeneous and isotropic fluid. The most common examples of such
fluids are electrolytes,[**] and liquid metals such as mercury and
sodium-potassium alloy (Na K). In addition, the channel that is
considered is rectangular and has a high aspect ratio. Further-
more, two forms of electrical excitation are considered: the
direct-current conduction drive, in which a uniform transverse
magnetic field that is parallel to the shorter sides of the
channel cross section interacts with a non-uniform direct-current
density that flows parallel to the longer sides of the channel
cross section (see Fig. 3-1); and the alternating-current induction
drive, in which surface current sheets (with either even or odd
symmetry) flowing on the longer sides of the channel and traveling
in the direction of the fluid flow produce a traveling magnetic
field that "drags along" the conducting fluid (see Fig. 5-1).
Finally, throughout this investigation a conscious effort has been
made to make no assumptions that cannot be practically realized
experimentally. (e.g., An infinite slit channel is not
physically realizable, but a long rectangular channel with a
twenty to one aspect ratio approximates it very closely.) Flow

---

[*]The results that are obtained here should also be applicable to
gas flows at low Mach numbers. See, for example, Shapiro.[20]

[**]Electrolytes pose other problems such as dielectric polarization
and electrochemical action.

devices that are designed to conform to these theoretical assumptions may not be the best possible energy converters, but their operating characteristics should provide an unambiguous check of the theoretical results, and they should be magnetohydrodynamic energy converters that are well understood.

1.3 The Importance of Laminar Flow

In view of the fact that most practical hydrodynamic flows are turbulent,[*] the restriction of this investigation to laminar magnetohydrodynamic flows deserves some discussion. There are three reasons for studying laminar magnetohydrodynamic flows. The first reason is analytical, the second is philosophical, and the third is practical.

The analytical reason is that laminar magnetohydrodynamic flows are susceptible of analysis by ordinary higher mathematical methods, whereas turbulent magnetohydrodynamic flows have so far escaped such treatment,[**] and have only been analyzed by the semi-empirical techniques of turbulent fluid mechanics (notably the work of Harris[12]). Thus, the restriction to laminar flows makes the mathematical analysis more tractable and thereby allows more involved results (e.g., efficiencies) to be obtained.

---

[*] See, for example, Hunsaker and Rightmire,[21] Ch. VIII.

[**] A rational theory of hydrodynamic and magnetohydrodynamic turbulence based on the calculus of random functionals is being developed by Poduska.[22]

The philosophical reason is that although the majority of practical hydrodynamic flows are turbulent, the great bulk of existing theoretical knowledge concerns laminar and even ideal fluid flow. Nevertheless, this knowledge of laminar flows has helped to guide and shape both theoretical and experimental work on more complicated turbulent flows. In the words of Pai,[*] "The understanding of the laminar viscous flow seems a prerequisite for the complete understanding of turbulent flow." Presumably, the same is true of magnetohydrodynamic flow.

The practical reason is that the high magnetic fields that are found to be necessary for efficient energy conversion (see Chs. IV and VII) have also been found to suppress turbulence. In their classic experiments, Hartmann and Lazarus[4] found that the transition from turbulent to laminar flow depends not only on the Reynolds number[**] but also on the strength of a transverse magnetic field. Later, Murgatroyd[25] carefully investigated the turbulent to laminar transition in a mercury flow in the presence of a transverse magnetic field, and found that the critical Reynolds number R_c [see Eq. (2.2.17)] was approximately related to the Hartmann number M [see Eq. (2.2.20)] by the equation

$$R_c \simeq 225\,M, \qquad\qquad (1.3.1)$$

---

[*] See the preface to Pai.[23]

[**] For an introduction to the experimental evidence concerning the laminar-turbulent transition in hydrodynamic flow, see Hunsaker and Rightmire,[21] Ch. VIII, and Pai,[24] Ch. I.

for large values of M. (In hydrodynamic flow $R_c \sim 500.$) This
linear dependence of R_c on M had been conjectured by
Lundquist[26] on physical grounds, and was predicted for the laminar
to turbulent transition by Lock[27] on the basis of linear stability
theory. (Lock predicted the much higher value $R_c \sim 5 \cdot 10^4 M$, for
large M.)

Recently, Globe[28] made a detailed experimental study of the
effect of a longitudinal magnetic field on the laminar to
turbulent transition* in a mercury channel flow. The effect of
the longitudinal field is much less than that of an equal trans-
verse field; in fact, the maximum change in the critical Reynolds
number that Globe obtained was a factor of about 1.9, for a
Hartmann number of about 20. The increase of the critical
Reynolds number for the laminar to turbulent transition under the
influence of a longitudinal magnetic field was predicted by
Stuart[30] on the basis of linear stability theory; and Globe has
shown that the ratios given by theory and experiment, of the
critical Reynolds numbers with a longitudinal magnetic field to
those without a field, are in reasonable agreement.

---

*Although Globe's experiments concerned the laminar to turbulent
transition, he was careful to provide sufficient initial dis-
turbance of the flow that the critical Reynolds numbers he
measured should correspond quite well to those for the turbulent
to laminar transition.

For a discussion of the effects of initial disturbances on the
laminar to turbulent transition in hydrodynamic flow, see
Prandtl and Tietjens[29], Art. 24.

In view of the very large Hartmann numbers (typically 100 to 1000) that are obtained in practical electromagnetic pumps, the investigations that are discussed above indicate the possibility of practical laminar magnetohydrodynamic energy converters, with their inherently smaller losses. From a practical standpoint, a transverse magnetic field is preferable, because it is required by most energy conversion schemes and produces a large increase in the critical Reynolds number. From an experimental viewpoint, however, a longitudinal field is also interesting, because it primarily affects the turbulence and only secondarily (through its effect on the random velocity correlations) affects the mean flow.

Chapter II

THE BASIC EQUATIONS

2.1 The Equations of Motion

The fluid that is considered in this investigation is homogeneous, isotropic, and incompressible; and is characterized by a permeability μ_o,[*] an electrical conductivity σ, a mass density ρ, and an absolute viscosity η. The equations that govern the motion of such a fluid are the Maxwell relations

$$\nabla \times \overline{H} = \overline{J}, \tag{2.1.1}$$

$$\nabla \times \overline{E} = -\mu_o \frac{\partial \overline{H}}{\partial t}, \tag{2.1.2}$$

and

$$\nabla \cdot \overline{H} = 0; \tag{2.1.3}$$

the constitutive relation

$$\overline{J} = \sigma(\overline{E} + \overline{v} \times \mu_o\overline{H}); \tag{2.1.4}$$

the magnetohydrodynamic Navier-Stokes equation

$$\rho(\frac{\partial}{\partial t} + \overline{v} \cdot \nabla)\overline{v} = -\nabla P + \eta\nabla^2\overline{v} + \overline{J} \times \mu_o\overline{H}; \tag{2.1.5}$$

and the incompressibility restriction

$$\nabla \cdot \overline{v} = 0. \tag{2.1.6}$$

---

[*] The fluid is assumed to have the permeability and permittivity of free space. For a discussion of the electrodynamics of moving polarizable and magnetizable media, see Fano, Chu and Adler.[31]

In Eqs. (2.1.1) through (2.1.6), ∇ is the vector operator $\overline{i}_x \frac{\partial}{\partial x} + \overline{i}_y \frac{\partial}{\partial y} + \overline{i}_z \frac{\partial}{\partial z}$, $\overline{H}$ is the magnetic field intensity, $\overline{J}$ is the conduction current density, $\overline{E}$ is the electric field intensity, $\overline{v}$ is the fluid velocity and P is the mechanical pressure. Throughout this investigation, all equations are written with respect to a fixed coordinate system (an Eulerian[*] formulation), and rationalized MKS units are employed.

In Eq. (2.1.1), displacement currents have been neglected, because they are extremely small in comparison with conduction currents in common magnetohydrodynamic fluids at any reasonable frequency.[**] Equation (2.1.5) is the ordinary Navier-Stokes equation for an incompressible fluid,[***] with the addition of the electromagnetic body force density $\overline{J} \times \mu_o \overline{H}$, and without the force of gravity, which may be neglected since no free surfaces are to be considered.

Equations (2.1.1) through (2.1.4), and Eq. (2.1.6) can be combined to form the Bullard relation

$$\nabla^2 \overline{H} - \sigma\mu_o [\frac{\partial \overline{H}}{\partial t} + (\overline{v} \cdot \nabla)\overline{H} - (\overline{H} \cdot \nabla)\overline{v}] = 0 , \qquad (2.1.7)$$

---

[*] For a discussion of the alternative Eulerian and Lagrangian formulations of the hydrodynamic equations, see Lamb,[32] Ch. I.

[**] If a sinusoidal disturbance of frequency ω exists in a static, homogeneous, and isotropic medium with permittivity ε and conductivity σ, the frequency at which the displacement current is equal to the conduction current is $\omega' = \sigma/\varepsilon$. For example, in mercury $\omega' \sim 6.3 \ 10^{17}$ rad./sec.

[***] See, for example, Pai,[23] Ch. III.

while Eqs. (2.1.1), (2.1.3), and (2.1.5) can be combined to yield

$$\rho(\frac{\partial}{\partial t} + \overline{v} \cdot \nabla)\overline{v} = -\nabla(P + \frac{1}{2} \mu_o H^2) + \eta\nabla^2\overline{v} + \mu_o(\overline{H} \cdot \nabla)\overline{H}. \quad (2.1.8)*$$

Equations (2.1.7) and (2.1.8) are compact in form, contain only the variables $\overline{H}$, $\overline{v}$ and P, and are often a convenient starting point in the search for the solution of a specific problem.

2.2 The Equations of Motion in Dimensionless Form

Any complicated analysis involving the equations of motion [Eqs. (2.1.1) through (2.1.8)] is greatly simplified by considering these equations in dimensionless form. The equations of motion can be rendered dimensionless by making the following normalizations with respect to a characteristic length L_o, a characteristic velocity v_o, and a characteristic magnetic field H_o. Let

$$(\tilde{x}, \tilde{y}, \tilde{z}) = (x, y, z)/L_o, \quad (2.2.1)$$

and therefore

$$\tilde{\nabla} = L_o\nabla. \quad (2.2.2)$$

Also let

$$\tau = tv_o/L_o, \quad (2.2.3)$$

$$\overline{u} = \overline{v}/v_o, \quad (2.2.4)$$

---

*Note that if $\overline{A}$ is a vector, A^2 is used throughout to denote $\overline{A} \cdot \overline{A}$.

$$p = P/\rho v_o^2 \ , \tag{2.2.5}$$

$$\bar{h} = \bar{H}/H_o \ , \tag{2.2.6}$$

$$\bar{j} = \bar{J}/\sigma\mu_o v_o H_o \ , \tag{2.2.7}$$

and

$$\bar{e} = \bar{E}/\mu_o v_o H_o \ . \tag{2.2.8}$$

If the normalized variables that are defined in Eqs. (2.2.1) through (2.2.8) are introduced in Eqs. (2.1.1) through (2.1.8), the results are

$$\tilde{\nabla} \times \bar{h} = R_m \bar{j} \ , \tag{2.2.9}$$

$$\tilde{\nabla} \times e = -\frac{\partial \bar{h}}{\partial \tau} \ , \tag{2.2.10}$$

$$\tilde{\nabla} \cdot \bar{h} = 0 \ , \tag{2.2.11}$$

$$\bar{j} = \bar{e} + \bar{u} \times \bar{h} \ , \tag{2.2.12}$$

$$(\frac{\partial}{\partial \tau} + \bar{u} \cdot \tilde{\nabla})\bar{u} = -\tilde{\nabla}p + \frac{1}{R} \tilde{\nabla}^2\bar{u} + R_m\beta(\bar{j} \times \bar{h}) \ , \tag{2.2.13}$$

$$\tilde{\nabla} \cdot \bar{u} = 0 \ , \tag{2.2.14}$$

$$\tilde{\nabla}^2\bar{h} - R_m[\frac{\partial \bar{h}}{\partial \tau} + (\bar{u} \cdot \tilde{\nabla})\bar{h} - (\bar{h} \cdot \tilde{\nabla})\bar{u}] = 0 \ , \tag{2.2.15}$$

and

$$(\frac{\partial}{\partial \tau} + \bar{u} \cdot \tilde{\nabla})\bar{u} = -\tilde{\nabla}(p + \frac{1}{2}\beta h^2) + \frac{1}{R} \tilde{\nabla}^2\bar{u} + \beta(\bar{h} \cdot \tilde{\nabla})\bar{h} \ . \tag{2.2.16}$$

In Eqs. (2.2.9) through (2.2.16),

$$R = \frac{\rho v_o^2}{\eta (v_o/L_o)^2 \cdot (L_o/v_o)} = \rho v_o L_o/\eta \ , \tag{2.2.17}$$

$$R_m = \frac{\sigma \mu_o L_o^2}{L_o/v_o} = \sigma \mu_o v_o L_o \ , \tag{2.2.18}$$

and

$$\beta = \frac{\mu_o H_o^2}{\rho v_o^2} \tag{2.2.19}$$

are respectively the hydraulic Reynolds number, the magnetic Reynolds number, and the energy ratio. In addition to these three dimensionless ratios, the Hartmann number M is often an important characteristic ratio. It is defined by the equation

$$M^2 = \frac{\sigma (v_o \mu_o H_o)^2}{\eta (v_o/L_o)^2} = (\mu_o H_o L_o)^2 \frac{\sigma}{\eta} \ , \tag{2.2.20}$$

and is related to the other dimensionless ratios by the identity

$$M^2 \equiv R \, R_m \, \beta \ . \tag{2.2.21}$$

Equations (2.2.17) through (2.2.20) indicate that from a dimensional viewpoint, on an average basis, the hydraulic Reynolds number can be thought of as the ratio of the kinetic-energy density to the product of the viscous power-loss density and the fluid transit time, the magnetic Reynolds number as the ratio of the magnetic-field diffusion time to the fluid transit time, the energy ratio as the ratio of the magnetic-energy density to the kinetic-energy

density, and the Hartmann number as the ratio of the ohmic power-loss density to the viscous power-loss density. These identifications are not rigorous, but they do give some physical feeling for the nature of the dimensionless ratios. In specific situations the physical significance of various dimensionless ratios can vary considerably (see Secs. 4.1 and 7.1)

2.3 Power and Energy Relations

The Poynting theorem for this magnetohydrodynamic situation can be derived as follows. In view of the vector identity

$$\nabla \cdot (\overline{A} \times \overline{B}) \equiv \overline{B} \cdot (\nabla \times \overline{A}) - \overline{A} \cdot (\nabla \times \overline{B}) , \qquad (2.3.1)$$

Eqs. (2.1.1) and (2.1.2) yield

$$-\nabla \cdot (\overline{E} \times \overline{H}) = \frac{\partial}{\partial t} (\frac{1}{2} \mu_o H^2) + \overline{E} \cdot \overline{J} . \qquad (2.3.2)$$

However, Eq. (2.1.4) allows $\overline{E}$ to be written as

$$\overline{E} = \frac{\overline{J}}{\sigma} - \overline{v} \times \mu_o \overline{H} , \qquad (2.3.3)$$

with the result that Eq. (2.3.2) becomes

$$-\nabla \cdot (\overline{E} \times \overline{H}) = \frac{\partial}{\partial t} (\frac{1}{2} \mu_o H^2) + \frac{J^2}{\sigma} - \overline{J} \cdot (\overline{v} \times \mu_o \overline{H}) . \qquad (2.3.4)$$

Finally, because of the vector identity

$$\overline{A} \cdot (\overline{B} \times \overline{C}) \equiv -\overline{B} \cdot (\overline{A} \times \overline{C}) , \qquad (2.3.5)$$

Eq. (2.3.4) can be written as

$$-\nabla \cdot (\overline{E} \times \overline{H}) = \frac{\partial}{\partial t}(\frac{1}{2}\mu_o H^2) + \frac{J^2}{\sigma} + \overline{v} \cdot (\overline{J} \times \mu_o \overline{H}) , \qquad (2.3.6)$$

which is the desired Poynting theorem. In Eq. (2.3.6), $-\nabla \cdot (\overline{E} \times \overline{H})$ is the rate at which electromagnetic energy is supplied per unit volume, $\frac{\partial}{\partial t}(\frac{1}{2}\mu_o H^2)$ is the rate at which the magnetic-energy storage is increased per unit volume, J^2/σ is the rate of ohmic dissipation per unit volume, and $\overline{v} \cdot (\overline{J} \times \mu_o \overline{H})$ is the rate at which the electromagnetic body force does work on the fluid per unit volume. Thus the electromagnetic energy that is supplied to a unit volume of the fluid is used in three ways: to increase the stored magnetic energy, to supply the ohmic dissipation, and to provide the energy that is converted to mechanical form (some of which is dissipated viscously).

An Energy Equation

An energy equation for the fluid can be obtained by forming the dot product of the fluid velocity $\overline{v}$ and the magnetohydrodynamic Navier-Stokes equation (2.1.5). The result is

$$(\frac{\partial}{\partial t} + \overline{v} \cdot \nabla)(\frac{1}{2}\rho v^2) = -\overline{v} \cdot \nabla P + \eta\overline{v} \cdot \nabla^2\overline{v} + \overline{v} \cdot (\overline{J} \times \mu_o \overline{H}).$$

$$(2.3.7)$$

In Eq. (2.3.7), $(\frac{\partial}{\partial t} + \overline{v} \cdot \nabla)(\frac{1}{2}\rho v^2)$ is the total rate of increase of the kinetic energy per unit volume; and $-\overline{v} \cdot \nabla P$, $\eta\overline{v} \cdot \nabla^2\overline{v}$, and $\overline{v} \cdot (\overline{J} \times \mu_o \overline{H})$ are respectively the rates at which the mechanical pressure, the viscous surface traction, and the electromagnetic body force do work on a unit volume of the

fluid as a whole. Thus the kinetic energy of the fluid can be increased by pressure forces, equivalent viscous body forces, and electromagnetic forces. [Note in particular that the term $\overline{\eta v} \cdot \nabla^2 \overline{v}$ is not a dissipation (see the following section).] The energy equation (2.3.7) is not the complete statement of conservation of energy for the fluid,[*] but is nevertheless a valid and informative result. The complete energy equation is not needed in this investigation, because the fluid is incompressible.

The Viscous Dissipation

The viscous stress tensor σ_{ij}[**] for an incompressible fluid is given by

$$\sigma_{ij} = \eta \left(\frac{\partial v_i}{\partial x_j} + \frac{\partial v_j}{\partial x_i} \right) , \qquad (2.3.8)[***]$$

in which x_i (i = 1,2,3) are the Cartesian coordinates, and v_i are the Cartesian components of the fluid velocity. The viscous power-loss density can be obtained by considering the rate at which work is done by the viscous surface traction on a surface S which encloses a volume V. The viscous surface-traction

---

[*] For a discussion of the complete energy equation of compressible magnetohydrodynamics, see Pai.[33]

[**] The symbol σ_{ij}, which is used only in this section to denote the viscous stress tensor, should not be confused with the scalar electrical conductivity σ.

[***] See, for example, Pai,[23] Eq. (3.31).

tensor σ_i can be obtained from the stress tensor as

$$\sigma_i = \sigma_{ij} n_j \ , \tag{2.3.9}$$

in which summation on a repeated index is understood, and n_i are the Cartesian components of the outward-pointing normal to the surface S. An expression for the rate at which work is done by the viscous surface tractions Φ can be obtained by integrating the dot product of the viscous surface traction and the fluid velocity over the surface S, i.e.

$$\Phi = \int_S \sigma_i v_i \, dS = \int_S v_i \sigma_{ij} n_j \, dS \ . \tag{2.3.10}$$

The surface integrals in Eq. (2.3.10) can be converted into volume integrals with the aid of Green's theorem, with the result that

$$\Phi = \int_V \frac{\partial}{\partial x_j} (v_i \sigma_{ij}) \, dV \ , \tag{2.3.11}$$

which can be expanded to

$$\Phi = \int_V \left(v_i \frac{\partial \sigma_{ij}}{\partial x_i} + \sigma_{ij} \frac{\partial v_i}{\partial x_j} \right) dV \ . \tag{2.3.12}$$

Because the volume V is arbitrary, the integral in Eq. (2.3.12) may be identified as the density of power that is delivered by the viscous forces ϕ, i.e.

$$\phi = v_i \frac{\partial \sigma_{ij}}{\partial x_j} + \sigma_{ij} \frac{\partial v_i}{\partial x_j} \ . \tag{2.3.13}$$

If Eq. (2.3.8) is substituted in Eq. (2.3.13), and use is made of the incompressibility restriction $\partial v_j / \partial x_j = 0$, Eq. (2.3.13) becomes

$$\phi = \eta v_i \frac{\partial}{\partial x_j} \frac{\partial v_i}{\partial x_j} + \eta \left(\frac{\partial v_i}{\partial x_j} + \frac{\partial v_j}{\partial x_i} \right) \frac{\partial v_i}{\partial x_j} . \qquad (2.3.14)$$

The first term on the right-hand side of Eq. (2.3.14) can be written in vector form as

$$\eta v_i \frac{\partial}{\partial v_j} \frac{\partial v_i}{\partial x_j} = \eta \bar{v} \cdot \nabla^2 \bar{v} , \qquad (2.3.15)$$

and can be interpreted as the rate at which the equivalent viscous body force $\eta \nabla^2 \bar{v}$ does work on a unit volume of the fluid as a whole [cf. Eq. (2.3.7)]. This power is the rate at which the viscous stresses are increasing the sum of the kinetic, potential, and converted (to electrical form) energies within a unit volume, and is not a viscous dissipation producing heat.

The second term on the right-hand side of Eq. (2.3.14) is the viscous power-loss density p_v, i.e.

$$p_v = \eta \left(\frac{\partial v_i}{\partial x_j} + \frac{\partial v_j}{\partial x_i} \right) \frac{\partial v_i}{\partial x_j} . \qquad (2.3.16)$$

This power is the rate at which the viscous stresses are doing work to deform the fluid per unit volume, and is a viscous dissipation producing heat.

Chapter III

FUNDAMENTALS OF CONDUCTION DRIVEN FLOW

3.1 The Configuration and the Choice of Characteristic Quantities

The particular field-flow geometry that is analyzed in this
chapter is called Hartmann flow, after the scientist who first
obtained the fluid velocity profile for this situation (see
Ch. I, and Hartmann[1]). In this configuration, the fluid flows
between infinite parallel planes that are separated by a distance
2a. The electrical excitation is provided by a constant magnetic
field $\overline{H}_a$ that is applied perpendicular to these planes, and a
constant electric field $\overline{E}_a$ that is applied perpendicular to the
applied magnetic field and the fluid velocity, as shown in Fig. 3-1.
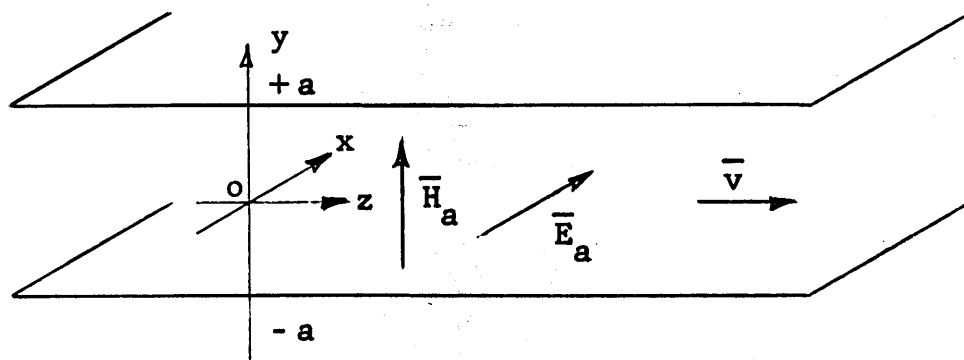
Fig. 3-1 Hartmann Flow Between
Infinite Parallel Planes

Because translation of the coordinate system in the x and
z directions does not alter the situation, the solution cannot

depend on x or z (note that although the pressure gradient is independent of z, the pressure varies linearly with z). The fluid velocity is assumed to be entirely in the z-direction, but to vary with y, i.e.

$$\overline{v} = v_z(y)\overline{i}_z \; . \tag{3.1.1}$$

The total magnetic field is assumed to consist of the applied field H_a, and an induced magnetic field H_z in the z-direction, viz.

$$\overline{H} = H_a\overline{i}_y + H_z(y)\overline{i}_z \; . \tag{3.1.2}$$

The assumption that the induced magnetic field is in the z-direction corresponds to the assumption that the current that flows through the fluid in the x-direction has its return path in an x-y plane.

The choice of the characteristic quantities is reasonably straight-forward in this simple situation. The channel half-width is taken as the characteristic length, i.e.

$$L_o = a \; , \tag{3.1.3}$$

the applied magnetic field is taken as the characteristic magnetic field, i.e.

$$H_o = H_a \; , \tag{3.1.4}$$

and the space-average of the fluid velocity is taken as the

characteristic velocity,[*] i.e.

$$v_o = \langle v_z \rangle = \frac{1}{2a} \int_{-a}^{a} v_z(y) \, dy \ . \qquad (3.1.5)[**]$$

With these choices of characteristic quantities, the deminsion-less parameters defined in Eqs. (2.2.17) through (2.2.20) become

$$R = \frac{\rho a}{\eta} \langle v_z \rangle \ , \qquad (3.1.6)$$

$$R_m = \sigma \mu_o a \langle v_z \rangle \ , \qquad (3.1.7)$$

$$\beta = \frac{\mu_o H_a^2}{\rho \langle v_z \rangle^2} \ , \qquad (3.1.8)$$

and

$$M^2 = (\mu_o H_a a)^2 \frac{\sigma}{\eta} \ . \qquad (3.1.9)$$

3.2 Basic Solutions

The normalized forms of Eqs. (3.1.1) and (3.1.2) for velocity and magnetic field are

$$\bar{u} = u_z(\tilde{y}) \bar{i}_z \ , \qquad (3.2.1)$$

and

$$\bar{h} = \bar{i}_y + h_z(\tilde{y}) \bar{i}_z \ . \qquad (3.2.2)$$

---

[*] Note that another possible choice for the characteristic velocity is the "electrical velocity" $E_a/\mu_o H_a$, although the choice that is made in Eq. (3.1.5) is more meaningful in this situation.

[**] The angular set of brackets is used throughout to denote an average with respect to space.

If Eqs. (3.2.1) and (3.2.2) are substituted in the dimensionless equations of motion (2.2.15) and (2.2.16), the former yields the single scalar equation

$$h_z'' + R_m u_z' = 0 \; ; \tag{3.2.3}*$$

while the latter yields the two scalar equations

$$-\frac{\partial p}{\partial \tilde{z}} + \frac{1}{R} u_z'' + \beta h_z' = 0 \; , \tag{3.2.4}$$

and

$$\frac{\partial p}{\partial \tilde{y}} + \beta h_z' = 0 \; , \tag{3.2.5}$$

in which the pressure p is in general a function of $\tilde{y}$ and $\tilde{z}$. However, Eq. (3.2.4) demands that

$$\frac{\partial^2 p(\tilde{y}, \tilde{z})}{\partial \tilde{z}^2} = 0 \; , \tag{3.2.6}$$

with the result that

$$p(\tilde{y}, \tilde{z}) = \tilde{z} f(\tilde{y}) + g(\tilde{y}) \; , \tag{3.2.7}$$

in which $f(\tilde{y})$ and $g(\tilde{y})$ are arbitrary functions of $\tilde{y}$. However, Eq. (3.2.5) demands that

$$\frac{\partial p}{\partial \tilde{y}} = \tilde{z} f' + g' \tag{3.2.8}$$

---

*A prime is used throughout to denote the differentiation of a function of one variable with respect to its argument.

must be a function of $\tilde{y}$ only, with the result that,

$$f' = 0 \ , \tag{3.2.9}$$

and

$$\frac{\partial p}{\partial \tilde{z}} = \text{a constant} \equiv p_o \ . \tag{3.2.10}$$

Equations (3.2.3) and (3.2.4), the definition (3.2.10), and the identity (2.2.2) can be combined to yield a single equation that governs the fluid velocity, viz.

$$(u_z'' - M^2 u_z)' = 0 \ . \tag{3.2.11}$$

Equation (3.2.11) must be solved subject to the boundary conditions

$$u_z(\pm 1) = 0 \tag{3.2.12}$$

that are imposed by the channel walls and the fluid viscosity, the symmetry condition

$$u_z(-\tilde{y}) = u_z(\tilde{y}) \ , \tag{3.2.13}$$

and the normalization

$$\int_o^1 u_z(\tilde{y}) \, d\tilde{y} = 1 \tag{3.2.14}$$

that is required by the definition of v_o [Eq. (3.1.5)]. The solution is readily found to be

$$u_z = (1 - \frac{\cosh M\tilde{y}}{\cosh M})/(1 - \frac{\tanh M}{M}) \ . \tag{3.2.15}$$

Thus the shape of the normalized velocity profile depends only on the Hartmann number M, although the average velocity v_o depends, of course, on the electrical and mechanical drives. Figure 3-2 shows a set of normalized velocity profiles for various values of M. When M is small, the profile is controlled by viscosity and has a parabolic shape; however, when M is large the profile is controlled by electromagnetic forces, and has a highly squared appearance.

Now that the velocity u_z has been determined, Eq. (3.2.4) can be solved for the induced magnetic field h_z. Subject to the symmetry requirement

$$h_z(-\tilde{y}) = -h_z(\tilde{y}) \tag{3.2.16}$$

the solution is

$$h_z = \frac{1}{R\beta} (Rp_o\tilde{y} - u_z') . \tag{3.2.17}$$

The symmetry condition (3.2.16) demands that any net current that flows through the fluid in the x-direction be returned symmetrically with respect to the channel.

Next, the current density $\bar{j}$ can be obtained from the magnetic field, by substituting Eqs. (3.2.17) and (3.2.2) in Eq. (2.2.9), with the result that

$$\bar{j} = \bar{i}_x j_x(\tilde{y}) = \bar{i}_x \frac{1}{M^2} (Rp_o - u_z'') . \tag{3.2.18}$$
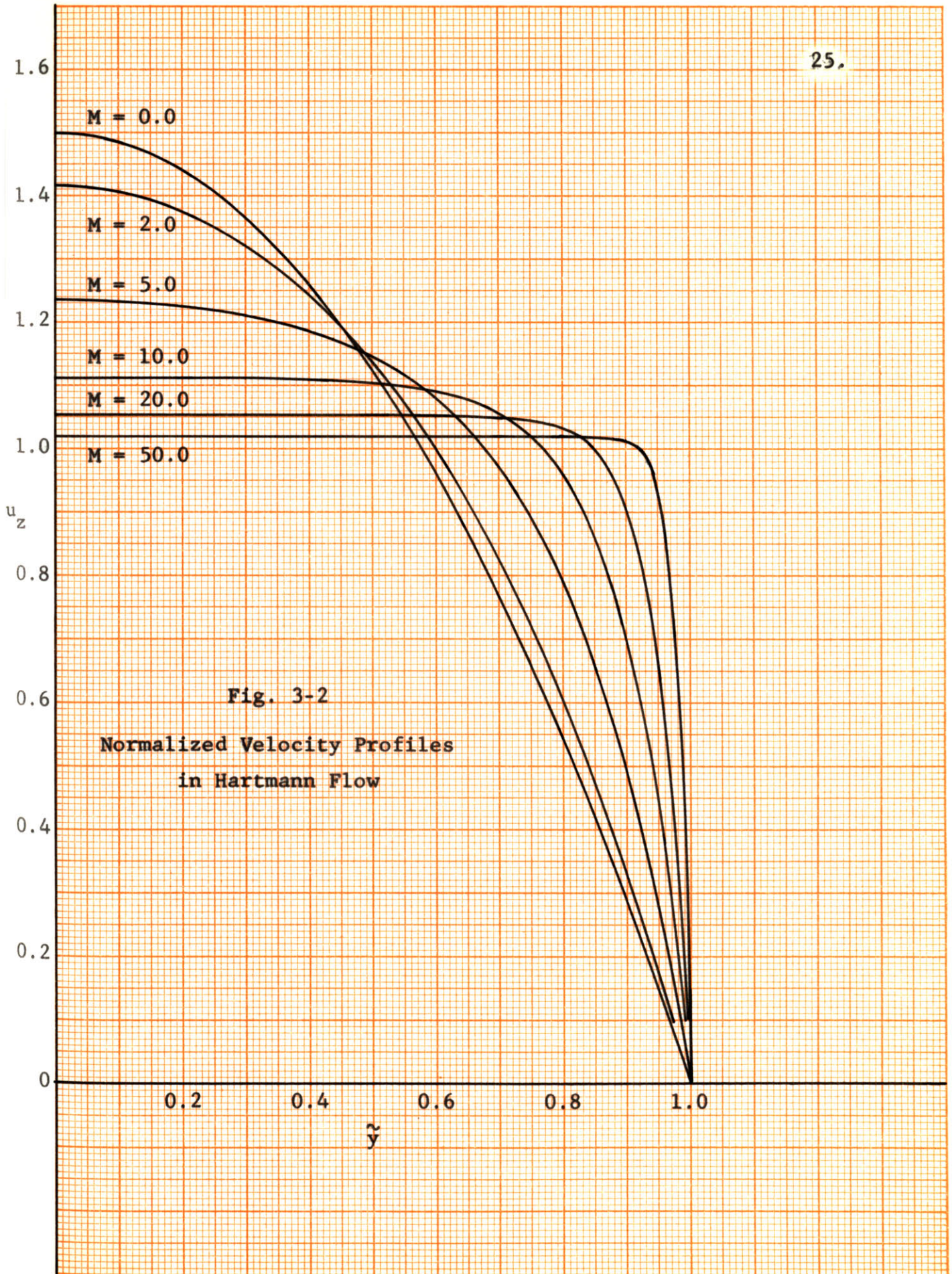
Fig. 3-2

Normalized Velocity Profiles
in Hartmann Flow

Finally, the electric field $\bar{e}$ can be computed by substituting Eqs. (3.2.18), (3.2.1) and (3.2.2) in Eq. (2.2.12), and is found to be

$$\bar{e} = \bar{j} - \bar{u} \times \bar{h} = \bar{i}_x \frac{1}{M^2} (Rp_o - u_z'' + M^2 u_z).$$

(3.2.19)

However, if Eq. (3.2.15) is substituted in Eq. (3.2.19), the result is

$$e_x = \frac{Rp_o}{M^2} + \frac{M}{M - \tanh M},$$

(3.2.20)

which is independent of $\tilde{y}$, and is, therefore, consistent with the idea of a constant applied electric field that was introduced in the problem specification (see Sec. 3.1 and Fig. 3-1).

3.3 A Variational Principle

The velocity profile for the conduction driven flow situation that is described in Sec. 3.1 can also be obtained from a variational principle. This principle states that out of all possible velocity profiles that are consistent with the boundary conditions, the fluid assumes the one that is associated with the least dissipation. The application of the principle follows.

In the conduction driven flow, there are two forms of dissipation; ohmic and viscous. The ohmic power dissipation per unit length in the z-direction P_{ohm} is given by

$$P_{ohm} = \int_{-a}^{a} \frac{J_x^2}{\sigma} \, dy = \sigma a (\mu_o H_a \langle v_z \rangle)^2 \int_{-1}^{1} j_x^2(\tilde{y}) d\tilde{y}$$

$$= \sigma a (\mu_o H_a \langle v_z \rangle^2 \int_{-1}^{1} (e_x - u_z)^2 \, d\tilde{y} \; , \qquad (3.3.1)$$

while the viscous power dissipation per unit length in the z-direction P_{vis} is given by [see Eq. (2.3.16)]

$$P_{vis} = \int_{-a}^{a} \eta \left(\frac{dv_z}{dy}\right)^2 \, dy = \frac{\eta \langle v_z \rangle^2}{a} \int_{-1}^{1} (u_z')^2 d\tilde{y} \; . \qquad (3.3.2)$$

Thus the total dissipation per unit length in the z-direction P_t is given by

$$P_t = \frac{\eta \langle v_z \rangle^2}{a} \int_{-1}^{1} [\, (u_z')^2 + M^2 (e_x - u_z)^2] d\tilde{y} \; , \qquad (3.3.3)$$

which is the integral that must be minimized by adjusting the function $u_z(\tilde{y})$, subject to the constraint

$$\int_{-1}^{1} u_z d\tilde{y} = 2 \; . \qquad (3.3.4)$$

The variational problem of minimizing the integral (3.3.3) subject to the constraint (3.3.4) is solved by first minimizing the integral

$$\int_{-1}^{1} F[u_z'(\tilde{y}), \, u_z(\tilde{y})] d\tilde{y} \; , \qquad (3.3.5)$$

in which

$$F = [(u_z')^2 + M^2(e_x - u_z)^2 + \lambda u_z] \ , \qquad (3.3.6)$$

subject to no constraint, and then determining the Lagrange multiplier λ, and the constants of integration in the solution of the Euler equation so that the boundary conditions and the constraint (3.3.4) are satisfied.[*] The function $F(u_z', u_z)$ must satisfy the Euler equation

$$\frac{d}{d\tilde{y}}(\frac{\partial F}{\partial u_z'}) - \frac{\partial F}{\partial u_z} = 0 \ , \qquad (3.3.7)$$

which yields

$$u_z'' - M^2 u_z + (\frac{\lambda}{2} + M^2 e_x) = 0 \ . \qquad (3.3.8)$$

Subject to the symmetry requirement $u_z(-\tilde{y}) = u_z(\tilde{y})$, and the boundary condition $u_z(\pm 1) = 0$, the solution of Eq. (3.3.8) is

$$u_z = (\frac{\lambda}{2M^2} + e_x)(1 - \frac{\cosh M\tilde{y}}{\cosh M}) \ . \qquad (3.3.9)$$

Finally, the Lagrange multiplier λ must be determined such that the constraint (3.3.4) is satisfied. The result is

$$u_z = (1 - \frac{\cosh M\tilde{y}}{\cosh M})/(1 - \frac{\tanh M}{M}) \ , \qquad (3.3.10)$$

---

[*] See Hildebrand,[34] Sec. 2.6.

which is identical to that obtained from the equations of motion in Sec. 3.2 [Eq. (3.2.15)].

This variational principle is an extension to a specific magnetohydrodynamic problem of similar principles for certain types of hydrodynamic flow.*

---

*See Lamb,[32] Art. 344.

Chapter IV

ENERGY CONVERSION IN CONDUCTION DRIVEN FLOW

4.1 Brake or Flow Damper Operation

The simplest conduction driven flow energy converter is the
brake or flow damper, in which the electromagnetic forces
produced by the interaction of induced currents and the applied
magnetic field, oppose the fluid motion and dissipate the fluid
energy in heat. There are two limiting forms of flow damper
that clearly illustrate this mode of operation. In the first,
the total current flowing through the fluid is zero (a non-
conducting channel, or conducting end plates that are open-
circuited); while in the second, the electric field in the fluid
is zero (conducting end plates that are short-circuited).

The I = 0 Flow Damper

The simplest type of flow damper consists of a non-
conducting rectangular channel across which a uniform magnetic
field is imposed. The rectangular channel is formed from the
infinite parallel planes of Fig. 3-1 by placing walls in the
y-z planes at $x = \pm d$ ($\tilde{x} = \pm d/a$), as shown in Fig. 4-1.
The distance 2d in the x-direction is assumed to be much
greater than the distance 2a that separates the original
parallel planes (a high-aspect-ratio channel), with the result
that the semi-infinite analysis of Ch. III may be assumed to be
applicable.

y

+a

-d ━━━━━━━━━━━━━━━━━━━━━━━━━━━━━━ +d ➤ x

o

-a
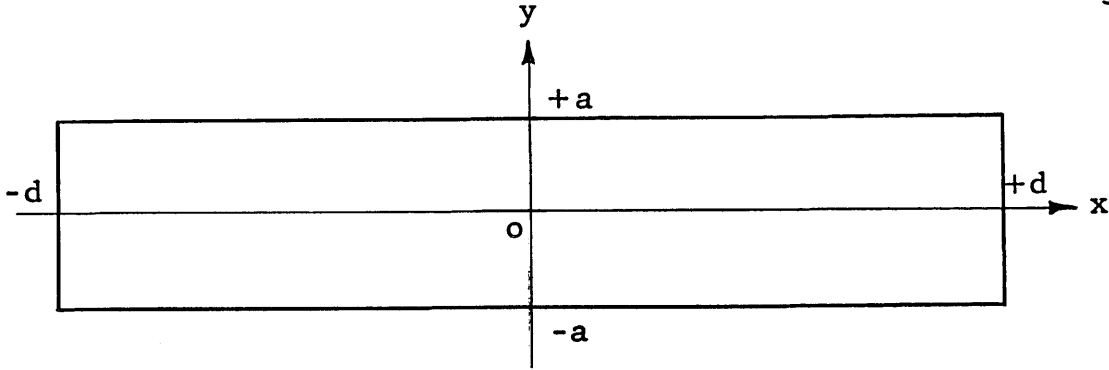
Fig. 4-1 A Channel Cross Section

The mathematical constraint for this type of flow damper is simply that the total current flowing in the x-direction must be zero; that is, that all the current circulates within the flow, by reversing direction at the walls $x = \pm d$.[*] If Eq. (3.2.18) is integrated across the channel, the total normalized current flowing in the x-direction, per unit length in $\tilde{z}$ is found to be

$$i_t = \int_{-1}^{1} j_x(\tilde{y}) d\tilde{y} = \frac{2}{M^2} [Rp_o - u_z'(1)] \ , \tag{4.1.1}$$

and is constrained to be zero. Thus the hydraulic Reynolds number is given by

$$\frac{\rho a}{\eta} \langle v_z \rangle = R = \frac{u_z'(1)}{P_o} = \frac{u_z'(1)}{a P_o/\rho \langle v_z \rangle^2} \ , \tag{4.1.2}$$

in which P_o is the unnormalized mechanical pressure gradient, i.e.

$$P_o \equiv \frac{\partial P}{\partial z} = a \ constant. \tag{4.1.3}$$

---

[*]This current reversal is facilitated by having electrically conducting planes at $x = \pm d$.

Equation (4.1.2) can be solved for the average velocity and yields, in view of the normalized velocity profile (3.2.15),

$$\frac{\langle v_z \rangle}{a^2 P_o/\eta} = \frac{1}{u_z'(1)} = - \frac{1}{M^2} (M \coth M - 1), \qquad (4.1.4)$$

in which the initial minus sign indicates that the fluid is driven in the minus z-direction by the mechanical pressure gradient P_o.

For small values of M, the average velocity tends to a constant as in hydrodynamic flow, in fact

$$\frac{\langle v_z \rangle}{a^2 P_o/\eta} \to - \frac{1}{3} (1 - \frac{M^2}{15}) , \quad \text{as } M \to 0 ; \qquad (4.1.5)$$

with the result that the volume flow rate is little affected for small magnetic fields.[*] However, for large values of M the average velocity is inversely proportional to M and is given by

$$\frac{\langle v_z \rangle}{a^2 P_o/\eta} \to - \frac{1}{M} , \quad \text{as } M \to \infty , \qquad (4.1.6)$$

with the result that the volume flow rate is inversely proportional to the magnetic field strength for large magnetic fields.

---

[*] Because experimentally the magnetic field strength is the most easily varied quantity in $M = \mu_o H_o L_o \sqrt{\sigma/\eta}$, the variation of a quantity with M can often be instructively interpreted as its variation with the magnetic field strength.

The velocity profiles for this flow damper are conveniently displayed by normalizing the velocity $v(\tilde{y})$ with respect to the center channel velocity in hydrodynamic flow $(M = 0)$, i.e.

$$\frac{v(\tilde{y})}{a^2 P_0/\eta} = \frac{\langle v_z \rangle}{a^2 P_0/\eta} \, u_z(\tilde{y}) = \frac{(1 - \frac{\cosh M\tilde{y}}{\cosh M})}{M \tanh M} \, . \qquad (4.1.7)$$

Figure 4-2 shows a set of these velocity profiles for several values of M. For M = 0, the velocity distribution reduces to the viscosity controlled parabolic contour. As M is increased, however, the magnetic field begins to flatten the profile and to decrease its amplitude. Finally, for large M, the amplitude of the velocity is greatly reduced, the central region of the profile is completely controlled and flattened by the magnetic field, and viscosity is important only in thin boundary layers near the walls.

The unnormalized current density $J_x(\tilde{y})$ can be obtained by combining Eqs. (3.2.18) and (4.1.2) and is given by

$$\frac{J_x(\tilde{y})}{a P_0 \sqrt{\sigma/\eta}} = -(\frac{1}{M} - \frac{\cosh M\tilde{y}}{\sinh M}) \, , \qquad (4.1.8)$$

in which the renormalization shown is convenient. Figure 4-3 shows a set of normalized (to $-a P_0 \sqrt{\sigma/\eta}$) current density curves for various values of the parameter M. The current always flows in the negative x-direction in the central region of the channel, and in the positive x-direction along the walls, however, the shape of the current distribution varies quite drastically with M. For small values of M $(M \leqslant 0.1)$, the magnitude of the circulating current is small, the distribution is quite flat throughout, and the zero crossing approaches
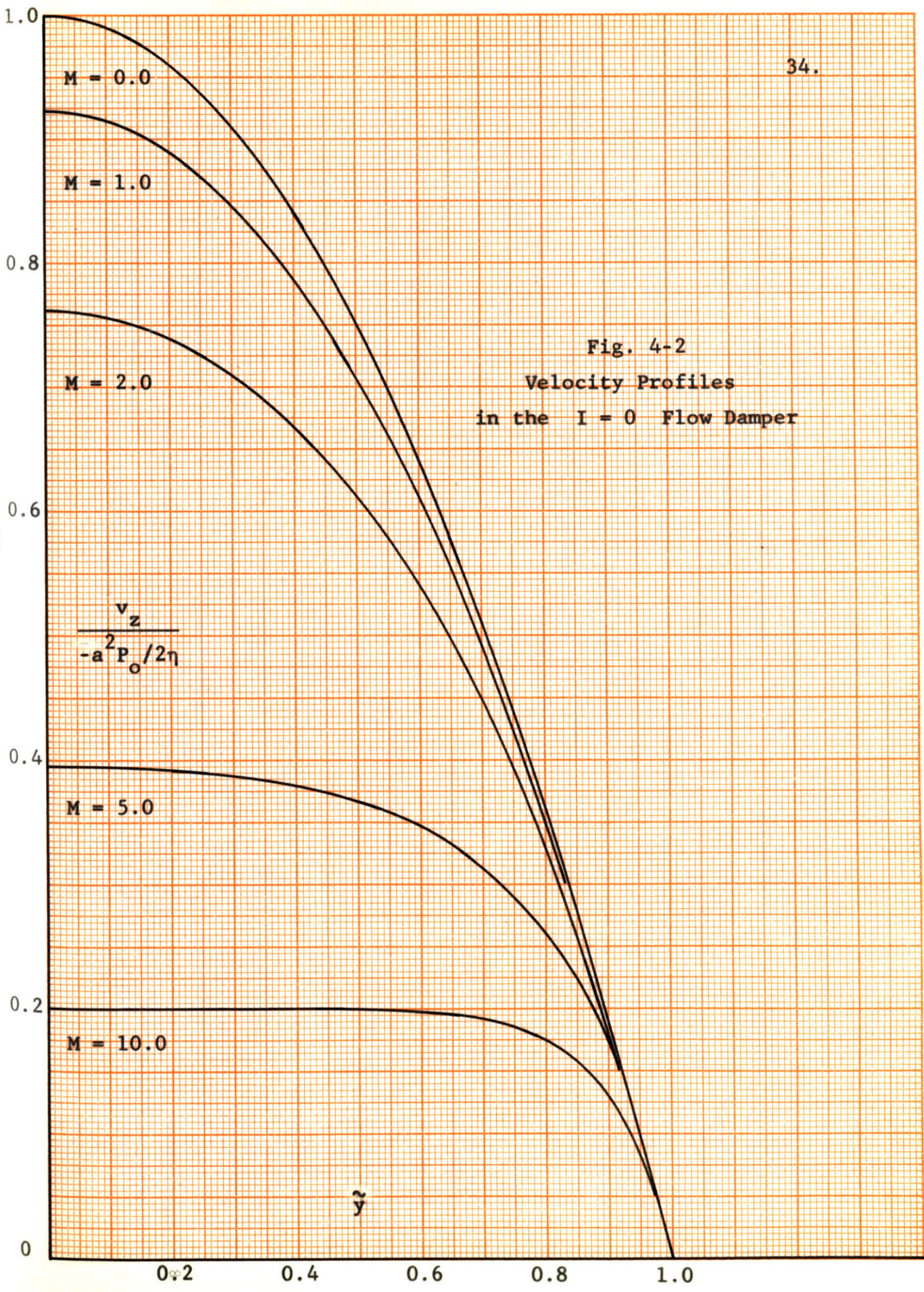
Fig. 4-2
Velocity Profiles
in the I = 0 Flow Damper

34.

34a.

Fig. 4-3
Current Density Profiles
in the I = 0 Flow Damper
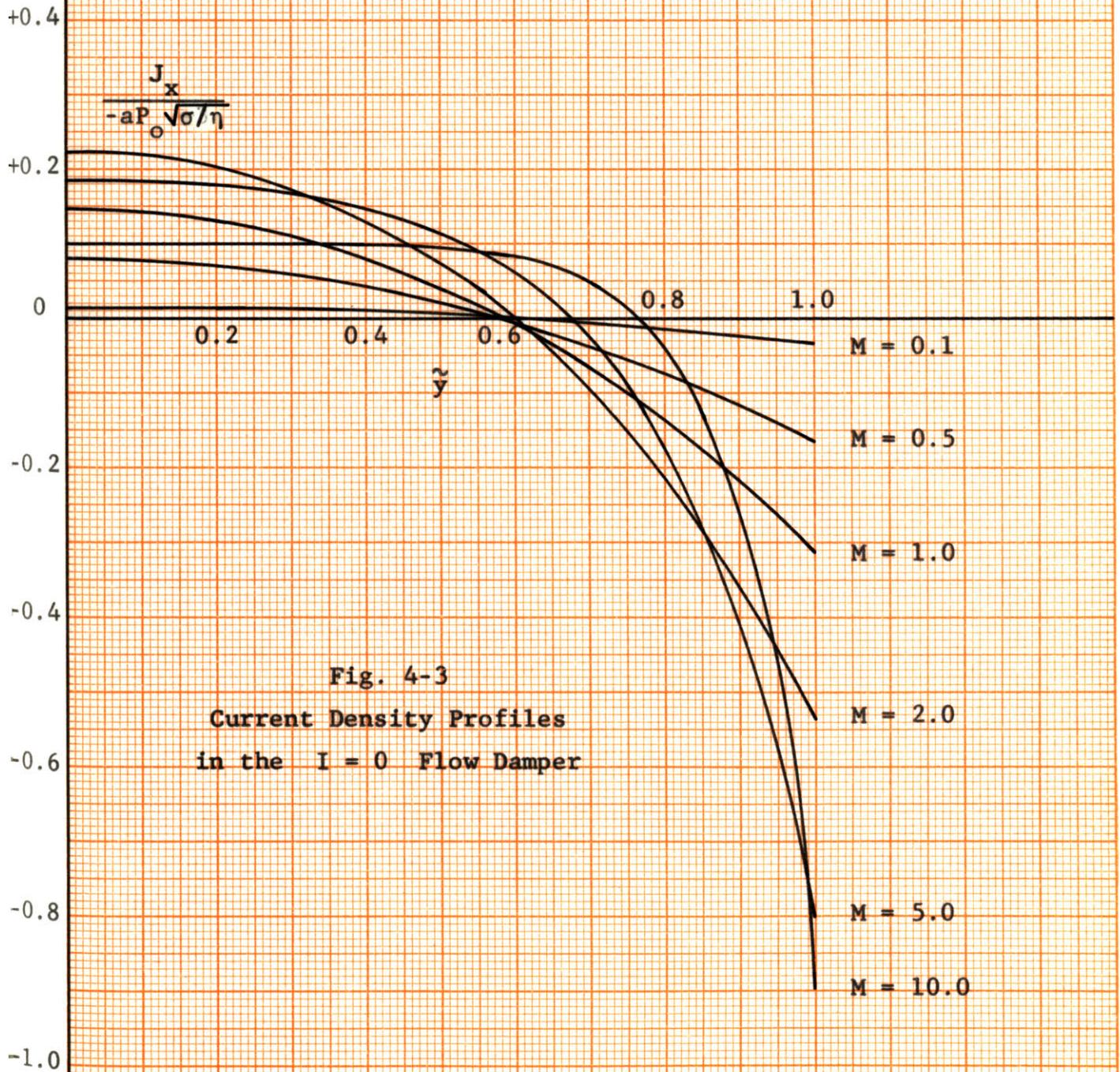
$\tilde{y} = 1/\sqrt{3} \simeq 0.577$ as M approaches zero. As M increases
$(0.1 < M < \sim 5.0)$ the magnitude of the circulating current
increases and the distribution remains flat near the center of
the channel, but develops a sharp negative peak near the walls.
Finally, as M increases still further $(M \to \infty)$, the magnitude
of the circulating current decreases, the zero crossing tends
to $\tilde{y} = 1$ monotonically, and the shape of the distribution
becomes flatter to the left of the zero crossing and more
peaked near the wall, with the peak rising to a limiting
value of one.

The square of the Hartmann number is commonly interpreted
as a measure of the ratio of the ohmic power loss to the
viscous power loss [see Eq. (2.2.20)]. Since the identifica-
tion is made on the basis of a rough dimensional argument,
the calculation of the actual ratio for the I = 0 flow
damper provides a check on the dimensional reasoning. The
exact calculations are somewhat involved algebraically, but
the result is that the ratio of the ohmic power loss to the
viscous power loss (both averaged with respect to $\tilde{y}$) is
given by

$$\frac{P_{ohm}}{P_{vis}} = \frac{[\sinh 2M + 2M - \frac{2}{M}(\cosh M - 1)]}{(\sinh 2M - 2M)} . \tag{4.1.9}$$

Although the expression (4.1.9) is a rather complicated function
of M, the following limiting properties can be deduced in a
straightforward manner. First, for small values of M the
ratio becomes

$$\frac{P_{ohm}}{P_{vis}} \to \frac{M^2}{15} , \text{ as } M \to 0 . \tag{4.1.10}$$

Second, for large values of M the ratio tends to one, in fact

$$\frac{P_{ohm}}{P_{vis}} \to 1 - \frac{2}{M} \; , \quad \text{as} \quad M \to \infty \; . \tag{4.1.11}$$

Thus for small values of M the actual power loss ratio differs from the ratio M^2 determined by dimensional arguments [Eq. (2.2.20)] only by the numerical factor 15. However, for large values of M the dimensional ratio is considerably in error, since it assumes a large value while the actual limiting value is one.

This detailed discussion of the actual power loss ratio for the I = 0 flow damper, and the results that follow for the E = 0 flow damper, demonstrate that dimensional reasoning, of the type that led to the identification of the square of the Hartmann number with the ratio of ohmic to viscous power dissipation, can quite often be misleading in specific situations. So-called "physical" and "dimensional" arguments of this type are often helpful for obtaining a general idea of the nature of a particular parameter or a physical situation; however, they should be employed as aides to, and not substitutes for, more rigorous analysis.

The E = 0 Flow Damper

In this second type of flow damper, the electrically conducting planes at $x = \pm d$ are short-circuited, which constrains the uniform electric field within the flow to be zero. If e_x is set equal to zero in Eq. (3.2.20), the hydraulic Reynolds number can be determined from the relation

$$\frac{a^2 P_o}{\eta \langle v_z \rangle} = Rp_o = - \frac{M^3}{M - \tanh M} , \qquad (4.1.12)$$

with the result that the average fluid velocity is given by

$$\frac{\langle v_z \rangle}{a^2 P_o / \eta} = - \frac{M - \tanh M}{M^3} , \qquad (4.1.13)$$

in which again the initial minus sign indicates that the fluid is driven in the minus z-direction by the mechanical pressure gradient P_o.

For small values of M, the average velocity again tends to a constant, in fact

$$\frac{\langle v_z \rangle}{a^2 P_o / \eta} \rightarrow - \frac{1}{3}(1 - \frac{2}{5} M^2) , \quad \text{as} \quad M \rightarrow 0 ; \qquad (4.1.14)$$

which, when compared with expression (4.1.5) for the I = 0 flow damper, shows that the E = 0 flow damper has the greater effect on the volume flow rate for small values of M. For large values of M, the comparison is more striking, since

$$\frac{\langle v_z \rangle}{a^2 P_o / \eta} \rightarrow - \frac{1}{M^2} , \quad \text{as} \quad M \rightarrow \infty , \qquad (4.1.15)$$

whereas the expression (4.1.6) goes as only 1/M as $M \rightarrow \infty$. Thus the E = 0 flow damper is far more effective than the I = 0 flow damper for large values of M.

The actual ratio of the ohmic power loss to the viscous power loss can also be computed for this type of flow damper, and the result is

$$\frac{P_{ohm}}{P_{vis}} = \frac{2M \cosh 2M - 3 \sinh 2M + 2(2M)}{\sinh 2M - 2M} , \qquad (4.1.16)$$

Again the expression is rather complicated, but the limiting
forms are given by

$$\frac{P_{ohm}}{P_{vis}} \to \frac{2}{5} M^2 \ , \quad \text{as} \quad M \to 0; \tag{4.1.17}$$

and

$$\frac{P_{ohm}}{P_{vis}} \to 2M \ , \quad \text{as } M \to \infty \ . \tag{4.1.18}$$

Thus the agreement between the ratio predicted on dimensional
grounds (M^2) and the actual ratio is quite good for small
values of M, but is still poor for large values of M.

4.2 Generator Operation

The operation of the conduction driven flow as a generator
is quite similar to brake or flow damper operation, except that
a net current is allowed to flow through the fluid and an
external load. A rectangular channel is again formed as shown
in Fig. 4-1, and conducting electrodes of length 2b in the
z-direction form the walls at x = ± d, as shown in Fig. 4-4.
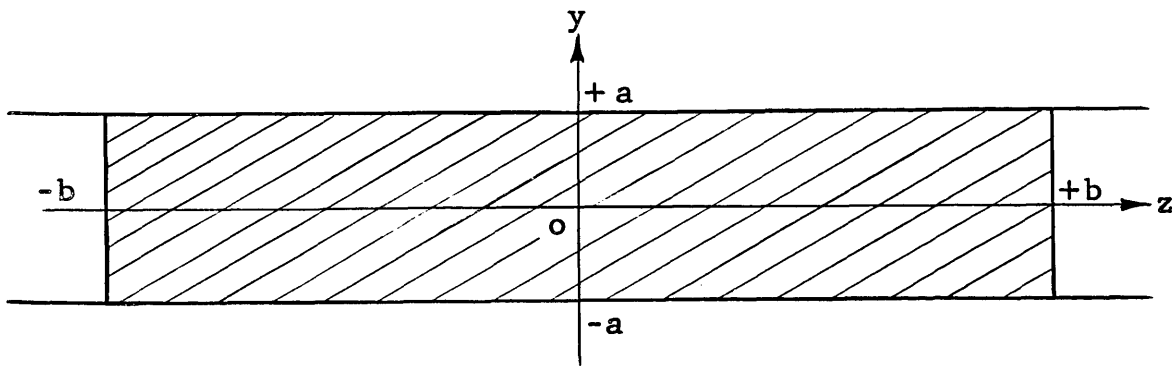
Fig. 4-4   A Channel Electrode

The length of the electrodes 2b is assumed to be much greater than the channel width 2a, or the channel depth 2d, with the result that end effects at $z = \pm b$ can be neglected. In order to exactly preserve the direction and symmetry of the induced magnetic field solution [see Eq. (3.2.16)], the external load must be connected to the electrodes in such a way that the load current flows in x-y planes and symmetrically with respect to the x-axis, as shown schematically in Fig. 4-5.
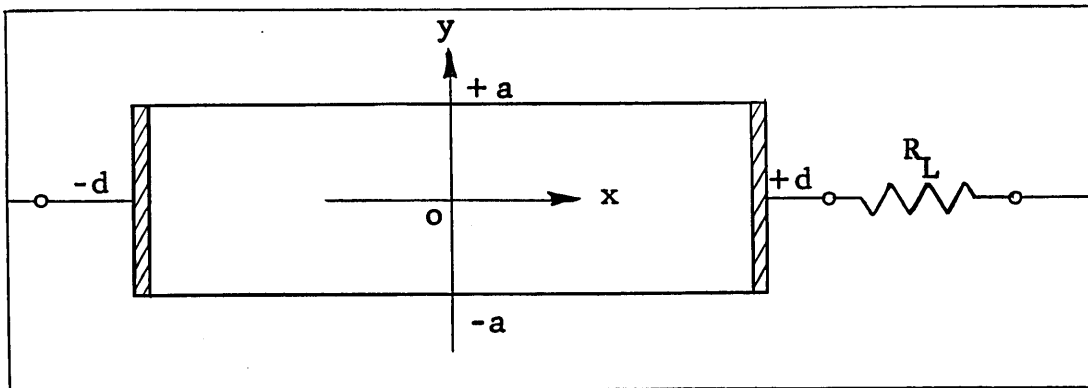
Fig. 4-5 Schematic Diagram of Symmetrical
Generator Loading

The electrical load that is placed on the generator is most conveniently characterized by its resistance per unit length in z, R_L. Therefore, the hydraulic Reynolds number must be determined as a function of this external load resistance. The total unnormalized current per unit length in z can be obtained by integrating Eq. (3.2.18) across the channel, and is found to be

$$I = \int_{-a}^{a} J_x dy = a\sigma\mu_o H_a \langle v_z \rangle \int_{-1}^{1} j_x d\tilde{y}$$

$$= a\sigma\mu_o H_a \langle v_z \rangle \frac{2}{M^2} [Rp_o - u_z'(1)] . \qquad (4.2.1)$$

Furthermore, the voltage V between the electrodes at $x = \pm d$ can be obtained from the uniform electric field (3.2.20) as

$$V = -2d\ E_x = -2d\mu_o H_a\ \langle v_z \rangle\ e_x$$

$$= -2d\mu_o H_a\ \langle v_z \rangle\ \frac{1}{M^2}\ (Rp_o + \frac{M^3}{M - \tanh M})\ . \qquad (4.2.2)$$

Therefore, the external load resistance R_L can be expressed as

$$R_L = \frac{V}{I} = -\frac{d}{a\sigma}\ \frac{Rp_o + M^3/(M - \tanh M)}{Rp_o + M^2\tanh M/(M - \tanh M)}\ . \qquad (4.2.3)$$

The ensuing calculations, and the presentation of the results are greatly simplified by normalizing the external load resistance per unit length R_L with respect to the internal resistance of the generator per unit length $d/a\sigma$ and defining

$$\alpha \equiv \frac{R_L}{d/a\sigma}\ ; \qquad (4.2.4)$$

and by making the further identification

$$\beta \equiv M/\tanh M\ . \qquad (4.2.5)$$

Equation (4.2.3) can be solved for the average fluid velocity $\langle v_z \rangle$ in terms of the dimensionless ratios α and β, with the result that

$$\frac{\langle v_z \rangle}{a^2 P_o/\eta} = \frac{1}{Rp_o} = -\frac{1}{M^2}\ \frac{(\alpha + 1)(\beta - 1)}{(\alpha + \beta)}\ . \qquad (4.2.6)$$

In order to optimize the operation of the flow as a generator, the electrical power output and the energy conversion

efficiency are next expressed in terms of the parameters α and β. If Eq. (4.2.6) is substituted in Eq. (4.2.1), the total current per unit length in z is found to be

$$I = - \frac{2aP_o}{\mu_o H_a} \frac{(\beta - 1)}{(\alpha + \beta)} ; \qquad (4.2.7)$$

and, therefore, the power delivered to the load per unit length is given by

$$P_L = I^2 R_L = \frac{4a^3 d \ P_o^2}{\eta M^2} \frac{\alpha(\beta - 1)^2}{(\alpha + \beta)^2} . \qquad (4.2.8)$$

Furthermore, the mechanical power input density is just $-\bar{v} \cdot \nabla P$, with the result that the mechanical power input per unit length in z is found to be

$$P_m = -4a \ d \ P_o \ \langle v_z \rangle = \frac{4a^3 d \ P_o^2}{\eta M^2} \frac{(\alpha + 1)(\beta - 1)}{(\alpha + \beta)} . \qquad (4.2.9)$$

Therefore, the energy conversion efficiency ε can be expressed as a function of only α and β, viz.

$$\varepsilon(\alpha,\beta) = \frac{\alpha(\beta - 1)}{(\alpha + 1)(\alpha + \beta)} ; \qquad (4.2.10)$$

in which the range of α is

$$0 \leq \alpha \leq \infty , \qquad (4.2.11)$$

while that of β is

$$1 \leq \beta \leq \infty . \qquad (4.2.12)$$

The important properties of ε can be deduced quite easily from Eq. (4.2.10). First, ε is equal to zero when either α is equal to zero or β is equal to one, i.e.

$$\varepsilon(0,\beta) = \varepsilon(\alpha,1) = 0 \ , \qquad\qquad (4.2.13)$$

which implies physically that the efficiency is zero for either a short-circuit load, or zero applied magnetic field. Second, the partial derivative of ε with respect to β is given by

$$\frac{\partial \varepsilon}{\partial \beta} = \frac{\alpha}{(\alpha + \beta)^2} \ , \qquad\qquad (4.2.14)$$

which is non-negative for the ranges of α and β under consideration [eqs. (4.2.11) and (4.2.12)]. Therefore, for any fixed value of α (except $\alpha = 0$), the efficiency is a monotonically increasing function of β. For such a fixed value of α, the limiting value of ε is

$$\varepsilon \to \frac{\alpha}{\alpha + 1} \ , \quad \text{as} \quad \beta \to \infty \ . \qquad\qquad (4.2.15)$$

Thus, for a fixed value of the external load resistance, the efficiency increases monotonically from zero to the limit (4.2.15) as the applied magnetic field increases from zero to infinity. Third, the partial derivative of ε with respect to α is given by

$$\frac{\partial \varepsilon}{\partial \alpha} = \frac{(\beta - 1)(\beta - \alpha^2)}{(\alpha + 1)^2 (\alpha + \beta)^2} \ , \qquad\qquad (4.2.16)$$

which is equal to zero for

$$\beta = 1 \ , \qquad\qquad (4.2.17)$$

and for

$$\beta = \alpha^2 .$$ (4.2.18)

For $\beta = 1$, the efficiency is a minimum ($\varepsilon = 0$), while for $\beta = \alpha^2$ it is a maximum, and is given by

$$\varepsilon(\alpha, \alpha^2) = \frac{\sqrt{\beta} - 1}{\sqrt{\beta} + 1} .$$ (4.2.19)

Also, for a fixed value of β, the limiting value of ε is

$$\varepsilon \rightarrow 0, \quad \text{as} \quad \alpha \rightarrow \infty .$$ (4.2.20)

Thus, for a fixed value of β, the efficiency increases from zero to a maximum given by Eq. (4.2.19), and then decreases to zero again, as α increases from zero to infinity. Therefore, for a fixed value of the applied magnetic field, the maximum possible efficiency is

$$\varepsilon = \frac{\sqrt{M/\tanh M} - 1}{\sqrt{M/\tanh M} + 1} ,$$ (4.2.21)

which is attained for a load resistance given by

$$R_L = \frac{d}{a\sigma} \sqrt{\frac{M}{\tanh M}} .$$ (4.2.22)

In order to make the variation of the efficiency as a function of the parameters α and β completely clear, Fig. 4-6 shows a family of curves of ε as a function of α, with β as a parameter.

The final subject to be discussed concerning generator operation is the dependence of the electrical power output P_L [Eq. (4.2.8)] on the load resistance R_L (through α). The
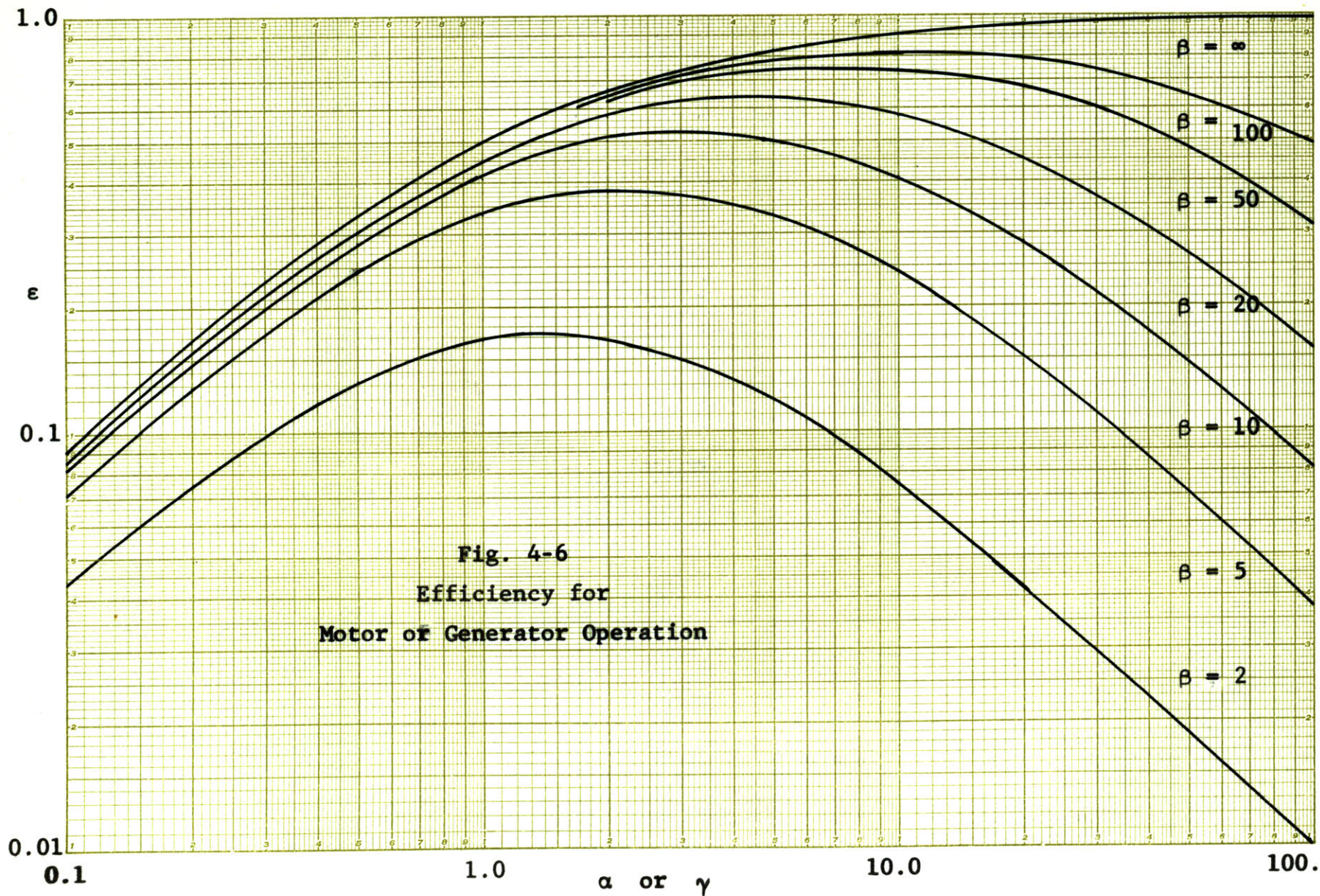
Fig. 4-6
Efficiency for
Motor or Generator Operation

$\beta = \infty$

$\beta = 100$

$\beta = 50$

$\beta = 20$

$\beta = 10$

$\beta = 5$

$\beta = 2$

ε

α or γ

44.

partial derivative of P_L with respect to α is given by

$$\frac{\partial P_L}{\partial \alpha} = \frac{4a^3 \, d \, P_o^2}{\eta M^2} \frac{(\beta - 1)^2 (\beta - \alpha)}{(\alpha + \beta)^3} \, , \qquad (4.2.23)$$

which is zero for

$$\alpha = \beta \, , \qquad (4.2.24)$$

which corresponds to a maximum of P_L. Therefore, if all other parameters are held fixed, the power output is a maximum when the load resistance per unit length is given by

$$R_L = \frac{d}{a\sigma} \frac{M}{\tanh M} \, . \qquad (4.2.25)$$

A comparison of Eq. (4.2.25) with Eq. (4.2.22) shows, as would be expected from physical experience, that the value of the load resistance for maximum power output is different from that for maximum efficiency. If the value of α for maximum power output [Eq. (4.2.24)] is substituted in the efficiency relation (4.2.10), the result is

$$\varepsilon(\beta,\beta) = \frac{1}{2} \frac{\beta - 1}{\beta + 1} \, . \qquad (4.2.26)$$

Therefore, if the load resistance is adjusted so as to give the maximum power output for each value of the applied magnetic field, the highest possible efficiency is one-half, which is obtained as the value of the applied magnetic field tends to infinity. However, this does not mean, contrary to some opinion, that efficiencies greater than one-half are not possible; only that such efficiencies are obtained at the expense of less than

maximum power output. In fact, as has been demonstrated in the preceding discussion, efficiencies approaching one are possible, although they are accompanied by power outputs approaching zero.

4.3 Motor or Pump Operation

The physical configuration for motor or pump operation is identical to that for generator operation, as shown in Figs. 4-4 and 4-5, except that the load resistance is replaced by a voltage source. If the magnitude of this applied voltage source is $2V_a$, the uniform electric field within the fluid is constrained to be

$$\frac{V_a}{d} = E_x = \mu_o H_a \langle v_z \rangle \, e_x$$

$$= \mu_o H_a [\frac{P_o a^2}{\eta M^2} + \frac{\langle v_z \rangle M}{M - \tanh M}] \, . \tag{4.3.1}$$

Equation (4.3.1) can be solved for $\langle v_z \rangle$, with the result that

$$\langle v_z \rangle = \frac{a^2 P_o}{\eta M^2} \frac{\gamma(\beta - 1)}{\beta} , \tag{4.3.2}$$

in which the dimensionless parameter γ, which is defined by

$$\gamma \equiv \frac{\sigma \frac{V_a}{d} \mu_o H_a}{P_o} - 1 , \tag{4.3.3}$$

has been introduced. The parameter γ can be interpreted physically as a measure of the ratio of the applied electromagnetic force density $\sigma \frac{V_a}{d} \mu_o H_a$ to the pressure force density P_o. Furthermore, Eqs. (4.3.2) and (4.3.3) show that if γ is positive, the electromagnetic force is greater than the pressure

force, and the fluid flows in the positive z-direction; while if γ is negative, the reverse is true. Thus the inequality

$$V_a \geq \frac{P_o d}{\sigma \mu_o H_a} \tag{4.3.4}$$

is a necessary condition for pump operation.

The mechanical power-output density is simply $\overline{v} \cdot \nabla P$, with the result that the total mechanical power output per unit length in z is given by

$$P_m = 4adP_o \langle v_z \rangle = \frac{4a^3 dP_o^2}{\eta M^2} \frac{\gamma(\beta - 1)}{\beta} , \tag{4.3.5}$$

in view of Eq. (4.3.2). Also, the total current per unit length can be obtained by substituting Eq. (4.3.2) in Eq. (4.2.1) and is found to be

$$I = \frac{2aP_o}{\mu_o H_a} \frac{(\beta + \gamma)}{\beta} , \tag{4.3.6}$$

with the result that the total electrical power input per unit length is given by

$$P_e = 2V_a I = \frac{4a^3 dP_o^2}{\eta M^2} \frac{(\gamma + 1)(\beta + \gamma)}{\beta} . \tag{4.3.7}$$

Therefore, the energy conversion efficiency of the pump can be expressed as

$$\varepsilon(\gamma, \beta) = \frac{\gamma(\beta - 1)}{(\gamma + 1)(\gamma + \beta)} , \tag{4.3.8}$$

in which γ is restricted to the range

$$0 \le \gamma \le \infty \qquad\qquad (4.3.9)$$

for pump operation [see Eq. (4.3.4)].

A comparison of Eqs. (4.3.8) and (4.3.9) with Eqs. (4.2.10) and (4.2.11) shows that the expression for the efficiency in pump operation is <u>identical</u> to that for generator operation if γ is replaced by α. Thus all of the discussion in Sec. 4.2 concerning the efficiency of generator operation is directly applicable to pump operation. Restated in terms of pump operation, the principal results are as follows. First, for a fixed value of γ (applied voltage), the efficiency increases monotonically from zero to a limiting value given by

$$\varepsilon \to \frac{\gamma}{\gamma + 1} \,, \quad \text{as} \quad \beta \to \infty \,, \qquad\qquad (4.3.10)$$

as the applied magnetic field varies from zero to infinity. Second, for a fixed value of M (magnetic field), the efficiency becomes a maximum given by

$$\varepsilon = \frac{\sqrt{M/\tanh M} - 1}{\sqrt{M/\tanh M} + 1} \,, \qquad\qquad (4.3.11)$$

when $\gamma^2 = \beta$, that is when

$$V_a = \frac{P_o d}{\sigma \mu_o H_a} \left(\sqrt{M/\tanh M} + 1 \right) \,, \qquad\qquad (4.3.12)$$

Finally, inspection of the expression (4.3.5) for the mechanical power output shows that it varies linearly with γ, with the result that increasing the applied voltage monotonically increases the power output.

4.4 Relation to Existing Experiments

The principal scientific experimental results concerning laminar conduction driven flow are still those obtained by Hartmann and Lazarus,[4] in 1937. At that time, they verified the fact that in an electrically insulating high-aspect-ratio channel (the I = 0 flow damper of Sec. 4.1), the volume flow rate is inversely proportional to the applied transverse magnetic field strength, for high values of the magnetic field. They did not, however, make any tests of E = 0 flow damper, pump, or generator operations; nor did they measure any velocity profiles. Recently, there has been an attempt by Kliman[36] to measure velocity profiles in magnetohydrodynamic channel flow by the use of an electromagnetic flow meter; although the results were somewhat inconclusive, and more work is needed to perfect the technique.

From a practical standpoint, a large number of conduction-driven electromagnetic pumps have been built and tested, primarily for pumping sodium in atomic reactor applications.[*] Unfortunately, such pumps do not conform to some of the assumptions that are made in this analysis. They are almost always uncompensated, and thus are effected by armature reaction; their channels are commonly rectangular or of low-aspect-ratio; and their flow rates are such that, in consideration of Murgatroyd's results (see Sec. 1.3), the flow within them is probably laminar for low flow rates, but undoubtedly is turbulent for high flow rates. The sort of experimental results that are

---

[*]See, for example, Cage,[6] Barnes,[7] and Watt.[8]

published concerning these pumps are terminal properties such as head-capacity and efficiency-capacity curves.* The head-capacity curves are invariably linear, which is in agreement with the prediction of Eqs. (4.3.2) and (4.3.3); but which is also predicted by far less detailed theories that completely ignore the magnetic field and velocity distributions. The efficiency-capacity curves also have the same form as those predicted by Eqs. (4.3.2) and (4.3.8), although again cruder theories predict a similar form.

Thus there is a real lack of careful, detailed experimental results of the type that would provide a rigorous experimental check on the theoretical results that are presented here. A discussion of some possible lines of experimental investigation is presented in Sec. 9.3.

---

*See, for example, Barnes.[37]

Chapter V

FUNDAMENTALS OF INDUCTION DRIVEN FLOW

5.1 The Configuration and the Choice of Characteristic Quantities

This chapter is concerned with the basic equations that govern the laminar flow of a viscous, incompressible, conducting fluid in a high-aspect-ratio channel under the influence of a traveling magnetic field. This type of magnetohydrodynamic channel flow is called "induction driven" because the currents that flow in the conducting fluid are induced by the traveling magnetic field, and because the gross operation of such a flow is similar to that of a conventional induction motor.[*]

In Fig. 5-1, the idealized situation that is analyzed here is
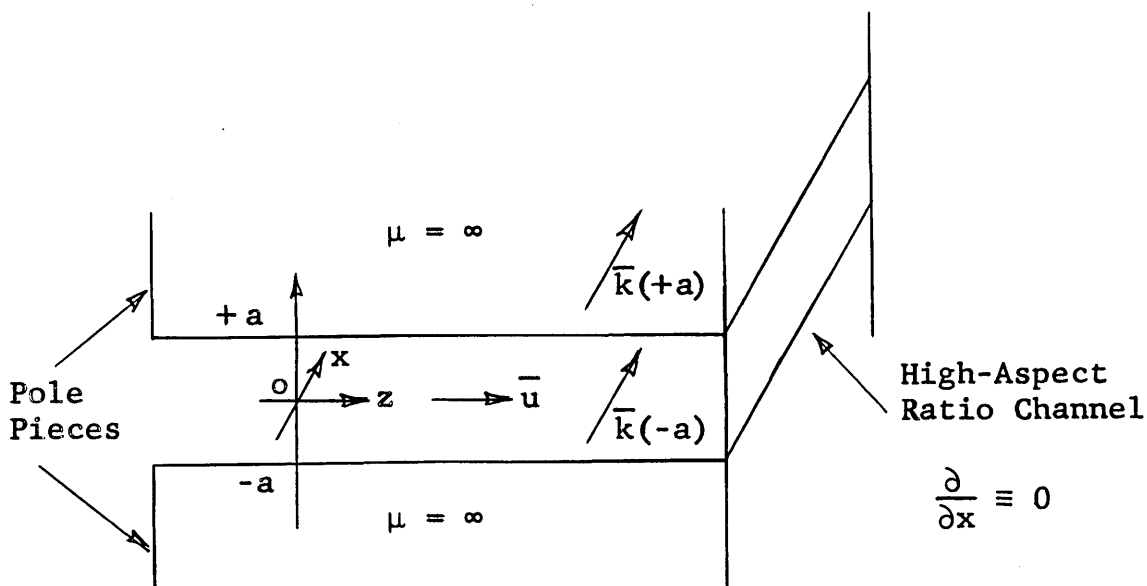
Fig. 5-1 An Induction Driven Magnetohydrodynamic
Channel Flow

---

[*]For an introduction to conventional induction machines, see White and Woodson,[35] Sec. 3.6.4. For a practical design analysis of induction pumps using induction motor theory, see Watt.[11]

shown schematically. The mean fluid flow is in the z-direction, and is confined by parallel, non-conducting planes at $y = \pm\,a$. Further, these planes extend sufficiently far in the x-direction (high-aspect-ratio) that none of the quantities of interest vary with x $(\frac{\partial}{\partial x} \equiv 0)$. The traveling magnetic field is excited by current sheets that vary sinusoidally in space and time, and flow in the x-direction on the surfaces of the infinitely permeable pole pieces which bound the channel on the planes $y = \pm\,a$. (In practice, the exciting structure might resemble the polyphase stator of a conventional induction motor.)

The excitation surface currents are assumed to be of the form:

$$\overline{K}(y = + a) = \overline{i}_x K_o \mathrm{Re}\; e^{i(\omega t - kz)} \tag{5.1.1}*$$

$$\overline{K}(y = -a) = \pm\, \overline{i}_x K_o \mathrm{Re}\; e^{i(\omega t - kz)} \tag{5.1.2}$$

with the result that the magnetic field travels with a phase velocity ω/k in the positive z-direction. If the positive sign is chosen in Eq. (5.1.2), the excitation has even symmetry with respect to y; if the negative sign is chosen, it has odd symmetry. Throughout this investigation, these two choices will be referred to respectively as even and odd excitation. The conventional induction motor, in which the coils are wound in the faces of the magnetic structure, is an example of even excitation; while the traveling wave tube,[**] in which the coil

---

[*] Throughout this analysis, i is used to denote $\sqrt{-1}$, and Re to denote "the real part of".

[**] Note that in the traveling wave tube electric as well as magnetic fields are important.

or helix is wound around the electron beam, is an example of odd excitation. Even excitation produces its maximum magnetic field transverse to the flow direction, while odd excitation produces its maximum magnetic field parallel to the flow direction. Because the transverse component of the magnetic field provides the electromagnetic $(\overline{J} \times \overline{B})$ force in the direction of the mean flow, even excitation qualitatively seems to be more effective than odd excitation. Even excitation is used exclusively in practical liquid metal induction pumps,* although odd excitation may be of interest in other applications.** Both types of excitation are analyzed in this investigation.

Equations (2.2.15) and (2.2.16) seem to indicate that there are only three independent dimensionless parameters in any magnetohydrodynamic problem, for example, R, R_m and β. This is not so, because there may be more than one independently variable characteristic length, velocity or magnetic field in a particular problem.

In the situation considered here, there are two characteristic lengths, the channel half-width a, and the excitation pole spacing π/k. In order to simplify the location of the boundary conditions on the velocity at the channel walls, the

---

*See, for example, Watt[8] and Blake.[10]

**Several groups are interested in using slow wave structures to accelerate plasma beams. See Marshall,[17] and Covert and Haldemann.[19]

channel half-width is chosen as <u>the</u> characteristic length, i.e.

$$L_o = a ,$$
(5.1.3)

and the dimensionless ratio

$$\alpha = ka$$
(5.1.4)

is introduced. There are also two characteristic velocities in this problem, the mean (space and time) fluid velocity, and the excitation phase velocity. The former is usually taken as characteristic in purely hydrodynamic problems because of its importance in the transition from laminar to turbulent flow. However, in this laminar magnetohydrodynamic situation the phase velocity of the excitation is given, and the fluid velocity must be determined. Thus the excitation phase velocity is appropriately chosen as the characteristic velocity, i.e.

$$v_o = \omega/k .$$
(5.1.5)

Finally, the peak value of the magnetic field at the channel walls is chosen as the characteristic magnetic field, i.e.

$$H_o = K_o .$$
(5.1.6)

Now that the characteristic quantities have been defined, the excitation [Eqs. (5.1.1) and (5.1.2)] can be written in normalized form as

$$\bar{k}(\tilde{y} = 1) = \bar{K}(y = a)/K_o = \text{Re } e^{i\alpha(\tau - \tilde{z})}$$
(5.1.7)

and

$$\overline{k}(\tilde{y} = -1) = \overline{K}(y = -a)/K_o = \pm \operatorname{Re} e^{i\alpha(\tau - \tilde{z})} \tag{5.1.8}$$

5.2 Difficulties Concerned with an Exact Solution

Considerable difficulty is encountered in trying to obtain an exact solution to Eqs. (2.2.15) and (2.2.16) subject to the excitation of Eqs. (5.1.7) and (5.1.8), and the boundary conditions at the channel walls. The crux of the difficulty is the non-linear terms of the form $(\overline{a} \cdot \tilde{\nabla})\overline{b}$ in the equations of motion.

Because the excitation is a periodic function of $\alpha(\tau - \tilde{z})$, a natural approach to the problem is to seek solutions for the magnetic field, the velocity, and the pressure which have the same form. Unfortunately, due to the non-linearities in the equations of motion, the responses are not confined to the driving frequency, but in general contain various harmonics of this frequency as well as d-c components. For this reason, solutions to the equations of motion must be sought in Fourier series form, e.g.

$$\overline{h}(\tilde{y},\tilde{z},\tau) = \sum_{\substack{n=-\infty \\ n \neq 0}}^{\infty} [\overline{i}_y \underline{h}_{yn}(\tilde{y}) + \overline{i}_z \underline{h}_{zn}(\tilde{y})] e^{in\alpha(\tau - \tilde{z})}, \tag{5.2.1*}$$

$$\overline{u}(\tilde{y},\tilde{z},\tau) = \overline{i}_z u_{zo}(\tilde{y}) + \sum_{\substack{n=-\infty \\ n \neq 0}}^{\infty} [\overline{i}_y \underline{u}_{yn}(\tilde{y}) + \overline{i}_z \underline{u}_{zn}(\tilde{y})] e^{in\alpha(\tau - \tilde{z})} \tag{5.2.2}$$

---

*A line under a function indicates that it is complex.

and

$$p(\tilde{y}, \tilde{z}, \tau) = -f\tilde{z} + \sum_{n=-\infty}^{\infty} \underline{p}_n(\tilde{y}) e^{in\alpha(\tau - \tilde{z})} \tag{5.2.3}$$

Because the variables $\bar{h}$, $\bar{u}$ and p are analytic functions of $(\tau - \tilde{z})$, the series in Eqs. (5.2.1), (5.2.2) and (5.2.3) are absolutely and uniformly convergent. They may be differentiated term by term any number of times, and the products (Cauchy) of them and their derivatives may be formed, and the series in these derivatives and products are also absolutely and uniformly convergent. Thus the series solutions given in Eqs. (5.2.1), (5.2.2) and (5.2.3) may be formally substituted in Eqs. (2.2.15) and (2.2.16) and the operations may be performed as indicated. When this is accomplished, use is made of the restrictions $\nabla \cdot \bar{h} = 0$ and $\nabla \cdot \bar{u} = 0$ to set $\underline{h}_{zn} = \underline{h}'_{yn}/in\alpha$ and $\underline{u}_{zn} = \underline{u}'_{yn}/in\alpha$, and Eqs. (2.2.15) and (2.2.16) are separated into components with regard to direction and frequency, four infinite sets of completely coupled non-linear differential equations, each with an infinite number of terms are obtained. Obviously such a set of equations is untractable. Even if these equations are drastically simplified by retaining only the fundamental frequency in the magnetic field, and the d-c and double-frequency terms in the velocity and the pressure, the resulting set of coupled non-linear equations is still formidable.

There are three essential difficulties in the method of formulating the solution that is outlined above. These difficulties are the non-linearity of the differential equations, the completely coupled nature of the sets of equations, and the large numbers of equations and variables involved. Any one of these difficulties is formidable enough by itself.

In order to avoid the second and third difficulties, the problem will be attacked with a method of successive approximations. This method proceeds as follows. First, a simple, but physically reasonable, first approximation is made concerning the form of the fluid velocity (that it is independent of time and entirely in the direction of the mean flow). Next, solutions are obtained to the coupled non-linear differential equations which govern the magnetic field and the velocity profile. Finally, the conditions under which this first approximation is an acceptable total solution, and those under which harmonic eddies in the fluid velocity tend to form are investigated.

5.3 The Non-Linear Equations that Govern the Approximate Solution

As a first approximation, the fluid velocity is assumed to be entirely along the channel (z-direction), and independent of time, i.e.

$$\bar{u} = \bar{i}_z u_z(\tilde{y}) . \tag{5.3.1}$$

This first approximation is physically appealing from the following qualitative viewpoint. The a-c component of the electromagnetic body force can be considered as the input to a low-pass filter, characterized by the density and viscosity of the fluid, whose output is the a-c component of the fluid velocity. When the applied frequency and the density are high, the inertia of the fluid very effectively filters out the time variations in the electromagnetic body force and the

fluid velocity is essentially independent of time. However, if the applied frequency and the density are low, the fluid velocity can be expected to attempt to follow the instantaneous variations in the electromagnetic body force. The actual situation is complicated by the fact that, due to the variation in fluid velocity across the channel, different elements of fluid experience electromagnetic body forces at different frequencies. This problem of the generation of a-c components in the fluid velocity is discussed quantitatively in Ch. VIII.

In view of the simplified form of the fluid velocity assumed in Eq. (5.3.1), solutions will be sought in which the magnetic field varies at the fundamental frequency only, viz.

$$\bar{h} = \mathrm{Re}\left\{[\bar{i}_y\,\underline{h}_y(\tilde{y}) + \bar{i}_z\,\underline{h}_z(\tilde{y})]e^{i\alpha(\tau - \tilde{z})}\right\}. \tag{5.3.2}$$

If Eqs. (5.3.1) and (5.3.2) are substituted in Eq. (2.2.15), two scalar equations are obtained. The y-component of (2.2.15) yields

$$\frac{d^2\underline{h}_y}{d\tilde{y}^2} - \alpha^2[1 + i\,\frac{R_m}{\alpha}\,(1 - u_z)]\underline{h}_y = 0, \tag{5.3.3}$$

while the z-component yields

$$\frac{d^2\underline{h}_z}{d\tilde{y}^2} - \alpha^2[1 + i\,\frac{R_m}{\alpha}\,(1 - u_z)]\underline{h}_z = -R_m\underline{h}_y\,\frac{du_z}{d\tilde{y}}. \tag{5.3.4}$$

Substitution of Eq. (5.3.2) in Eq. (2.2.9) shows that the current density $\bar{j}$ is of the form

$$\bar{j} = \bar{i}_x \text{Re}[\underline{j}_x(\tilde{y})e^{i\alpha(\tau - \tilde{z})}] \, ,$$

(5.3.5)

in which $\underline{j}_x$ is given by

$$\underline{j}_x = \frac{1}{R_m} \left(\frac{dh_z}{d\tilde{y}} + i\alpha \, \underline{h}_y \right) \, .$$

(5.3.6)

However, the divergence relation (2.2.11) requires that

$$\frac{dh_y}{d\tilde{y}} - i\alpha \, \underline{h}_z = 0 \, ,$$

(5.3.7)

with the result that the use of Eqs. (5.3.3) and (5.3.7) in Eq. (5.3.6) produces a simplified form for the current density, viz.

$$\underline{j}_x = (1 - u_z)\underline{h}_y \, .$$

(5.3.8)

Equation (5.3.8) shows that the assumption that the magnetic field varies at the fundamental frequency only [Eq. (5.3.2)] is consistent with the assumption that the velocity is independent of time [Eq. (5.3.1)], because the current induced in the fluid, and hence the magnetic field it produces, varies at the fundamental frequency only. If, however, the fluid velocity is a function of time, the induced current and magnetic field contain sums and differences of the velocity and magnetic field frequencies, and a spectrum of harmonics is generated.

Next, consider the electromagnetic force in the magneto-hydrodynamic Navier-Stokes equation (2.2.13). If Eqs. (5.3.2), (5.3.5) and (5.3.8) are used to form an expression for $\bar{j} \times \bar{h}$, the result is

$$\bar{j} \times \bar{h} = \frac{1}{2}(1 - u_z)\text{Re}[i_y \frac{1}{i\alpha} (\underline{h}_y \underline{h}_y'^* - \underline{h}_y \underline{h}_y' e^{i2\alpha(\tau - \tilde{z})})$$

$$+ \bar{i}_z(\underline{h}_y \underline{h}_y^* + \underline{h}_y^2 e^{i2\alpha(\tau - \tilde{z})})] . \qquad (5.3.9)*$$

Furthermore, the curl of Eq. (5.3.9) is given by

$$\nabla \times (\bar{j} \times \bar{h}) = \bar{i}_x\text{Re}[(1 - u_z)\underline{h}_y \underline{h}_y'^*$$

$$- \frac{1}{2} u_z'(\underline{h}_y \underline{h}_y^* + \underline{h}_y^2 e^{i2\alpha(\tau - \tilde{z})})] . \qquad (5.3.10)$$

Because this curl is not equal to zero, $\bar{j} \times \bar{h}$ cannot be entirely represented as the gradient of a scalar magnetic pressure, and is in fact more conveniently dealt with in the form given in Eq. (5.3.9). Also, since the right-hand side of Eq. (5.3.10) contains an a-c term, while under the assumed solutions [Eqs. (5.3.1) and (5.3.2)] the curl of the remaining terms in Eq. (2.2.13) has no a-c terms, the form of the approximate solutions cannot be an exact solution.

---

*A star over a complex function denotes the complex conjugate.

If Eqs, (5.3.1) and (5.3.9) are substituted into Eq. (2.2.13), the result is two scalar equations. The y-component of Eq. (2.2.13) yields

$$0 = - \frac{\partial p}{\partial \tilde{y}} + \frac{1}{2} R_m \beta (1 - u_z) \text{Re}[\frac{1}{i\alpha} (\underline{h}_y \underline{h}_y'^* - \underline{h}_y \underline{h}_y' e^{i2\alpha(\tau - z)})],$$

(5.3.11)

while the z-component yields

$$0 = - \frac{\partial p}{\partial \tilde{z}} + \frac{1}{R} u_z'' + \frac{1}{2} R_m \beta (1 - u_z)(\underline{h}_y \underline{h}_y^* + \text{Re } \underline{h}_y^2 e^{i2\alpha(\tau - z)}) .$$

(5.3.12)

Next, Eqs. (5.3.11) and (5.3.12) are averaged with respect to time.[*] Equation (5.3.11) yields

---

[*] An objection to this averaging operation may be raised on the following grounds. Consider an element of fluid that is traveling at very nearly the traveling magnetic field wave speed. This element of fluid experiences an a-c force with a period that is so long that the fluid is bound to react to the a-c force.

This objection can be answered as follows. As a measure of the tendency of the fluid element to respond to the a-c force, consider the impulse (integral of force with respect to time) that is applied to the fluid element in one direction before the force changes sign. If the fluid element is traveling with a normalized velocity u that is nearly equal to one, the form of the a-c part of the electromagnetic body force f is

$$f \sim (1 - u) \cdot \sin[(1 - u)\omega t] .$$

Since the period of this force is $2\pi/(1 - u)\omega$, the form of the impulse I is

$$I = \int_0^{\pi/(1 - u)\omega} (1 - u) \cdot \sin[(1 - u)\omega t] dt = 2/\omega.$$

Thus the impulse is inversely proportional to the external applied frequency ω and independent of the velocity of the fluid element. Therefore the averaging process is equally valid for all elements of the fluid, and the pertinent question is whether or not the applied frequency ω is high enough so that a-c motions may be neglected.

$$- \frac{\overline{\partial p}}{\partial \tilde{y}} + \frac{1}{4} R_m \beta (1 - u_z)(h_y h_y'^* + h_y^* h_y') = 0 \;,$$

while Eq. (5.3.12) yields

$$- \frac{\overline{\partial p}}{\partial \tilde{z}} + \frac{1}{R} u_z'' + \frac{1}{2} R_m \beta (1 - u_z) \underline{h}_y \, \underline{h}_y^* = 0 \;.$$

(5.3.14)

Consideration of Eqs. (5.3.13) and (5.3.14), in the light of the fact that averaging with respect to time commutes with differentiation with respect to space, shows that (cf. Sec. 3.2)

$$\frac{\overline{\partial p}}{\partial \tilde{z}} = \text{a constant} = p_o \;.$$

(5.3.15)

Finally, therefore, Eq. (5.3.14) can be written in the form

$$\frac{d^2 u_z}{d\tilde{y}^2} + \frac{1}{2} M^2 (1 - u_z) \underline{h}_y \, \underline{h}_y^* - R p_o = 0 \;,$$

(5.3.16)

in which the Hartmann number M, given by

$$M^2 \equiv R \, R_m \beta = (\mu_o K_o a)^2 \sigma / \eta \;,$$

(5.3.17)

has been introduced.

The preceding analysis has reduced the general problem of obtaining an approximate flow solution to the specific problem

---

of obtaining solutions to the three, coupled, second-order, non-linear differential equations given by Eqs. (5.3.3) and (5.3.16). [Equation (5.3.4) is not another independent equation; it can be obtained from Eqs. (5.3.3) and (5.3.7).] These equations can be simplified by introducing the normalized velocity defect ϵ_z, which is defined by

$$\epsilon_z = 1 - u_z .$$

(5.3.18)

This substitution reduces Eqs. (5.3.3) and (5.3.16) to

$$\frac{d^2 h_y}{d\tilde{y}^2} - \alpha^2 (1 + i \frac{R_m}{\alpha} \epsilon_z) h_y = 0 ,$$

(5.3.19)

and

$$\frac{d^2 \epsilon_z}{d\tilde{y}^2} - \frac{1}{2} M^2 h_y h_y^* \epsilon_z + Rp_o = 0 .$$

(5.3.20)

Harris[12] obtained equations similar to Eqs. (5.3.19) and (5.3.20), and showed that under the drastic mathematical simplification that h_y is a constant Eq. (5.3.20) becomes linear and has solutions that resemble the Hartmann profiles for d-c conduction driven flow (see Sec. 3.2). These solutions apply to the situation in which even excitation is employed, and in which the excitation pole spacing is much larger than the channel half width and the magnetic Reynolds number is small ($| \alpha^2 + i\alpha R_m \epsilon_z | \ll 1$).

5.4 Power, Efficiency, and Mode of Operation

The purpose of this section is to develop expressions for the electrical and mechanical power inputs, the ohmic and viscous power losses, and the efficiency and dissipation ratio that are associated with the induction driven flow. The forms of these expressions are instructive in themselves, and they provide the basis for the numerical calculation of the efficiency curves that are presented in Sec. 7.5.

Power Inputs

First, consider the electrical power input. Let P_e be the time-average electrical power input to the fluid per unit length in the x and z-directions. Consideration of the magneto-hydrodynamic Poynting theorem (2.3.2) shows that the time-average electrical power input density is equal to $\overline{E} \cdot \overline{J}$, with the result that

$$P_e = 2 \int_0^a \overline{\overline{E} \cdot \overline{J}} \, dy \ . \tag{5.4.1}$$

In terms of the normalized variables that are introduced in Secs. 2.2 and 5.1, Eq. (5.4.1) can be written in the form

$$P_e = 2\sigma(\mu_o v_o H_o)^2 L_o \int_0^1 \overline{\overline{e} \cdot \overline{j}} \, d\tilde{y} \ . \tag{5.4.2}$$

An expression for the normalized electric field $\overline{e}$ can be obtained by substituting Eqs. (5.3.1), (5.3.2), (5.3.5) and (5.3.8) in Eq. (2.2.12), and is given by

$$\overline{e} = - \overline{u} \times \overline{h} + \overline{j} = \overline{i}_x \ \text{Re} \ \underline{h}_{-y} \ e^{i\alpha(\tau - \tilde{z})} \tag{5.4.3}$$

This expression for $\bar{e}$ can be combined with that of Eqs. (5.3.5) and (5.3.8) for $\bar{j}$ to yield

$$\overline{\bar{e} \cdot \bar{j}} = \frac{1}{2} (1 - u_z)\underline{h}_y \underline{h}_y^* .$$ (5.4.4)

Using Eq. (5.4.4), P_e can be written in the form

$$P_e = \sigma(\mu_o H_o v_o)^2 L_o \int_0^1 (1 - u_z)\underline{h}_y \underline{h}_y^* d\tilde{y} ,$$ (5.4.5)

or upon introducing the specific characteristic quantities of this flow [Eqs. (5.1.3), (5.1.5) and (5.1.6)] as

$$P_e = \sigma a(\mu_o K_o \omega/k)^2 \int_0^1 (1 - u_z)\underline{h}_y \underline{h}_y^* d\tilde{y} .$$ (5.4.6)

Second, consider the mechanical power input. Let P_m be the time-average mechanical power input per unit length in the x and z-directions. Consideration of the fluid energy Equation (2.3.7) shows that the mechanical power input density is given by $-\bar{v} \cdot \nabla P$, with the result that

$$P_m = -2 \int_0^a \overline{\bar{v} \cdot \nabla P} \, dy .$$ (5.4.7)

In terms of the normalized variables, Eq. (5.4.7) becomes

$$P_m = -2\rho v_o^3 \int_0^1 \overline{\bar{u} \cdot \nabla p} \, d\tilde{y}$$ (5.4.8)

However, using Eqs. (5.3.1) and (5.3.15), Eq. (5.4.8) can be written in the form

$$P_m = -2\rho v_o^3 p_o \int_0^1 u_z d\tilde{y} ,$$ (5.4.9)

or alternatively as

$$P_m = -2\rho P_o (\frac{\omega}{k})^3 \int_0^1 u_z d\tilde{y} \ . \qquad (5.4.10)$$

Power Dissipations

First, consider the ohmic power loss. Let P_{ohm} be the time-average ohmic power loss per unit length in the x and z-directions. Again, consideration of the magnetohydrodynamic Poynting theorem [Eq. (2.3.6)] shows that the ohmic power loss density is given by $\overline{J} \cdot \overline{J}/\sigma$, with the result that

$$P_{ohm} = \frac{2}{\sigma} \int_0^a \overline{\overline{J \cdot J}} \ d\tilde{y} \ . \qquad (5.4.11)$$

In terms of the dimensionless variables, Eq. (5.4.11) becomes

$$P_{ohm} = 2\sigma L_o (\mu_o H_o v_o)^2 \int_0^1 \overline{\overline{j \cdot j}} \ d\tilde{y} \ . \qquad (5.4.12)$$

An expression for $\overline{\overline{j \cdot j}}$ can be obtained from consideration of Eqs. (5.3.5) and (5.3.8), viz.

$$\overline{\overline{j \cdot j}} = \frac{1}{2} (1 - u_z)^2 \ \underline{h}_y \ \underline{h}_y^* \ , \qquad (5.4.13)$$

with the result that (5.4.12) can be written in the form

$$P_{ohm} = \sigma L_o (\mu_o H_o v_o)^2 \int_0^1 (1 - u_z)^2 \ \underline{h}_y \ \underline{h}_y^* \ d\tilde{y} \qquad (5.4.14)$$

or alternatively as

$$P_{ohm} = \sigma a (\mu_o K_o \ \omega/k)^2 \int_0^1 (1 - u_z)^2 \ \underline{h}_y \ \underline{h}_y^* \ d\tilde{y} \ . \qquad (5.4.15)$$

Next, consider the viscous power dissipation. Let P_{vis} be the time-average viscous power dissipation per unit length in the x and z-directions. In Sec. 2.3, an expression is obtained for the viscous power-loss density [Eq. (2.3.16)], which in this case reduces to $\eta(dv_z/dy)^2$, with the result that

$$P_{vis} = 2\eta \int_0^a (\frac{dv_z}{dy}) dy \ . \qquad (5.4.16)$$

In terms of the dimensionless variables, Eq. (5.4.16) can be written in the form

$$P_{vis} = 2\eta \ v_o^2/L_o \int_0^1 (u_z')^2 \ d\tilde{y} \ , \qquad (5.4.17)$$

or alternatively as

$$P_{vis} = 2\eta(\omega/k)^2/a \int_0^1 (u_z')^2 \ d\tilde{y} \ . \qquad (5.4.18)$$

Modes of Operation, Efficiency, and Dissipation Ratio

The energy conversion modes in which the flow can operate can be classified in the following manner. First, if the electrical power input is positive and the mechanical power input is negative, the flow is operating as a pump or motor. Second, if the electrical power input is negative and the mechanical power input is positive, the flow is operating as a generator. Third, if both the electrical and the mechanical power inputs are positive, the flow is operating as a flow

damper or brake. Clearly, if both the electrical and the mechanical power inputs are negative, an error has occurred.

If the flow is operating as a generator $(P_e < 0, P_m > 0)$, the efficiency ε_g is given by $-P_e/P_m$, which can be obtained from Eqs. (5.4.5) and (5.4.9) in the form

$$\varepsilon_g = \frac{\sigma(\mu_o H_o)^2 L_o}{2\rho \, v_o P_o} \frac{\int_0^1 (1 - u_z)\underline{h}_y \, \underline{h}_y^* \, d\tilde{y}}{\int_0^1 u_z d\tilde{y}} \, , \qquad (5.4.19)$$

which may be written in terms of dimensionless groups as

$$\varepsilon_g = \frac{M^2}{2Rp_o} \frac{\int_0^1 (1 - u_z)\underline{h}_y \, h_y^* \, d\tilde{y}}{\int_0^1 u_z \, d\tilde{y}} \, . \qquad (5.4.20)$$

Similarly, if the flow is operating as a pump $(P_e > 0, P_m < 0)$, the efficiency ε_p is given by $-P_m/P_e$, or

$$\varepsilon_p = \frac{2Rp_o}{M^2} \frac{\int_0^1 u_z d\tilde{y}}{\int_0^1 (1 - u_z)\underline{h}_y \, \underline{h}_y^* \, d\tilde{y}} \qquad (5.4.21)$$

If, however, the flow is operating as a flow damper, it is not characterized by an efficiency, but by a dissipation ratio. There are two possible dissipation ratios. The first is simply an extension of the concept of efficiency to the flow damper mode of operation, and measures the ratio of electrical to mechanical power input when both powers are entirely dissipated. If ε_d is this ratio, it is equal to P_e/P_m and is given by

$$\varepsilon_d = - \frac{M^2}{2Rp_o} \frac{\int_0^1 (1 - u_z) \underline{h}_y \, \underline{h}_y^* \, d\tilde{y}}{\int_0^1 u_z d\tilde{y}} \qquad (5.4.22)$$

The second dissipation ratio is more general, because it is applicable to all modes of operation; and more deserving of the name, because it measures the ratio of ohmic to viscous dissipation in the fluid. If D is this ratio, it is equal to P_{ohm}/P_{vis} and through use of Eqs. (5.4.15) and (5.4.18) can be written as

$$D = \frac{M^2}{2} \frac{\int_0^1 (1 - u_z)^2 \, \underline{h}_y \, \underline{h}_y^* \, d\tilde{y}}{\int_0^1 (u_z')^2 \, d\tilde{y}} . \qquad (5.4.23)$$

The simple form of many of the expressions obtained in this section seems to indicate that a general discussion of them would be possible at this time. In fact, this is not the case, because each of the integrals in these expressions is a rather complicated function of the four parameters α, M, R_m and Rp_o. For this reason further discussion is deferred until Sec. 7.5, in which curves of ε_g, ε_p and ε_d as functions of Rp_o for various values of α, M and R_m are shown.

Chapter VI

SOLUTIONS TO THE NON-LINEAR DIFFERENTIAL EQUATIONS
THAT GOVERN THE APPROXIMATE SOLUTION

6.1 Boundary and Symmetry Conditions

The problem at hand is to determine solutions to Eqs. (5.3.19) and (5.3.20), subject to the excitations given in Eqs. (5.1.7) and (5.1.8), and the boundary and symmetry conditions discussed below. First, consider the restrictions on the fluid velocity. Since the channel, the pressure drive (Rp_o), and the electromagnetic drive $(\sim \underline{h}_y \underline{h}_y^*)$ all have even symmetry with respect to $\tilde{y}$, the velocity will also have even symmetry. Further, since the fluid has finite viscosity, the tangential component of the velocity must also be zero at the channel walls. Next, consider the boundary conditions on the magnetic field. Inspection of the excitation [Eqs. (5.1.7) and (5.1.8), and Fig. 5-1], shows that the y-component of the magnetic field has the same symmetry as the excitation, while the z-component has the opposite symmetry. Further, since the magnetic field is assumed to be equal to zero in the highly permeable pole pieces, the magnitude of the tangential (z) component of the field at the channel walls must be equal to the magnitude of the surface current. (The signs in this equality are, of course, also determined.)

All of the boundary and symmetry conditions discussed above and some simple consequences thereof are tabulated below for convenience.

1) Boundary and Symmetry Conditions on Velocity

$$u(-\tilde{y}) = u(\tilde{y}) \Rightarrow \varepsilon(-\tilde{y}) = \varepsilon(\tilde{y})$$

$$u(\pm 1) = 0 \quad \Rightarrow \varepsilon(\pm 1) = 1$$

(6.1.1)

2) Boundary and Symmetry Conditions on Magnetic Field

a) Even Excitation

$$\underline{h}_y(-\tilde{y}) = \underline{h}_y(\tilde{y})$$

$$\underline{h}_z(-\tilde{y}) = -\underline{h}_z(\tilde{y})$$

$$\underline{h}_z(1) = -1 \Rightarrow \underline{h}_y'(1) = -i\alpha$$

(6.1.2)

$$\underline{h}_z(-1) = + 1 \Rightarrow \underline{h}_y'(-1) = + i\alpha$$

b) Odd Excitation

$$\underline{h}_y(-\tilde{y}) = -\underline{h}_y(\tilde{y})$$

$$\underline{h}_z(-\tilde{y}) = \underline{h}_z(\tilde{y})$$

$$\underline{h}_z(1) = -1 \Rightarrow \underline{h}_y'(1) = -i\alpha$$

(6.1.3)

$$\underline{h}_z(-1) = -1 \Rightarrow \underline{h}_y'(-1) = -i\alpha$$

6.2 A Perturbation Expansion in Magnetic Reynolds Number

Since the magnetic Reynolds number tends to be small in most liquid metal flows,[*] there is utility in expanding a set of solutions in this parameter. Furthermore, inspection of Eq. (5.3.19)

---

[*] In mercury, with $v_o = 1$ m./sec. (a high velocity) and $L_o = 0.1$ m. (a large channel), $R_m \sim 0.13$.

indicates that it becomes uncoupled from Eq. (5.3.20) when the magnetic Reynolds number is equal to zero. The actual expansions are made in the parameter R_m/α, which can be interpreted as the magnetic Reynolds number based on the excitation pole spacing, and are given by

$$\varepsilon_z(\tilde{y}) = \sum_{n=0}^{\infty} \varepsilon_{zn}(\tilde{y}) \left(\frac{R_m}{\alpha}\right)^n , \qquad (6.2.1)$$

and

$$\underline{h}_y(\tilde{y}) = \sum_{n=0}^{\infty} \underline{h}_{yn}(\tilde{y}) \left(\frac{R_m}{\alpha}\right)^n . \qquad (6.2.2)$$

From a practical standpoint, the series in Eqs. (6.2.1) and (6.2.2) need not even converge; all that is necessary is that the finite number of terms that are retained approximate the correct solution to the desired degree of accuracy over the required range of the parameter R_m/α.*

If the expansions given in Eqs. (6.2.1) and (6.2.2) are substituted in Eqs. (5.3.19) and (5.3.20) and terms containing like powers of R_m/α are equated, the results for the magnetic field equation are

$$\underline{h}_{y0}'' - \alpha^2 \underline{h}_{y0} = 0, \quad n = 0 ; \qquad (6.2.3)$$

---

*Such series are often called asymptotic. For further information concerning asymptotic expansions, see Erdélyi.[38]

and

$$\underline{h}_{yn}'' - \alpha^2 \underline{h}_{yn} = i\alpha^2 \sum_{k=0}^{n-1} \varepsilon_{zk} \underline{h}_{y,n-1-k} \quad , \quad n \geq 1 \; ; \tag{6.2.4}$$

while the velocity defect equation yields

$$\varepsilon_{z0}'' - \frac{1}{2} M^2 \underline{h}_{y0} \underline{h}_{y0}^* \varepsilon_{z0} = -Rp_o, \quad n = 0 \; ; \tag{6.2.5}$$

and

$$\varepsilon_{zn}'' - \frac{1}{2} M^2 \underline{h}_{y0} \underline{h}_{y0}^* \varepsilon_{z0} = \frac{1}{2} M^2 \sum_{k=0}^{n-1} \varepsilon_{zk} \sum_{\ell=0}^{n-k} \underline{h}_{y\ell} \underline{h}_{y,n-k-\ell} \quad , \quad n \geq 1. \tag{6.2.6}$$

Inspection of the system of equations (6.2.3) through (6.2.6) reveals several important features. First, the system is uncoupled from below, because there is a progressive way of solving the system of equations in which the coefficients in a particular equation depend only on solutions that have previously been obtained. This situation is in striking contrast with the completely coupled systems of equations discussed in Sec. 5.2, in which the coefficients in each equation depend on the solution to every other equation. Second, since the coefficients in a particular equation are known functions of $\tilde{y}$ by the time that the equation is considered, the equations are linear and superposition may be applied. Thus the very powerful perturbation expansion technique converts the three original coupled, nonlinear, differential equations into a system of linear equations that is uncoupled from below.

The properties of this system of linear differential equations can be more clearly recognized if the first few equations resulting from Eqs. (6.2.4) and (6.2.6) are written out. The

first two equations produced by Eq. (6.2.4) are

$$\underline{h}''_{y1} - \alpha^2 \underline{h}_{y1} = i\alpha^2 \, \varepsilon_{z0} \, \underline{h}_{y0} \, , \quad (n = 1); \qquad (6.2.7)$$

and

$$\underline{h}''_{y2} - \alpha^2 \underline{h}_{y2} = i\alpha^2 (\varepsilon_{z0} \, \underline{h}_{y1} + \varepsilon_{z1} \, \underline{h}_{y0}) \, , \quad (n = 2). \qquad (6.2.8)$$

Similarly, the first two equations resulting from Eq. (6.2.6) are

$$\varepsilon''_{z1} - \frac{1}{2} M^2 \, \underline{h}_{y0} \, \underline{h}^*_{y0} \, \varepsilon_{z1} = \frac{1}{2} M^2 (\underline{h}_{y0} \, \underline{h}^*_{y1} + \underline{h}_{y1} \, \underline{h}^*_{y0}) \varepsilon_{z0} \, ,$$

$$(n = 1) \; ; \quad (6.2.9)$$

and

$$\varepsilon''_{z2} - \frac{1}{2} M^2 \, \underline{h}_{y0} \, \underline{h}^*_{y0} \, \varepsilon_{z2} = \frac{1}{2} M^2 [\, (\underline{h}_{y0} \, \underline{h}^*_{y2} + \underline{h}_{y1} \, \underline{h}^*_{y1}$$

$$+ \, \underline{h}_{y2} \, \underline{h}^*_{y0}) \varepsilon_{z0}$$

$$+ \, (\underline{h}_{y0} \, \underline{h}^*_{y1} + \underline{h}_{y1} \, \underline{h}^*_{y0}) \varepsilon_{z1}] \, , \quad (n = 2).$$

$$(6.2.10)$$

Inspection of Eqs. (6.2.3) and (6.2.5), and Eqs. (6.2.7) through (6.2.10) indicates the sequence in which this set of equations should be solved. Equation (6.2.3) has constant coefficients, and can, therefore, be solved immediately for the zero-order magnetic field. Once the zero-order magnetic field is known, Eq. (6.2.5) becomes linear, and can be solved for the zero-order velocity defect. However, once the zero-order magnetic field and the zero-order velocity defect are known, Eq. (6.2.7) becomes linear, and can be solved for the first-order magnetic

field. This process of solving first a magnetic field equation, then a velocity defect equation, and then the next-higher-order magnetic field equation can be continued, at least in theory, until any desired degree of accuracy is obtained in the expansions in the magnetic Reynolds number [Eqs. (6.2.1) and (6.2.2)]. In practice, however, the driving functions in the differential equations rapidly become so complicated that numerical methods must be employed.

6.3 An Analytical-Numerical Method of Solving the Resulting Set of Linear Differential Equations

This section describes a combined analytical and numerical method of obtaining solutions to and properties of the set of linear differential equations given by Eqs. (6.2.3) through (6.2.6). The philosophy of this procedure is to do analytically that which can be done conveniently and reasonably compactly, and to do numerically that which cannot. However, the two methods are not separated; rather they are intermixed, each where it seems most applicable. For example, general properties of the system of equations are deduced analytically, while homogeneous and particular solutions to the higher-order equations are integrated numerically.

First, a note concerning the boundary conditions. Since the series (6.2.1) and (6.2.2) must satisfy the boundary conditions (6.1.1), (6.1.2) and (6.1.3) for a continuous range of values of the parameter R_m/α, the zero-order terms in these series must satisfy the stated inhomogeneous boundary conditions, while all higher-order terms must satisfy the corresponding homogeneous boundary conditions. [For example, $\varepsilon_{z0}(\pm 1) = 1$, while $\varepsilon_{zn}(\pm 1) = 0, n \neq 0.$]

The system of equations starts off simply enough with Eq. (6.2.3), the solutions of which have the form $\sinh \alpha \tilde{y}$ and $\cosh \alpha \tilde{y}$. When subject to the symmetry and inhomogeneous boundary conditions of Eqs. (6.1.2) and (6.1.3) these solutions become

$$\underline{h}_{y0} = -i \cosh \alpha\tilde{y}/\sinh \alpha \qquad (6.3.1)$$

for even excitation, and

$$\underline{h}_{y0} = -i \sinh \alpha\tilde{y}/\cosh \alpha \qquad (6.3.2)$$

for odd excitation. Note that physically these are the exact magnetic field solutions if the fluid is non-conducting so that the magnetic field is produced solely by the excitation surface currents and satisfies the homogeneous equation $\nabla^2 \bar{h} = 0$.

The next step is to substitute Eqs. (6.3.1) and (6.3.2) in Eq. (6.2.5), which governs the zero-order velocity defect. The results of this substitution are

$$\varepsilon_{z0}'' - \frac{1}{2} M^2 \frac{\cosh^2 \alpha\tilde{y}}{\sinh^2 \alpha} \varepsilon_{z0} = -Rp_0 \qquad (6.3.3)$$

for even excitation, and

$$\varepsilon_{z0}'' - \frac{1}{2} M^2 \frac{\sinh^2 \alpha\tilde{y}}{\cosh^2 \alpha} \varepsilon_{z0} = - Rp_0 \qquad (6.3.4)$$

for odd excitation. Equations (6.3.3) and (6.3.4) have the form

of an inhomogeneous, modified Mathieu equation.[*] Unfortunately, relatively little theoretical work has been done on this form of Mathieu equation; most of the effort has centered on characteristic values and solutions of the homogeneous Mathieu equation $y'' + (a + b \cos 2x)y = 0$. Appendix A presents a discussion of the relation of Eqs. (6.3.3) and (6.3.4) to the Mathieu equation, and presents some approximate solutions to these equations. The usefulness of such approximate solutions in this particular problem is limited, however, by the difficulty of constructing an approximate solution that is valid over a wide range of the parameters M, α and Rp_o. Furthermore, because the higher-order equations have driving functions that are more and more complicated functions of the previous solutions, the process of carrying an approximate solution through successive equations rapidly becomes untenable. For these reasons, numerical integration is used to obtain the required homogeneous and particular solutions for each differential equation. The numerical methods used in these calculations are described in Appendix B.

The solution of the zero-order velocity-defect equation [Eq. (6.2.5)] is obtained in the following manner. First, a homogeneous solution ε_{z0h} to the equation

$$\varepsilon_{z0h}'' - \frac{1}{2} M^2 \underline{h}_{y0} \underline{h}_{y0}^* \varepsilon_{z0h} = 0 \qquad (6.3.5)**$$

---

[*] For information concerning the general theory of Mathieu equations, see McLachlan[39] and Campbell.[40]

** The subscripts h and p are used throughout to denote homogeneous and particular solutions of a differential equation.

with the properties $\varepsilon_{z0h}(-\tilde{y}) = \varepsilon_{z0h}(\tilde{y})$ and $\varepsilon_{z0h}(0) = 1^*$ is integrated numerically. Next, a particular solution ε_{z0p} to the equation

$$\varepsilon_{z0p}'' - \frac{1}{2} M^2 \underline{h}_{y0} \underline{h}_{y0}^* \varepsilon_{z0p} = -1 \tag{6.3.6}$$

with the properties $\varepsilon_{z0p}(-\tilde{y}) = \varepsilon_{z0p}(\tilde{y})$ and $\varepsilon_{z0p}(0) = 0$ is computed. Finally, these solutions are combined to form the total solution

$$\varepsilon_{z0} = \frac{\varepsilon_{z0h}}{\varepsilon_{z0h}(1)} + Rp_0 [\varepsilon_{z0p} - \frac{\varepsilon_{z0p}(1)}{\varepsilon_{z0h}(1)} \varepsilon_{z0h}] \tag{6.3.7}$$

which satisfies Eq. (6.2.5) and the boundary conditions $\varepsilon_{z0}(-\tilde{y}) = \varepsilon_{z0}(\tilde{y})$ and $\varepsilon_{z0}(\pm 1) = 1$ [Eq. (6.1.1)]. The combinations of homogeneous and particular solutions appearing in Eq. (6.3.7) are formed during the numerical calculations; and the solution is presented in the reduced form

$$\varepsilon_{z0} = \varepsilon_{z00} + Rp_0 \varepsilon_{z01} . \tag{6.3.8}$$

---

*The initial conditions, which are not related to symmetry, for the various homogeneous and particular solutions are arbitrary, except that in the homogeneous solutions care must be taken to avoid the situation described on p.82 , in which starting a solution with both zero value and zero slope makes it identically zero.

Thus the principle of superposition for linear differential equations allows the parameter Rp_o to be carried through the solutions analytically. This greatly reduces the number of different numerical solutions that are required, since only two parameters (M and α) must be varied numerically and not three. Note that if the original non-linear equations [Eqs. (5.3.19) and (5.3.20)] are integrated numerically, four parameters (M, R_m, α and Rp_o) must be varied numerically.

Now that the zero-order velocity defect has been obtained in the form of Eq. (6.3.8), the first-order magnetic field equation [Eq. (6.2.7)] can be written as

$$\underline{h}_{y1}'' - \alpha^2 \underline{h}_{y1} = i\alpha^2 \underline{h}_{y0}(\varepsilon_{z00} + Rp_o\,\varepsilon_{z01}).$$
(6.3.9)

Furthermore, the first-order magnetic field $\underline{h}_{y1}$ must have the same symmetry as the excitation and must satisfy the homogeneous boundary condition $\underline{h}_{y1}'(1) = 0$. If Eq. (6.3.9) is separated into its real and imaginary parts, the results are

$$h_{y1r}'' - \alpha^2 h_{y1r} = -\alpha^2 h_{y0i0}(\varepsilon_{z00} + Rp_o\varepsilon_{z01}),$$
(6.3.10)*

and

$$h_{y1i}'' - \alpha^2 h_{y1i} = 0,$$
(6.3.11)

---

*A zero has been arbitrarily added to the subscript of h_{y0i} (viz. h_{y0i0}) to make it conform to the notation introduced later in which this added number indicates the power of Rp_o which multiplies a solution.

in which the subscripts r and i denote the real and imaginary parts of the various magnetic field quantities, and where use has been made of the fact that $h_{y0r} = 0$ for both even and odd excitation [see Eqs. (6.3.1) and (6.3.2)].

Equation (6.3.11) can be readily disposed of; its solution is either $a \cdot \cosh \alpha \tilde{y}$ for even excitation or $a \cdot \sinh \alpha \tilde{y}$ for odd excitation. However, in either of these solutions the boundary condition $h'_{y1i}(1) = 0$ implies that $a = 0$. Thus

$$h_{y1i} = 0 . \qquad (6.3.12)$$

The solution to Eq. (6.3.10) is obtained in the following way. First, the homogeneous solutions are just those mentioned above ($\cosh \alpha \tilde{y}$ and $\sinh \alpha \tilde{y}$), and furthermore the correct symmetry can be automatically obtained by letting

$$h_{y1rh} = h_{y0i0} . \quad [\text{cf. Eqs. (6.3.1) and (6.3.2)}] \qquad (6.3.13)$$

Next, an even $\langle\text{odd}\rangle^*$ particular solution h_{y1rp0} to the equation

$$h''_{y1rp0} - \alpha^2 h_{y1rp0} = -\alpha^2 h_{y0i0} \varepsilon_{z00} , \qquad (6.3.14)$$

which satisfies the condition $h_{y1rp0}(0) = 0 \quad \langle h'_{y1rp0}(0) = 0 \rangle$, is integrated numerically. Also, to provide for the second driving term in Eq. (6.3.10), an even $\langle\text{odd}\rangle$ particular solution h_{y1rp1} to the equation

$$h''_{y1rp1} - \alpha^2 h_{y1rp1} = -\alpha^2 h_{y0i0} \varepsilon_{z01} , \qquad (6.3.15)$$

---

*The discussion is presented in terms of even excitation, and the changes that are required for odd excitation are given in angular brackets.

which satisfies the condition $h_{y1rp1}(0) = 0$ $\langle h'_{y1rp1}(0) = 0 \rangle$, is computed. Finally, the three solutions are combined to form the total solution

$$h_{y1r} = [h_{y1rp0} + \frac{1}{\alpha} h'_{y1rp0}(1) \cdot h_{y0i0}]$$

$$+ Rp_o[h_{y1rp1} + \frac{1}{\alpha} h'_{y1rp1}(1) \cdot h_{y0i0}], \quad (6.3.16)$$

which satisfies Eq. (6.3.10), the symmetry requirement $h_{y1r}(-\tilde{y}) = h_{y1r}(\tilde{y})$ $\langle h_{y1r}(-\tilde{y}) = -h_{y1r}(\tilde{y}) \rangle$, and the homogeneous boundary condition $h'_{y1r}(1) = 0$. Again the combinations of solutions required in Eq. (6.3.16) are formed during the numerical computation, and the total solution is presented in the form

$$h_{y1r} = h_{y1r0} = Rp_o h_{y1r1} . \quad (6.3.17)$$

Once the zero-order velocity defect and the zero and first-order magnetic fields are known, Eq. (6.2.9) can be solved for the first-order velocity defect. The driving term in this equation is

$$\frac{1}{2} M^2 (\underline{h}_{y0} \underline{h}^*_{y1} + \underline{h}_{y1} \underline{h}^*_{y0}) \varepsilon_{z0} ; \quad (6.3.18)$$

however, the zero-order magnetic field is now known to be purely imaginary [Eqs. (6.3.1) and (6.3.2)] with the result that $\underline{h}^*_{y0} = -\underline{h}_{y0}$, and the first-order magnetic field is now known to be purely real [Eq. (6.3.12)] with the result that $\underline{h}^*_{y1} = \underline{h}_{y1}$. Thus $(\underline{h}_{y0} \underline{h}^*_{y1} + \underline{h}_{y1} \underline{h}^*_{y0}) = 0$, and the driving function vanishes. Therefore, the first-order velocity defect satisfies the homogeneous equation

$$\varepsilon_{z1}'' = \frac{1}{2} M^2 \underline{h}_{y0} \underline{h}_{y0}^* \varepsilon_{z1} \cdot \tag{6.3.19}$$

Since $\underline{h}_{y0} \underline{h}_{y0}^* = \cosh^2 a\tilde{y}/\sinh^2 a$ $\langle \sinh^2 a\tilde{y}/\cosh^2 a \rangle$ is non-negative, ε_{z1}'' has the same sign as ε_{z1} for all values of $\tilde{y}$. However, ε_{z1} must also satisfy the symmetry condition $\varepsilon_{z1}(-\tilde{y}) = \varepsilon_{z1}(\tilde{y})$, which implies that $\varepsilon_{z1}'(0) = 0$, and the homogeneous boundary condition $\varepsilon_{z1}(1) = 0$.

Three situations are possible depending on the value of $\varepsilon_{z1}(0)$ as shown in Fig. 6-1.
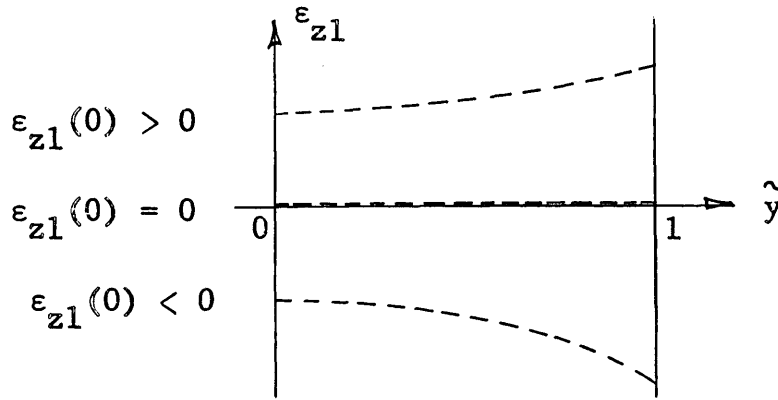
Fig. 6-1 Possible Solutions for the
First-Order Velocity Defect

First, if $\varepsilon_{z1}(0) > 0$, then $\varepsilon_{z1}''(0) > 0$, and ε_{z1} is a mono-tone, non-decreasing function of $\tilde{y}$ for $\tilde{y} \geq 0$. Second, if $\varepsilon_{z1}(0) < 0$, then $\varepsilon_{z1}''(0) < 0$, and ε_{z1} is a monotone, non-increasing function of $\tilde{y}$ for $\tilde{y} \geq 0$. Third, if $\varepsilon_{z1}(0) = 0$, then $\varepsilon_{z1} \equiv 0$. Clearly the third situation is the only one which satisfies the boundary condition $\varepsilon_{z1}(1) = 0$. Therefore,

$$\varepsilon_{z1} = 0 \cdot \tag{6.3.20}$$

Now that the zero-order velocity defect and the first-order magnetic field are determined in the form of Eqs. (6.3.8) and (6.3.17), and the first-order velocity defect has been found to be zero, the second-order magnetic field equation [Eq. (6.2.8)] can be written in the form

$$\underline{h}_{y2}'' - \alpha^2 \underline{h}_{y2} = i\alpha^2 (\varepsilon_{z00} + Rp_o \varepsilon_{z01})(h_{y1r0} + Rp_o h_{y1r1}). \quad (6.3.21)$$

If Eq. (6.3.21) is separated into its real and imaginary parts, and the driving function is multiplied out, the results are

$$h_{y2r}'' - \alpha^2 h_{y2r} = 0, \quad (6.3.22)$$

and

$$h_{y2i}'' - \alpha^2 h_{y2i} = \alpha^2 [\varepsilon_{z00} h_{y1r0} + Rp_o(\varepsilon_{z00} h_{y1r1}$$

$$+ \varepsilon_{z01} h_{y1r0}) + (Rp_o)^2 \varepsilon_{z01} h_{y1r1}]. \quad (6.3.23)$$

As in the case of h_{y1i}, the only solution to Eq. (6.3.22) that satisfies the symmetry requirement $h_{y2r}(-\tilde{y}) = h_{y2r}(\tilde{y})$ $\langle h_{y2r}(-\tilde{y}) = -h_{y2r}(\tilde{y})\rangle$, and the homogeneous boundary condition $h_{y2r}'(1) = 0$ is

$$h_{y2r} = 0, \quad (6.3.24)$$

with the result that the second-order magnetic field is purely imaginary.

Equation (6.3.23) is solved for h_{y2i} in the same way that Eq. (6.3.13) was solved for h_{y1r}, except that three particular solutions, each corresponding to a single term in the

drive, are required for Eq. (6.3.23). The homogeneous solution to Eq. (6.3.23) is again identified with the zero-order magnetic field, viz.

$$h_{y2ih} = h_{y0i0} \; \cdot \tag{6.3.25}$$

Among the particular solutions, h_{y2ip0} is the solution of

$$h''_{y2ip0} - \alpha^2 h_{y2ip0} = \alpha^2 \varepsilon_{z00} h_{y1r0} \tag{6.3.26}$$

that satisfies $h_{y2ip0}(-\tilde{y}) = h_{y2ip0}(\tilde{y})$ $\langle h_{y2ip0}(-\tilde{y}) = -h_{y2ip0}(\tilde{y})\rangle$ and $h_{y2ip0}(0) = 0$ $\langle h'_{y2ip0}(0) = 0\rangle$; h_{y2ip1} is the solution of

$$h''_{y2ip1} - \alpha^2 h_{y2ip1} = \alpha^2 (\varepsilon_{z00} h_{y1r1} + \varepsilon_{z01} h_{y1r0}) \tag{6.3.27}$$

that satisfies $h_{y2ip1}(-\tilde{y}) = h_{y2ip1}(\tilde{y})$ $\langle h_{y2ip1}(-\tilde{y}) = -h_{y2ip1}(\tilde{y})\rangle$ and $h_{y2ip1}(0) = 0$ $\langle h'_{y2ip1}(0) = 0\rangle$; and h_{y2ip2} is the solution of

$$h''_{y2ip2} - \alpha^2 h_{y2ip2} = \alpha^2 \varepsilon_{z01} h_{y1r1} \tag{6.3.28}$$

that satisfies $h_{y2ip2}(-\tilde{y}) = h_{y2ip2}(\tilde{y})$ $\langle h_{y2ip2}(-\tilde{y}) = -h_{y2ip2}(\tilde{y})\rangle$ and $h_{y2ip2}(0) = 0$ $\langle h'_{y2ip2}(0) = 0\rangle$.

Again these solutions can be combined to form the total solution

$$h_{y2i} = [h_{y2ip0} + \frac{1}{\alpha} h'_{y2ip0}{}^{(1)} \cdot h_{y0i0}]$$

$$+ Rp_o[h_{y2ip1} + \frac{1}{\alpha} h'_{y2ip1}{}^{(1)} \cdot h_{y0i0}]$$

$$+ (Rp_o)^2[h_{y2ip2} + \frac{1}{\alpha} h'_{y2ip2}{}^{(1)} \cdot h_{y0i0}] , \qquad (6.3.29)$$

which satisfies Eq. (6.3.23), the symmetry requirement $h_{y2i}(-\tilde{y}) = h_{y2i}(\tilde{y})$ $\langle h_{y2i}(-\tilde{y}) = -h_{y2i}(\tilde{y}) \rangle$, and the homogeneous boundary condition $h'_{y2i}(1) = 0$. The solution is presented in the simplified form

$$h_{y2i} = h_{y2i0} + Rp_o h_{y2i1} + (Rp_o)^2 h_{y2i2} . \qquad (6.3.30)$$

Finally, consider the second-order velocity defect equation [Eq. (6.2.10)], which now can be written in the form

$$\varepsilon''_{z2} - \frac{1}{2}M^2 h_{y0} h^*_{y0} \varepsilon_{z2} = \frac{1}{2} M^2 (2h_{y0i} h_{y2i} + h^2_{y1r}) \varepsilon_{z0} = D . \qquad (6.3.31)$$

A homogeneous solution to Eq. (6.3.31) that satisfies the conditions $\varepsilon_{z2h}(-\tilde{y}) = \varepsilon_{z2h}(\tilde{y})$ and $\varepsilon_{z0h}(0) = 1$ has already been determined, viz.

$$\varepsilon_{z2h} = \varepsilon_{z0h} . \quad [\text{cf. Eq. (6.3.5)}] \qquad (6.3.32)$$

To determine the drives for the various particular solutions, Eq. (6.3.8), (6.3.17) and (6.3.30) must be substituted int the

expression (6.3.31) for the total drive D. The result is

$$D = \frac{1}{2} M^2 \left\{ \varepsilon_{z00}(2h_{y0i0}\, h_{y2i0} + h_{y1r0}^2) \right.$$

$$+ Rp_o[2\varepsilon_{z00}(h_{y0i0}\, h_{y2i1} + h_{y1r0}\, h_{y1r1})$$

$$+ \varepsilon_{z01}(2h_{y0i0}\, h_{y2i0} + h_{y1r0}^2)]$$

$$+ (Rp_o)^2[\varepsilon_{z00}(2h_{y0i0}\, h_{y2i2} + h_{y1r1}^2)$$

$$+ 2\varepsilon_{z01}(h_{y0i0}\, h_{y2i1} + h_{y1r0}\, h_{y1r1})]$$

$$\left. + (Rp_o)^3 \varepsilon_{z01}(2h_{y0i0}\, h_{y2i2} + h_{y1r1}^2) \right\} \, . \qquad (6.3.33)$$

Of the four particular solutions that must be obtained in this case, ε_{z2p0} is the solution of

$$\varepsilon_{z2p0}'' - \frac{1}{2} M^2 h_{y0i0}^2 \varepsilon_{z2p0} = \frac{1}{2} M^2 \varepsilon_{z00}(2h_{y0i0}\, h_{y2i0} + h_{y1r0}^2)$$

$$(6.3.34)$$

that satisfies the conditions $\varepsilon_{z2p0}(-\tilde{y}) = \varepsilon_{z2p0}(\tilde{y})$ and $\varepsilon_{z2p0}(0) = 0$; ε_{z2p1} is the solution of

$$\varepsilon_{z2p1}'' - \frac{1}{2} M^2 h_{y0i0}^2 \varepsilon_{z2p1} = \frac{1}{2} M^2[2\varepsilon_{z00}(h_{y0i0}\, h_{y2i1} + h_{y1r0}\, h_{y1r1})$$

$$+ \varepsilon_{z01}(2h_{y0i0}\, h_{y2i0} + h_{y1r0}^2)] \qquad (6.3.35)$$

that satisfies the conditions $\varepsilon_{z2p1}(-\tilde{y}) = \varepsilon_{z2p1}(\tilde{y})$ and

$\varepsilon_{z2p1}(0) = 0$; ε_{z2p2} is the solution of

$$\varepsilon''_{z2p2} - \frac{1}{2} M^2 h^2_{y0i0} \varepsilon_{z2p2} = \frac{1}{2} M^2 [\varepsilon_{z00}(2h_{y0i0} h_{y2i2} + h^2_{y1r1})$$

$$+ 2\varepsilon_{z01}(h_{y0i0} h_{y2i1} + h_{y1r0} h_{y1r1})]$$

$$(6.3.36)$$

that satisfies the conditions $\varepsilon_{z2p2}(-\tilde{y}) = \varepsilon_{z2p2}(\tilde{y})$ and

$\varepsilon_{z2p2}(0) = 0$; and ε_{z2p3} is the solution of

$$\varepsilon''_{z2p3} - \frac{1}{2} M^2 h^2_{y0i0} \varepsilon_{z2p3} = \frac{1}{2} M^2 \varepsilon_{z01}(2h_{y0i0} h_{y2i2} + h^2_{y1r1}) \quad (6.3.37)$$

that satisfies $\varepsilon_{z2p3}(-\tilde{y}) = \varepsilon_{z2p3}(\tilde{y})$ and $\varepsilon_{z2p3}(0) = 0$. The homogeneous and particular solutions are combined to form the total solution

$$\varepsilon_{z2} = [\varepsilon_{z2p0} - \frac{\varepsilon_{z2p0}(1)}{\varepsilon_{z0h}(1)} \varepsilon_{zoh}]$$

$$+ Rp_o[\varepsilon_{z2p1} - \frac{\varepsilon_{z2p1}(1)}{\varepsilon_{z0h}(1)} \varepsilon_{zoh}]$$

$$+(Rp_o)^2[\varepsilon_{z2p2} - \frac{\varepsilon_{z2p2}(1)}{\varepsilon_{z0h}(1)} \varepsilon_{zoh}]$$

$$+(Rp_o)^3[\varepsilon_{z2p3} - \frac{\varepsilon_{z2p3}(1)}{\varepsilon_{z0h}(1)} \varepsilon_{zoh}], \qquad (6.3.38)$$

which satisfies Eq. (6.2.10), the symmetry requirement $\varepsilon_{z2}(-\tilde{y}) = \varepsilon_{z2}(\tilde{y})$ and the homogeneous boundary condition $\varepsilon_{z2}(1) = 0$. Again, this solution is presented in the more compact form

$$\varepsilon_{z2} = \varepsilon_{z20} + Rp_o \varepsilon_{z21} + (Rp_o)^2 \varepsilon_{z22} + (Rp_o)^3 \varepsilon_{z23} . \qquad (6.3.39)$$

The process of solving higher and higher order equations in the system given in Eqs. (6.2.3) through (6.2.6) can be continued indefinitely, although the algebraic and computational difficulties increase with each step. However, some general properties of the expansions in R_m/α [Eqs. (6.2.1) and (6.2.2)] are suggested by the solutions that have been obtained. First, velocity defects corresponding to even powers of R_m/α are nonzero, while those corresponding to odd powers of R_m/α are identically zero. Second, the expansion of ε_{zn} involves powers of Rp_o up to and including $n + 1$. Third, the magnetic field terms h_{yn} are purely imaginary if n is even and purely real if n is odd. Fourth, the expansion of h_{yn} involves powers of Rp_o up to and including n. For convenience, these properties are displayed for the first few values of n in Table 6-1 on the following page.

Of particular importance among the properties listed in Table 6-1 is the fact that the third-order velocity defect is equal to zero. This means that the error in the approximation to the velocity defect provided by ε_{z0} and ε_{z2} is proportional to the fourth power of R_m/α. The numerical error curves represented in Sec. 7.4 show that R_m/α can be reasonably large before this error is appreciable.

n	ε_{zn}	Highest Power of Rp_o in ε_{zn}	h_{yn}	Highest Power of Rp_o in ε_{zn}
0	$\neq 0$	1	Imaginary	0
1	$= 0$	—	Real	1
2	$\neq 0$	3	Imaginary	2
3	$= 0$	—	Real	3
4	$\neq 0$	5	Imaginary	4

Table 6-1

Properties of the Expansions

in R_m/α

Chapter VII

RESULTS OF THE NUMERICAL CALCULATIONS
CONCERNING INDUCTION-DRIVEN FLOW

This section presents and discusses the results of the
numerical calculations that were made to implement the method
of solution that is described in Ch. VI. Only the results of
these calculations are presented here, however, the numerical
methods that were employed are described in Appendix B,and
the digital computer techniques are outlined in Appendix C.

7.1 The Physical Significances of the Two Types of
Excitation and the Flow Parameters

The nature of the solutions that are presented in the
following sections is much more easily understood if the
physical significances of the two types of excitation (even
and odd) and of the various flow system parameters (α, M,
R_m/α and Rp_o) are made clear.

First, consider the differences between even and odd
excitation. The fundamental distinction is that in even
excitation the traveling current sheets on the surfaces of
the channel are in phase, while in odd excitation they are
180° out of phase [cf. Eqs. (5.1.7) and (5.1.8)]. Figure 7-1
depicts the two forms of excitation schematically. The
traveling current sheets are represented by sine waves, with
a dot indicating current directed out of the paper, and a
cross indicating current directed into the paper. The
dotted arrows indicate the direction of the magnetic field

produced by each "pole" of current, while the solid arrows indicate the position and direction of the principal field produced by the excitation. The phase velocity of the current waves is $\frac{\omega}{k}$, and their wave length is $\frac{2\pi}{k}$.
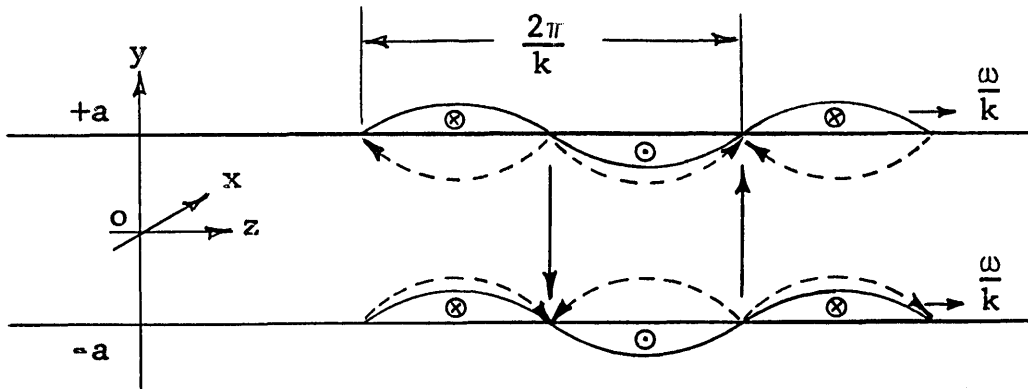

Fig. 7-1a   Even Excitation
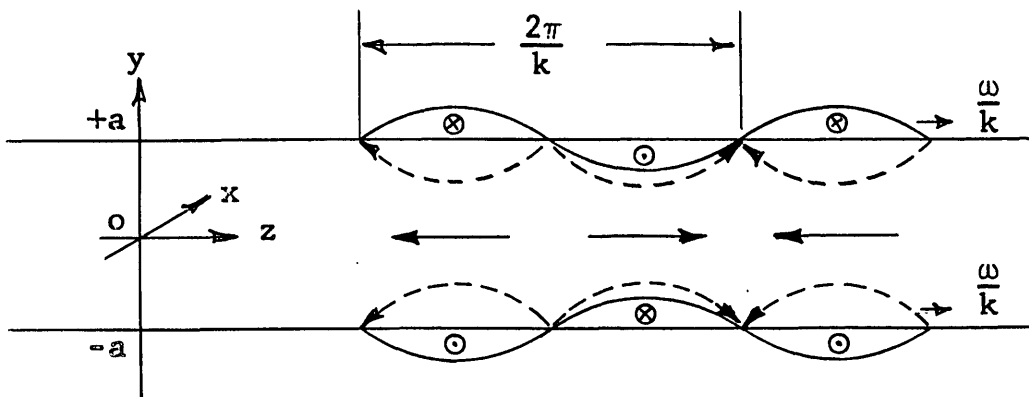

Fig. 7-1b   Odd Excitation

In general, even excitation produces a large component of transverse magnetic field (proportional to $\cosh a\tilde{y}/\sinh a$ when $R_m \ll 1$), while odd excitation produces exactly the reverse. Thus, for small values of a,   the field produced

by even excitation is almost entirely transverse, and that
produced by odd excitation is almost entirely longitudinal.
However, for large values of α, the transverse and longi-
tudinal fields produced by both types of excitation are
approximately the same. [When $R_m \ll 1$, the ratio of the
average transverse field to the average longitudinal field
produced by even excitation, or the ratio of the average
longitudinal field to the average transverse field produced
by odd excitation is $\cosh \alpha/(\cosh \alpha - 1)$.] Because the
transverse component of the traveling magnetic field
produces an electromagnetic force that is in the direction
of the mean fluid flow, while the longitudinal component
does not, even excitation has a greater effect on the fluid
motion than does odd excitation.

Next consider the significance of the parameter α.
Its definition [Eq. (5.1.4)] indicates that it measures the
ratio of the channel half-width a to the excitation pole
spacing π/k. Because of the way in which α effects the
magnetic field distribution, it may be thought of as a
measure of a sort of "geometrical skin effect". If α is
small, the magnetic fields are uniform (for R_m small);
while if α is large, they are strong near the channel walls
and weak near the center line.

The significance of the parameter M is already quite
clear from the discussion of Hartmann flow in Chs. III and
IV, but for the sake of completeness, it is discussed briefly
here. If the definition $M^2 = (\mu_o H_o L_o)^2 \sigma/\eta$ is rearranged
slightly, it becomes

$$M^2 = \frac{\sigma v_o (\mu_o H_o)^2}{\eta v_o / L_o^2} \tag{7.1.1}$$

which can be interpreted dimensionally as the ratio of the electromagnetic force $\bar{J} \times \mu_o \bar{H}$ due to the induced current $\sigma \bar{v} \times \mu_o \bar{H}$, to the viscous force $\eta \nabla^2 \bar{v}$. Thus, if M is small, viscous forces control the fluid motion and the velocity profiles have a parabolic character, while if M is large, electromagnetic forces dominate and the velocity profiles have a highly squared appearance.

Next consider the parameter R_m/α in which the perturbation expansions of Sec. 6.2 are made. If the specific characteristic quantities of induction-driven flow that are defined in Eqs. (5.1.3) through (5.1.6) are substituted in the general definition of R_m [Eq. (2.2.18)], R_m/α can be written as

$$R_m/\alpha = \frac{\sigma \mu_o \frac{\omega}{k} a}{ka} = \frac{1}{2\pi^2} \frac{(\frac{2\pi}{k})^2}{\frac{2}{\omega \mu \sigma}} . \tag{7.1.2}$$

The right-hand side of Eq. (7.1.2) shows that R_m/α is a measure of the square of the ratio of the excitation

wave length to the electromagnetic skin depth.[*] Therefore, when R_m/α is small, electrical skin effect is unimportant, while when R_m/α is large, this skin effect prevents the magnetic field from penetrating uniformly into the fluid. Thus two of the flow system parameters are concerned with skin effects: α with the geometrical skin effect; and R_m/α with the electrical skin effect.

Finally, consider the parameter Rp_0. In terms of the definitions of R and p_0 [Eqs. (2.2.17) and (5.3.15)], and the characteristic quantities of this flow, Rp_0 can be written as

$$Rp_0 = \frac{\overline{\frac{\partial P}{\partial z}}}{\eta \frac{\omega}{k}/a^2}, \qquad (7.1.3)$$

which can be interpreted physically as the ratio of the body force due to the mechanical pressure gradient to the viscous force that would exist if the average fluid velocity were the synchronous speed. Hence, if Rp_0 is small, the balance between electromagnetic and viscous forces determines the

---

[*] Because the fluid velocity varies across the channel, different elements of fluid experience electromagnetic fields at different frequencies. Hence, this skin effect problem is more complicated than the usual one for which the expression $\delta = \sqrt{2/\omega\mu\sigma}$ is derived. However, the analogy is useful in obtaining a physical understanding of the nature of the parameter R_m/α.

fluid motion, while if Rp_o is large, the balance is between external pressure forces and either viscous or electromagnetic forces. Note that when Rp_o is positive the mechanical pressure force is in the negative z-direction and vice versa.

7.2 Velocity Profiles

The key results of the numerical calculations concerning this induction-driven flow are fluid velocity profiles. Not only are they central in all further calculations of such quantities as flow rate and efficiency, but their form and its variation with the various flow parameters very graphically displays the physical phenomena that are significant in this flow.

The basic form in which the velocity profiles were calculated and in which the complete sets of profiles are presented in Appendix D consists of the first two non-zero terms in the perturbation expansion described in Secs. 6.2 and 6.3. Thus the velocity is written as the following functional polynomial in the parameters R_m/α and Rp_o ,

$$u_z(\tilde{y}) = u_{z00}(\tilde{y}) + Rp_o \cdot u_{z01}(\tilde{y})$$

$$+ (R_m/\alpha)^2 \, [u_{z20}(\tilde{y}) + Rp_o \cdot u_{z21}(\tilde{y})$$

$$+ (Rp_o)^2 \cdot u_{z22}(\tilde{y}) + (Rp_o)^3 \cdot u_{z23}(\tilde{y})]$$

$$+ O[(R_m/\alpha)^4], \quad \text{(cf. Table 6-1)} \quad\quad (7.2.1)$$

and the figures show plots of the functions $u_{z00}(\tilde{y})$ through $u_{z23}(\tilde{y})$.

Figure 7-2 shows a set of velocity profiles for $\alpha = 1.0$, $M = 1.0$, and even excitation. Because the Hartmann number is relatively low (cf. the Hartmann profiles, Fig. 3-2), the functions all have the parabolic appearance that characterizes profiles that are dominated by viscous forces. Since the functions all have roughly the same shape, the form of the velocity profile changes relatively little with changes in R_m/α or Rp_o.

Note that u_{z00} is positive, because with no pressure gradient along the channel the magnetic field, which travels in the positive z-direction, drives the fluid in the same direction. However u_{z01} is negative, because a positive pressure gradient (Rp_o) drives the fluid in the negative z-direction. A simple physical explanation of the fact that all of the second-order (in R_m/α) velocities are negative is somewhat more difficult to obtain, although this fact can be demonstrated by direct analytical consideration of Eqs. (6.3.31) and (6.3.33). In view of the interpretation of R_m/α as a measure of the importance of the electrical skin effect, the fact that the second-order velocities are negative is indicative of the fact that as the electrical skin effect becomes more pronounced the traveling magnetic field exerts less influence on the fluid motion (cf. the flow rate-pressure head curves of Sec. 7.5). In terms of the analogy

Fig. 7-2

Velocity Profiles

$\alpha = 1.0$

$M = 1.0$

even excitation
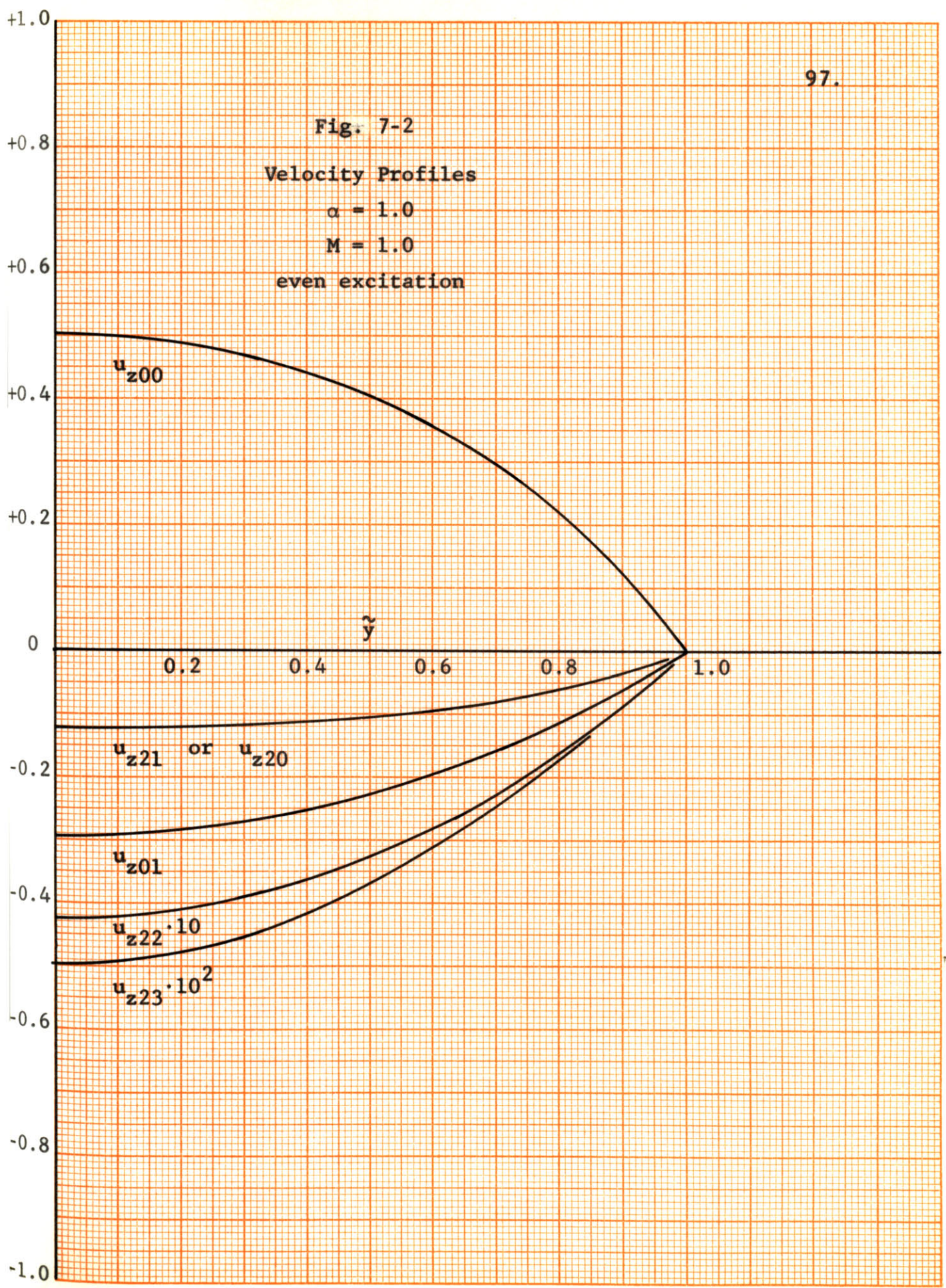
between an induction-driven flow and a conventional induction motor, the zero-order solutions correspond to the assumption that the induction machine rotor is completely resistive, while the second-order solutions begin to show the effects of inductance.

Figures 7-3 and 7-4 show a pair of sets of velocity profiles for even and odd excitations with $\alpha = 0.5$ and $M = 10.0$. In both sets of profiles, the effect of the electromagnetic forces in establishing more rectangular shaped profiles is evident, although far more pronounced with even excitation. This difference is due to the reasonably small value of α which implies that the transverse magnetic field produced by the odd excitation is weaker than that produced by the even excitation. (The "effective Hartmann number" is smaller with odd excitation than it is with even excitation.) The fact that even excitation controls the fluid much more effectively than odd excitation at this value of α is evident in two forms. First, the average value of u_{z00} is larger with even excitation (most of the fluid travels at very nearly the synchronous speed). Second, the average value of u_{z01} is much smaller with even excitation, indicating that a much larger pressure force (Rp_o) is required to alter the volume flow rate for even excitation than for odd excitation.

Although α is relatively small, the "geometrical skin effect" due to the non-uniformity of the transverse magnetic field is already evident in the case of even excitation in that u_{z01} has a more parabolic and less rectangular appearance than u_{z00}. Thus, for small values of Rp_o the
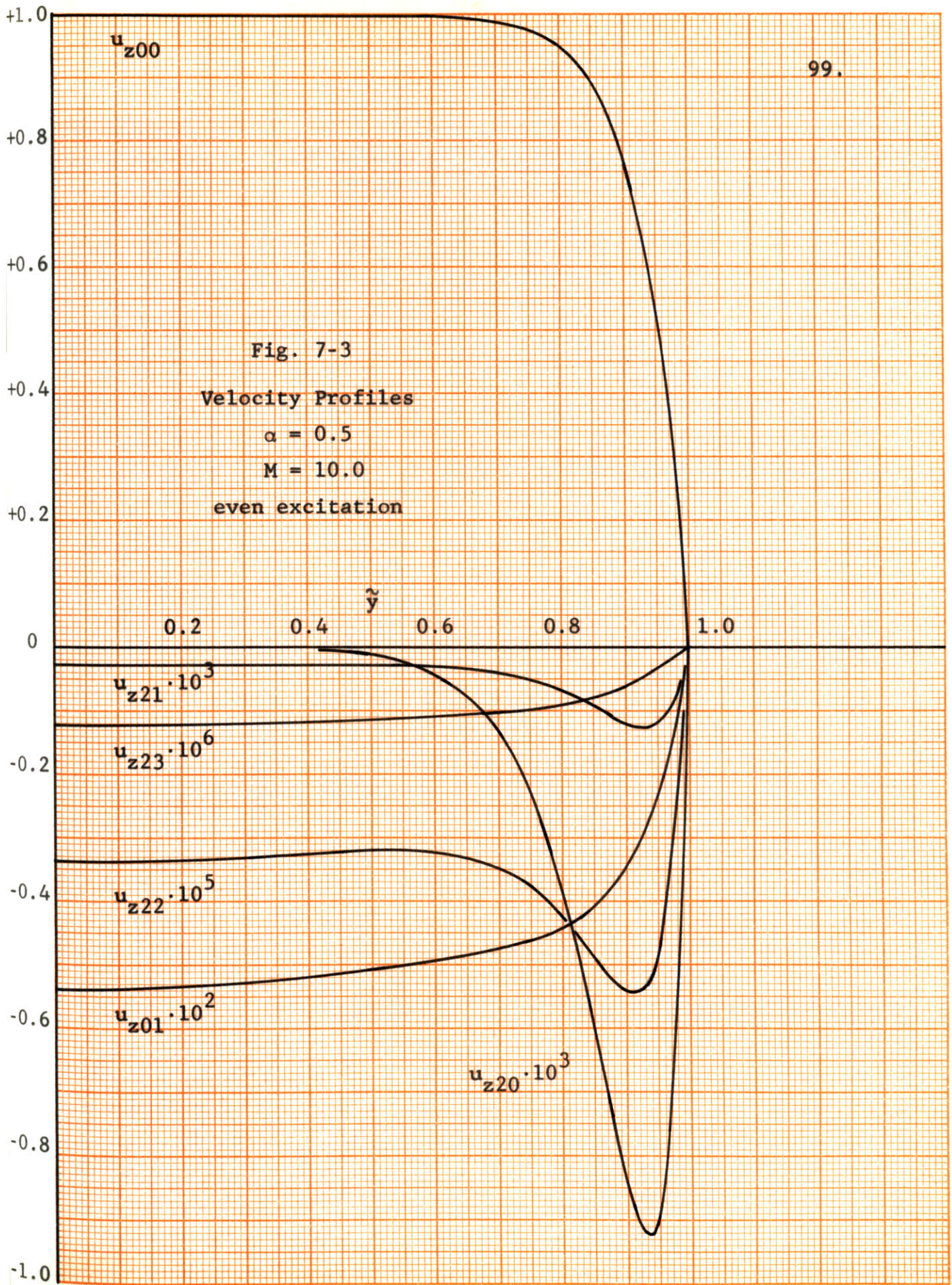
Fig. 7-3

Velocity Profiles

$\alpha = 0.5$

$M = 10.0$

even excitation

u_{z00}

$u_{z21} \cdot 10^3$

$u_{z23} \cdot 10^6$

$u_{z22} \cdot 10^5$

$u_{z01} \cdot 10^2$

$u_{z20} \cdot 10^3$

$\tilde{y}$

99.

Fig. 7-4

Velocity Profiles

$\alpha = 0.5$

$M = 10.0$

odd excitation
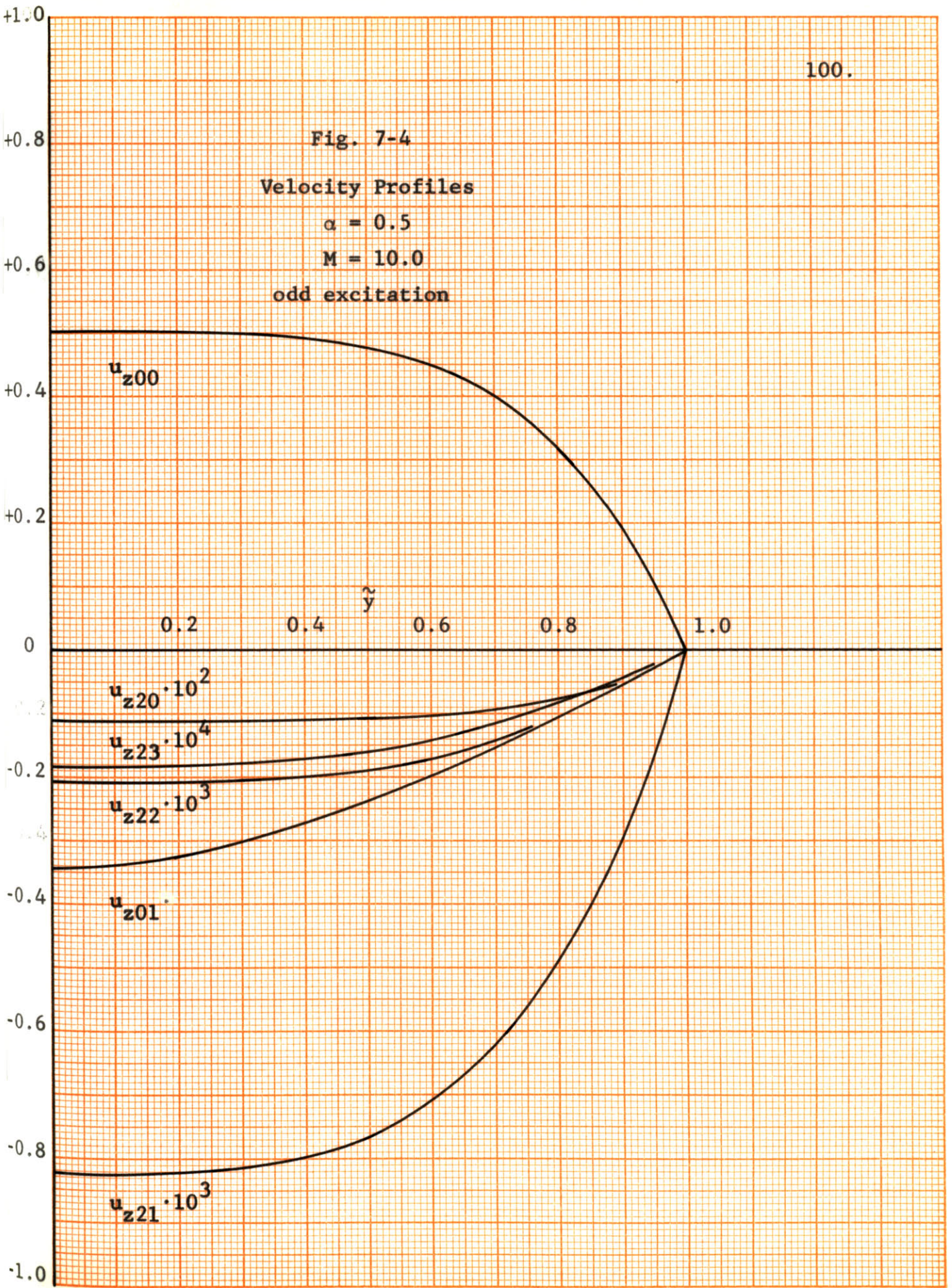
velocity has a more rectangular appearance, while for large values of Rp_0 it has a more parabolic appearance. This is in sharp contrast with Hartmann flow, in which the shape of the velocity profile is fixed by the Hartmann number alone (cf. Sec. 3.1). The "geometrical skin effect" is, or course, quite pronounced with odd excitation, because the transverse magnetic field in that case is zero in the center of the channel and increases in magnitude toward the channel walls (cf. Fig. 7-9).

In Fig. 7-3, with even excitation, the electrical skin effect is very apparent in the second-order (in R_m/α) velocity profiles. Furthermore, within this group of profiles the varying effect of the pressure drive can be seen. Since u_{z20} is multiplied by $(R_m/\alpha)^2$, but not Rp_0, its shape is entirely dominated by the electrical skin effect. By contrast, u_{z23} that is multiplied by $(R_m/\alpha)^2$ and $(Rp_0)^3$ is dominated by the pressure and viscous forces. In between these two extremes, u_{z21} and u_{z22} show progressively less electromagnetic skin effect and more viscous control. The pronounced electromagnetic skin effect is absent from the second-order profiles for odd excitation, because the magnetic fields in this case are already much stronger near the walls than in the center of the channel (cf. Fig. 7-9).

A final pair of sets of velocity profiles for $\alpha = 1.0$ and $M = 10.0$ is shown in Figs. 7-5 and 7-6. Notice that although M is the same in these figures as in Figs. 7-3 and 7-4, u_{z00} is less rectangular in Fig. 7-5 than in

Fig. 7-5

Velocity Profiles

$\alpha = 1.0$

$M = 10.0$

even excitation

u_{z00}

$u_{z20} \cdot 10^2$

$u_{z22} \cdot 10^3$

$u_{z01} \cdot 10$

$u_{z21} \cdot 10^3$

$u_{z23} \cdot 10^5$

$\tilde{y}$

102.

Fig. 7-6

Velocity Profiles

$\alpha = 1.0$

$M = 10.0$

odd excitation

u_{z00}

u_{z01}

$u_{z21} \cdot 10^2$

$u_{z20} \cdot 10^2$

$u_{z23} \cdot 10^4$

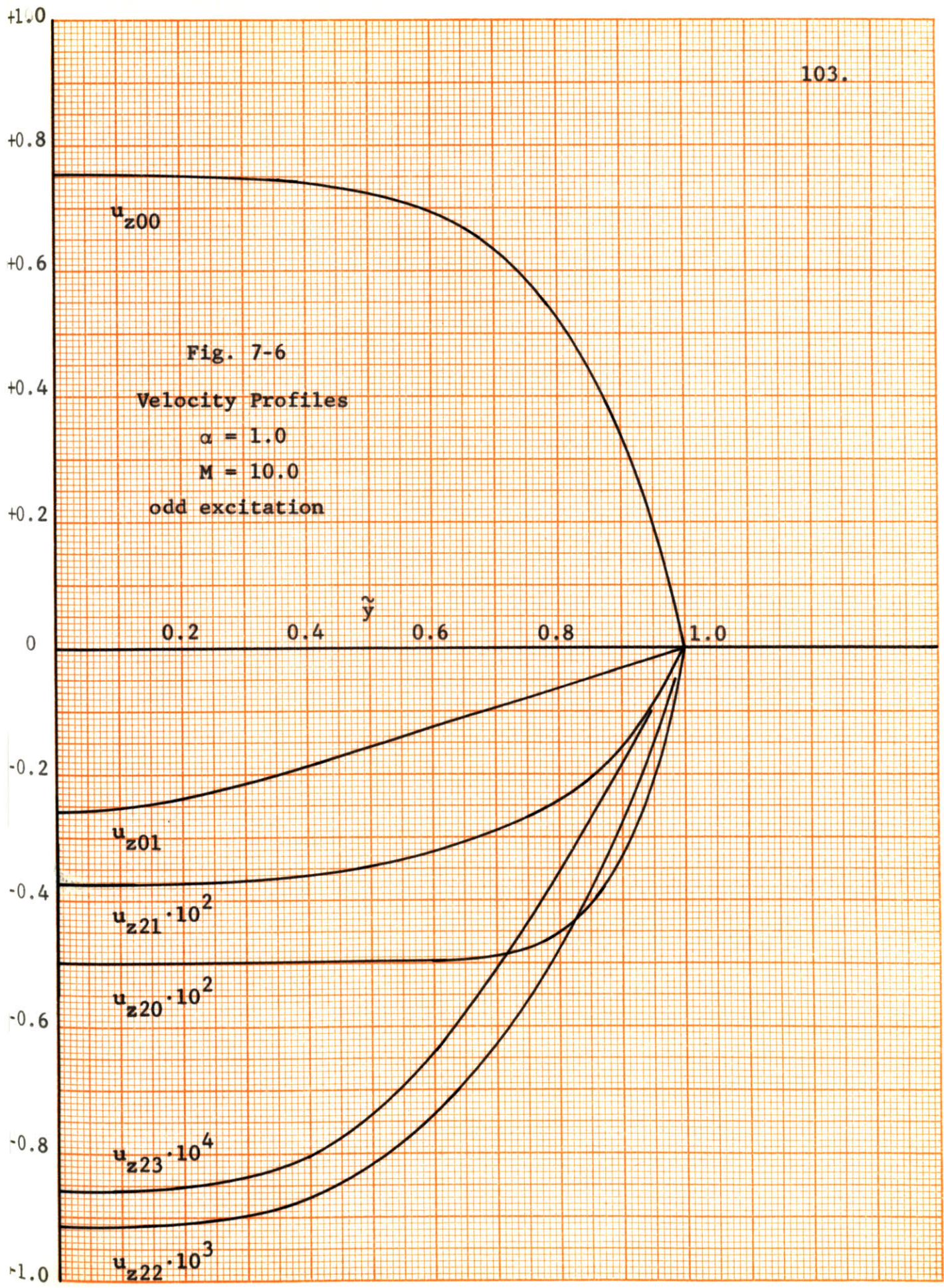$u_{z22} \cdot 10^3$

$\tilde{y}$

103.
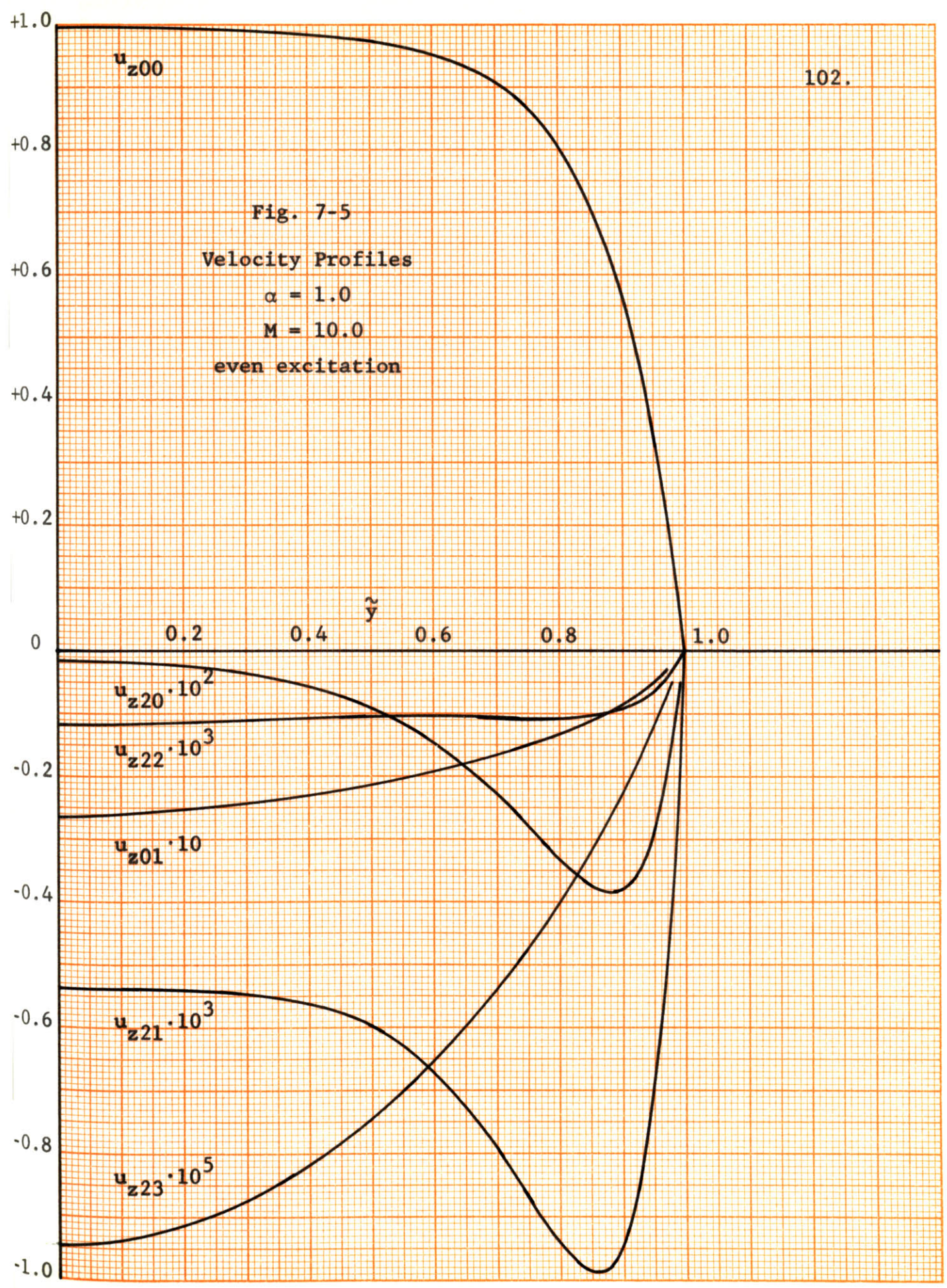
Fig. 7-3 and more rectangular in Fig. 7-6 than in Fig. 7-4. Both of these changes are due to the increase in α (from Figs. 7-3 and 7-4 to Figs. 7-5 and 7-6), which makes the two forms of excitation more nearly equally effective. Note also that the electromagnetic skin effect is less pronounced in Fig. 7-5 than in Fig. 7-3. This is also due to the change in α.

Figure 7-5 shows quite clearly that u_{z00} has a more rectangular appearance than u_{z01}, with the result that the shape of the velocity profile will change with changes in Rp_o. This variation in profile shape is shown graphically in Fig. 7-7 where the center channel velocity is deformed continuously from twice the synchronous speed to minus the synchronous speed by varying the pressure drive Rp_o. (Note that these profiles are for $R_m/\alpha = 0$.) The profiles in Fig. 7-7 show the somewhat startling possibility that the fluid velocity can have a point of inflection and can even be positive near the walls and negative near the center of the channel. This seemingly strange phenomenon appears in fact to be quite reasonable, because the mechanical pressure exerts a force that is uniform across the channel, while the traveling magnetic field exerts a force that is stronger near the walls than it is near the center of the channel. The question of the stability of such

Fig. 7-7

Variation of the
Velocity Profile with Rp_o
$\alpha = 1.0$
$M = 10.0$
even excitation

$Rp_o = -38.0$

$Rp_o = -25.4$

$Rp_o = -12.7$

$Rp_o = -0.1$

$Rp_o = +12.6$

$Rp_o = +25.2$

$Rp_o = +37.9$

$Rp_o = +50.5$

$Rp_o = +63.2$

$Rp_o = +75.8$

u_z

$\tilde{y}$
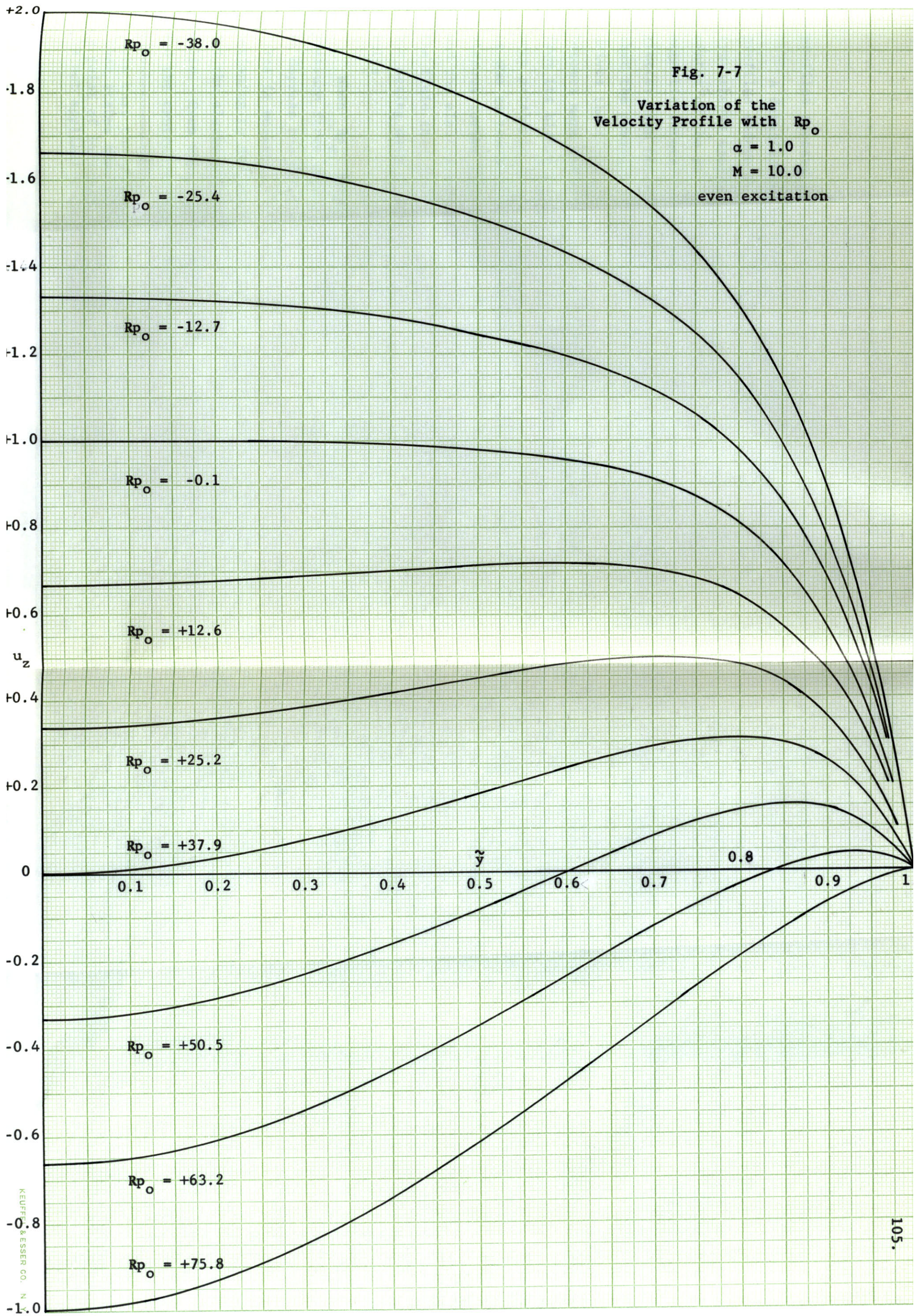
profiles appears to be a very interesting problem.[*]

A detailed examination of the way in which the velocity profiles deform in Fig. 7-7 is quite revealing. Near the synchronous speed, the pressure force is very small and the center of the profile is flat, being controlled by electromagnetic forces. In order to make the center channel velocity greater than the synchronous speed, Rp_0 must be negative so that the pressure force is in the positive z-direction and drives the fluid faster than the traveling field. As Rp_0 becomes more and more negative, the profile rapidly changes from its highly rectangular form at $u_z(0) = 1.0$ to a much more parabolic form at $u_z(0) = 2.0$. This rapid transition is due to the combination of two effects: the pressure and viscous forces that are striving to make the profile parabolic; and the electromagnetic force that is retarding all elements of the fluid that are traveling faster than the synchronous speed, but acting more strongly on those elements that are nearer the walls.

When Rp_0 increases in the positive direction, the pressure force opposes the electromagnetic force, and begins to depress the profile in the center where the electromagnetic force is weakest. When $u_z(0) = 0.0$, the pressure force is beginning to dominate in the central region of the channel, but the electromagnetic force is still in control near the walls. Even when Rp_0 is large enough to make $u_z(0) = -1.0$ and the central region of the profile has a decidedly parabolic

---

[*]Note that the theorem concerning parallel hydrodynamic flows that states that under certain circumstance the existance of a point of inflection implies instability (see Lin,[41] Sec. 4.3) is not applicable to this magnetohydrodynamic situation.

appearance, the effect of the electromagnetic force near the walls is still noticeable.

7.3 Magnetic Field Profiles

In Secs. 6.2 and 6.3, the transverse magnetic field was also expanded in a functional series in powers of R_m/α and Rp_o. This series has the form

$$
\begin{aligned}
h_y(\tilde{y}) = i \Bigg\{ &h_{y0i0}(\tilde{y}) + (R_m/\alpha)^2 \cdot [h_{y2i0}(\tilde{y}) \\
&+ Rp_o \cdot h_{y2i1}(\tilde{y}) + (Rp_o)^2 \cdot h_{y2i2}(\tilde{y})] \\
&+ 0[(R_m/\alpha)^4] \Bigg\} \\
&+ \Bigg\{ (R_m/\alpha) \cdot [h_{y1r0}(\tilde{y}) + Rp_o \cdot h_{y1r1}(\tilde{y})] \\
&+ 0[(R_m/\alpha)^3] \Bigg\} ,
\end{aligned}
\tag{7.3.1}
$$

and the numerical results consist of plots of the functions $h_{y0i0}(\tilde{y})$ through $h_{y2i2}(\tilde{y})$.

Because of the relatively large number of plots that would be required, the entire set of magnetic field profiles that corresponds to the set of velocity profiles shown in Appendix D is not shown; however, for the purposes of discussion, a typical pair of sets of magnetic field profiles for $\alpha = 1.0$ and $M = 10.0$ are shown in Figs. 7-8 and 7-9. The most striking difference between these sets of profiles is of course the
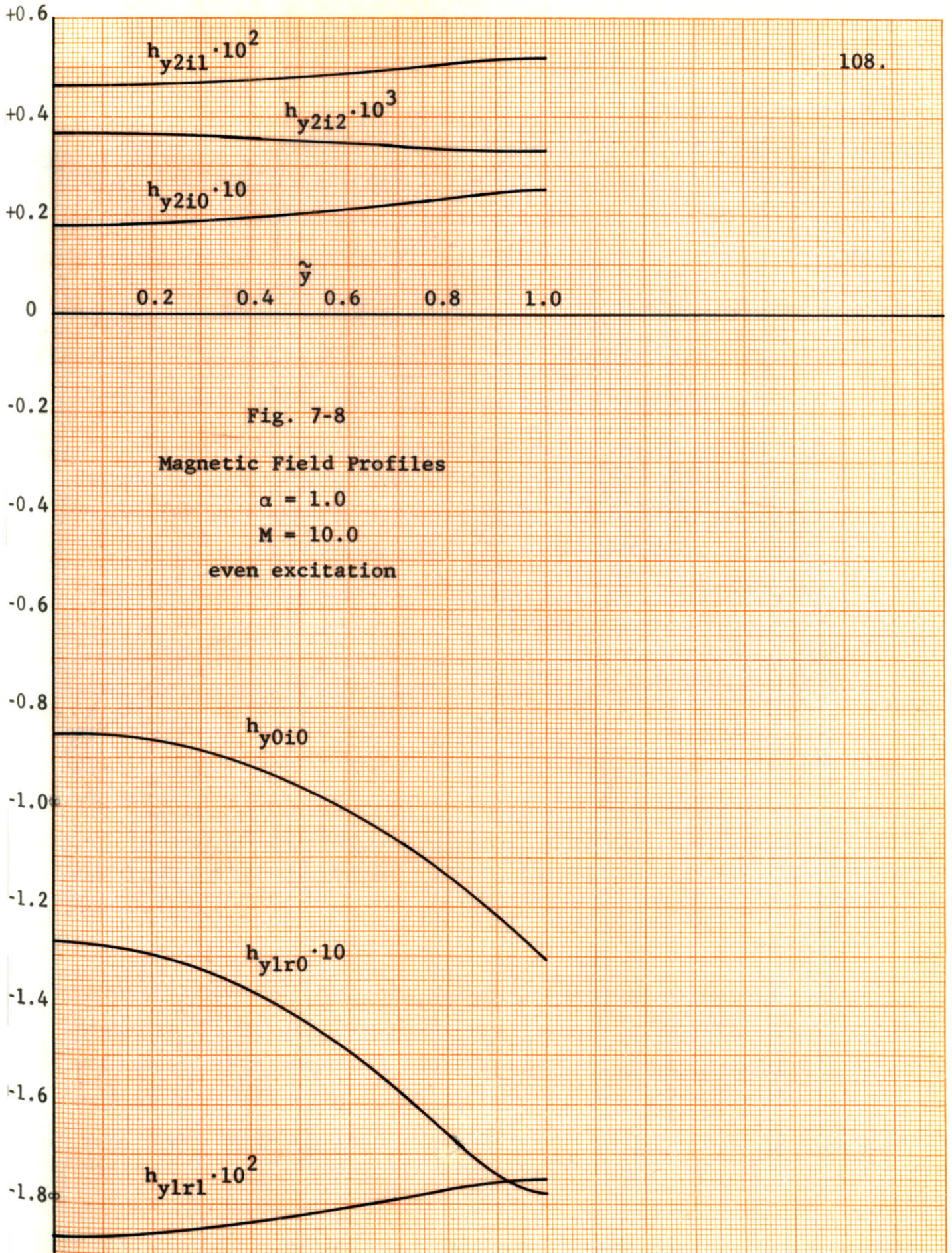
Fig. 7-8

Magnetic Field Profiles

$\alpha = 1.0$
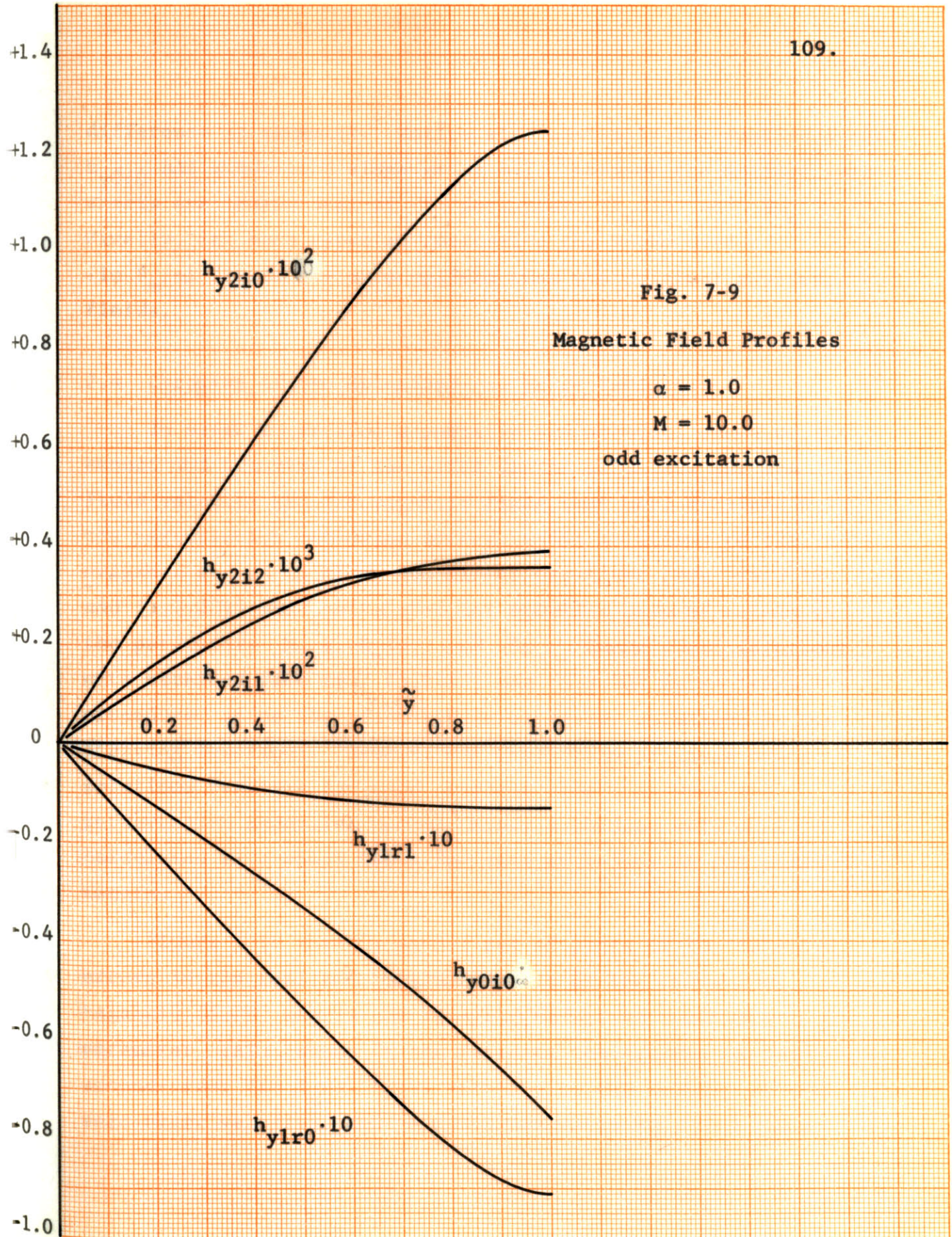
$M = 10.0$

even excitation

Fig. 7-9

Magnetic Field Profiles
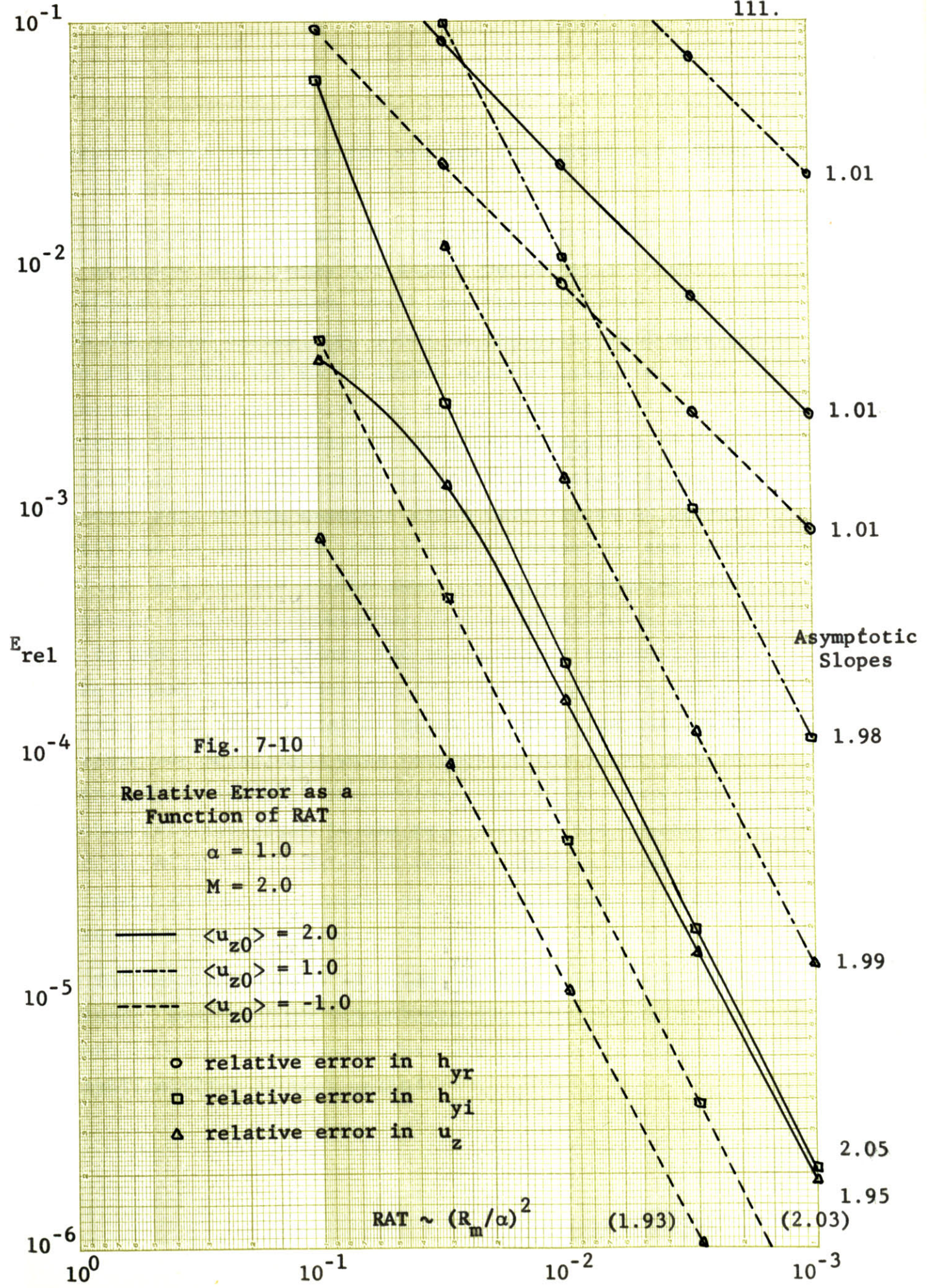
$\alpha = 1.0$

$M = 10.0$

odd excitation

$h_{y2i0} \cdot 10^2$

$h_{y2i2} \cdot 10^3$

$h_{y2i1} \cdot 10^2$

$\tilde{y}$

$h_{y1r1} \cdot 10$

h_{y0i0}

$h_{y1r0} \cdot 10$

difference in symmetry. Notice also that only the applied field h_{y010} has a non-zero slope at $\tilde{y} = 1$, because the surface current sheets are independent of the parameters (R_m/α) and Rp_0. Finally, for both types of excitation the higher-order (in R_m/α) fields are more uniform than the original applied fields.

7.4 Checking of the Solutions and Error Estimates

In order to provide a positive and accurate check on the amount and behavior of the error in the solutions for the fluid velocity and the magnetic field that were obtained by the perturbation expansion method, exact solutions to the original set of coupled, non-linear equations [Eqs. (5.3.19) and (5.3.20)] were calculated for specific sets of values of the parameters M, α, R_m/α, and Rp_0. These exact solutions were obtained from Eqs. (5.3.19) and (5.3.20) by an iterative procedure, using the perturbation expansion solutions as the starting functions. Because the production of these exact solutions requires far more computer time than does the perturbation expansion method, exact solutions were only calculated as a check for a few sets of values of the parameters.

Figure 7-10 shows a sample set of plots of the relative errors in the real and imaginary parts of the transverse magnetic field, and in the velocity defect as functions of a parameter RAT, which is the ratio of the average of the second-order (in R_m/α) fluid velocity to the average of the zero-order velocity, and is proportional to $(R_m/\alpha)^2$. Sets

Fig. 7-10

Relative Error as a
Function of RAT

$\alpha = 1.0$

$M = 2.0$

——— $\langle u_{z0} \rangle = 2.0$

—·—· $\langle u_{z0} \rangle = 1.0$

– – – $\langle u_{z0} \rangle = -1.0$

○ relative error in h_{yr}

□ relative error in h_{yi}

△ relative error in u_z

E_{rel}

Asymptotic
Slopes

111.

1.01

1.01

1.01

1.98

1.99

2.05

1.95

RAT $\sim (R_m/\alpha)^2$ (1.93)   (2.03)

of error curves are shown for average zero-order velocities of
2.0, 1.0 and -1.0.

The important feature of these error curves is that over
most of their length they are almost perfectly straight lines.
The slopes of these lines, which are the powers of RAT with
which the error varies, are shown in the right-hand margin.
These slopes turn out to be almost exactly integers, and
furthermore they agree with the error behavior that is
predicted in the truncated perturbation expansions (7.2.1)
and (7.3.1). Thus the errors in the fluid velocity and the
imaginary part of the magnetic field have slopes of almost
exactly two in Fig. 7-10, and therefore depend on the second
power of RAT or the fourth power of R_m/α. However, this
is exactly the error dependence that is predicted in Eqs.
(7.2.1) and (7.3.1). Since the expansion of the real part
of the magnetic field [see Eq. (7.3.1)] has no term which is
independent of R_m/α against which to normalize the error,
the error was normalized with respect to the first term in
the expansion, which is proportional to R_m/α. Thus the
expected relative error in the real part of the magnetic
field is $O[(R_m/\alpha)^2]$, which is exactly what is found in Fig.
7-10 where this error depends on the first power of RAT or
the second power of R_m/α.

The results of this solution checking procedure are quite
important, because they demonstrate the correctness of the
perturbation expansion solutions, and testify to the validity
and applicability of this method.

Finally, in order to give some idea of the range of values of R_m/α in which the truncated perturbation expansion solutions accurately approximate the exact solution, the relative errors in the velocity defect that are shown in Fig. 7-10 are re-plotted in Fig. 7-11 as functions of R_m/α. In general, the error is very small for $R_m/\alpha < \sim 0.5$, and often it is still relatively small for $R_m < \sim 10.0$.

7.5 Volume Flow Rate and Efficiency

The average fluid velocity, which is proportional to the volume flow rate, can be obtained in the form of a polynomial in R_m/α and Rp_o by averaging the functions u_{z00} through u_{z23} in Eq. (7.2.1) with respect to $\tilde{y}$. Figure 7-12 shows a typical set of curves of the average fluid velocity $\langle u_z \rangle$ as a function of the pressure gradient Rp_o, with R_m/α as a parameter. For $R_m/\alpha = 0$, the curve is, or course, a straight line, because only $\langle u_{z00} \rangle$ and $\langle u_{z01} \rangle$ are present in the polynomial. Again, note that a positive pressure gradient drives the fluid in the negative z-direction. As R_m/α is increased, the fluid velocity is affected very little near synchronous speed ($\langle u_z \rangle = 1.0$) where the pressure gradient Rp_o is small, however it is affected considerably in regions farther from this point ($\langle u_z \rangle > \sim 2.0$ or $< \sim 0.0$) where the pressure gradient is larger. As R_m/α is increased, the electromagnetic skin effect decreases the effect of the traveling magnetic field on the fluid, with the result that the fluid responds more and more to the pressure drive.

Fig. 7-11

Relative Error as a
Function of R_m/α

$\alpha = 1.0$

$M = 2.0$

——————— $\langle u_{z0} \rangle = 2.0$

—·—·—·— $\langle u_{z0} \rangle = 1.0$

— — — — $\langle u_{z0} \rangle = -1.0$

relative error in u_z only
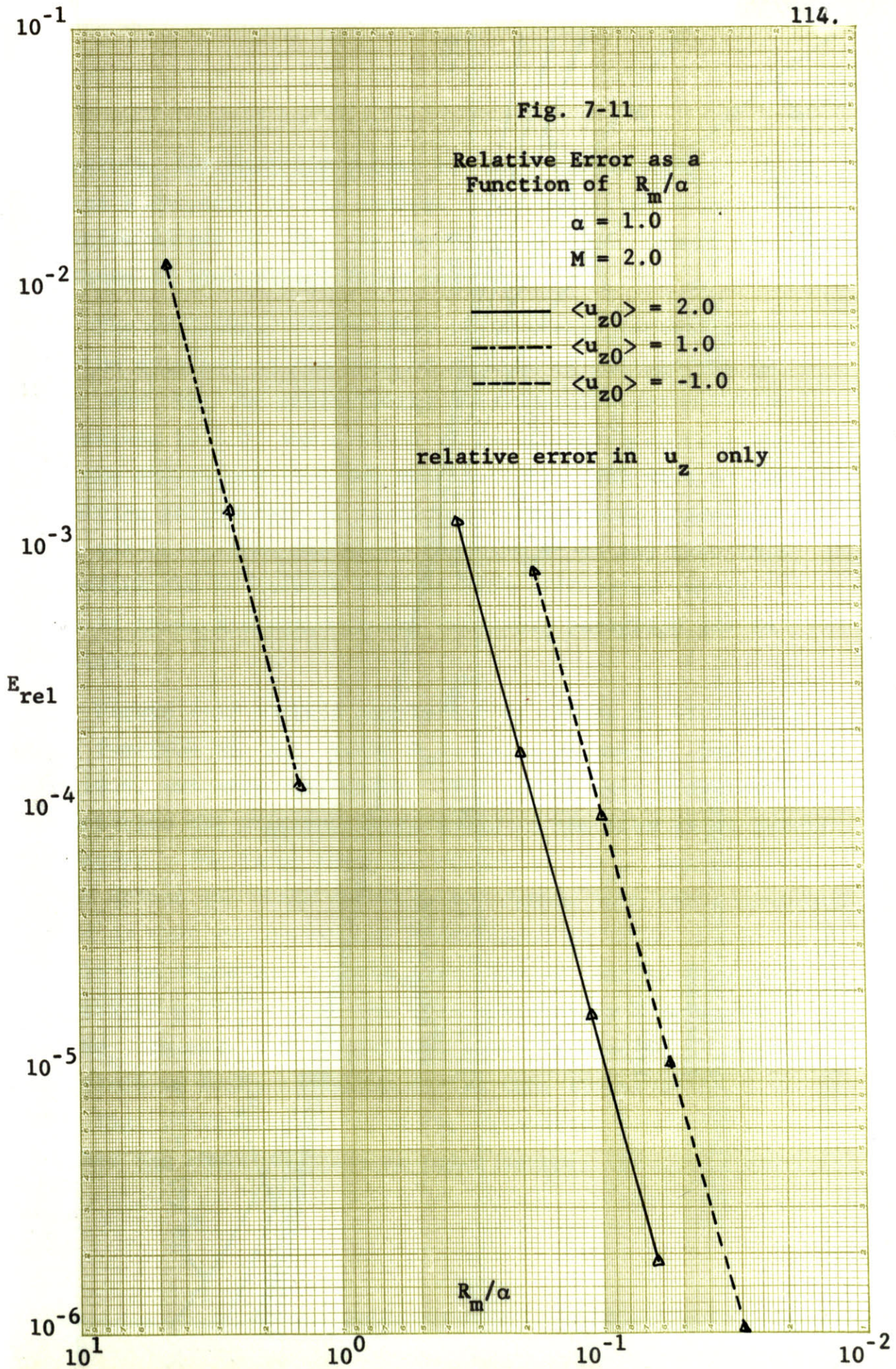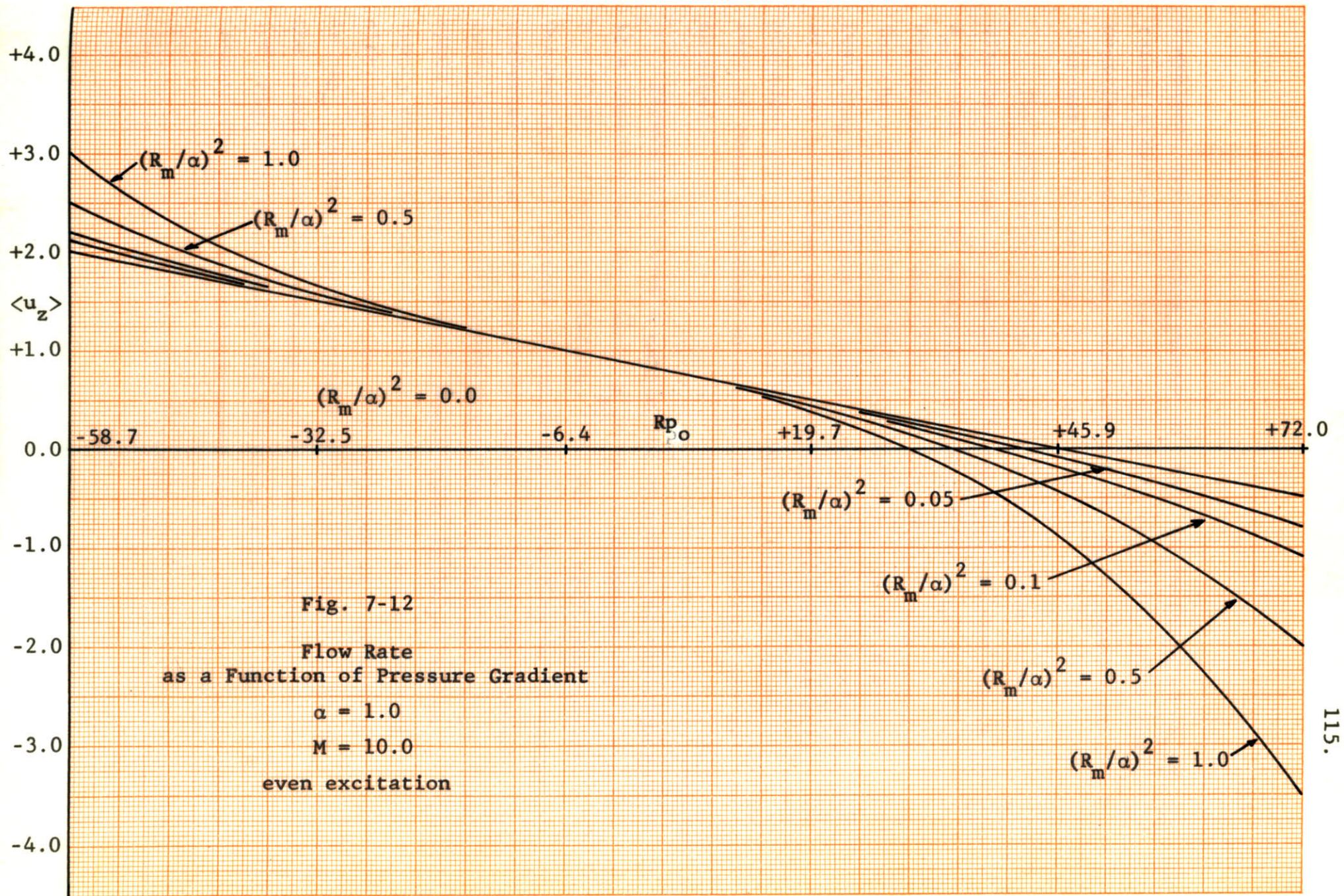
Fig. 7-12

Flow Rate
as a Function of Pressure Gradient
$\alpha = 1.0$
$M = 10.0$
even excitation

$(R_m/\alpha)^2 = 1.0$

$(R_m/\alpha)^2 = 0.5$

$(R_m/\alpha)^2 = 0.0$

$(R_m/\alpha)^2 = 0.05$

$(R_m/\alpha)^2 = 0.1$

$(R_m/\alpha)^2 = 0.5$

$(R_m/\alpha)^2 = 1.0$

$\langle u_z \rangle$

Rp_o

115.

Therefore, for positive values of Rp_0 an increase in R_m/α causes a decrease in the average fluid velocity, while for negative values of Rp_0 an increase in R_m/α causes an increase in the average fluid velocity.

The efficiency of the flow as an energy converter can also be obtained in the form of a ratio of polynomials in R_m/α and Rp_0 by substituting the truncated perturbation expansions (7.1.1) and (7.2.1) in the integral expressions for the efficiency (5.4.20) and (5.4.21). The form of the resulting polynomials is quite complicated and, therefore, will not be written out here. Suffice it to say that this procedure can be carried out and that efficiency curves such as those discussed in the following paragraph can be obtained.

Figure 7-13 shows a sample set of curves of efficiency as a function of Rp_0 with R_m/α as a parameter, for $\alpha = 1.0$, $M = 10.0$, and even excitation. The curves very graphically demonstrate the regions of operation of the flow as an energy converter. For large negative values of Rp_0, the pressure force drives the fluid sufficiently faster than the synchronous speed so that the mechanical power input is large enough to supply the ohmic and viscous power losses, and to provide electrical power output--the flow operates as a generator. As Rp_0 becomes less negative a point is reached at which the fluid is still traveling faster than synchronous speed (cf. Fig. 7-12), but at which the mechanical power input just matches the ohmic and viscous power losses, and the electrical

Fig. 7-13

Efficiency as a Function of Pressure Gradient

$\alpha = 1.0$

$M = 10.0$

even excitation

$(R_m/\alpha)^2 = 0.10$ $(R_m/\alpha)^2 = 0.0$

$(R_m/\alpha)^2 = 0.50$

Generator Operation   Brake Operation   Pump Operation   Brake Operation

$(R_m/\alpha)^2 = 0.50$ $(R_m/\alpha)^2 = 0.10$

$(R_m/\alpha)^2 = 1.0$ $(R_m/\alpha)^2 = 0.0$

Rp_o

117.
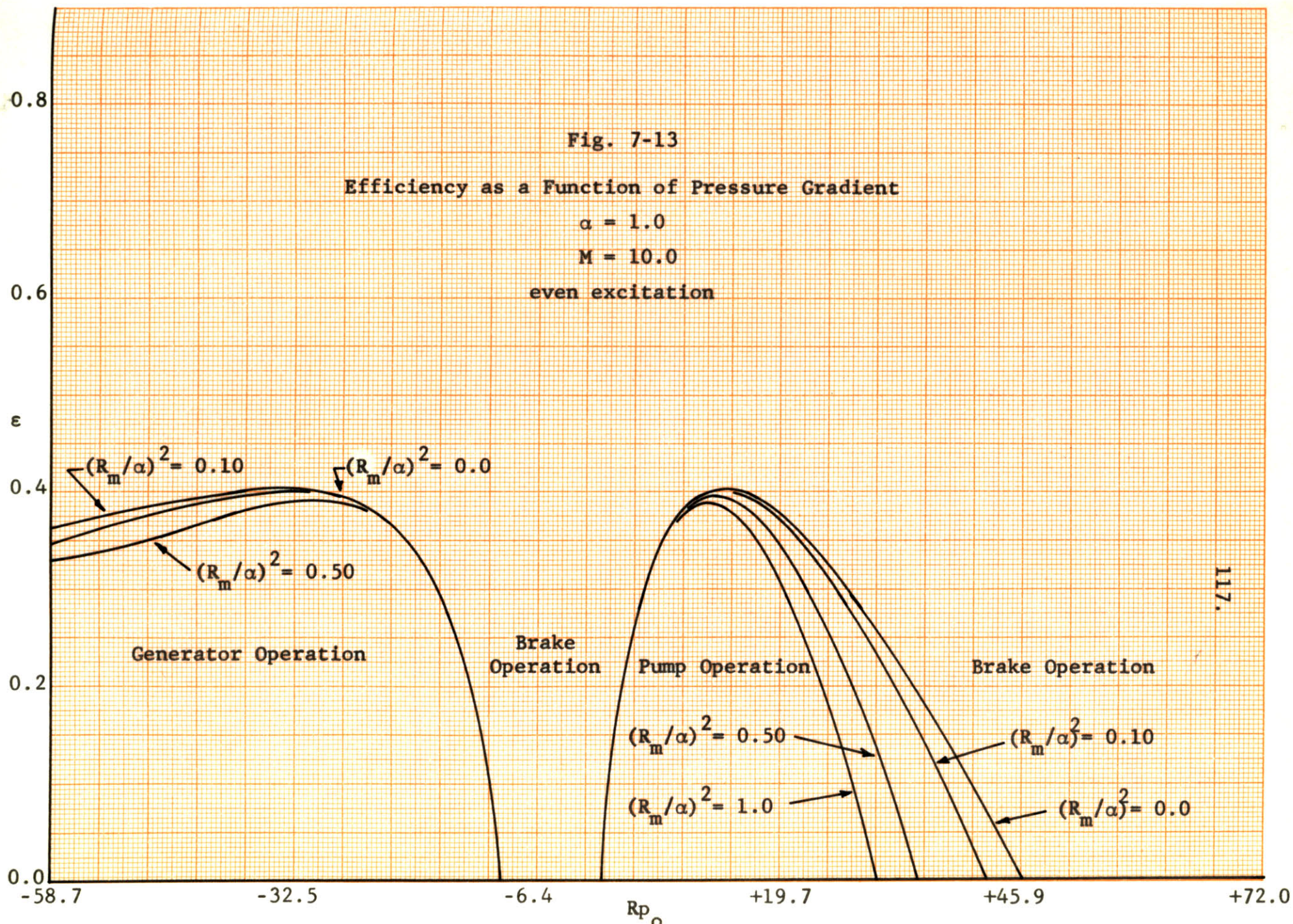
power output and the efficiency drop to zero. As Rp_0 becomes still less negative power comes into the flow from both the mechanical and the electrical power sources, but is entirely dissipated in ohmic and viscous loss--the flow operates as a brake or flow damper. When Rp_0 becomes positive, power begins to flow out of the mechanical terminals--the device operates as a pump or motor. The mechanical power output as well as the ohmic and viscous losses are now supplied by the electrical power input. As Rp_0 is increased, the efficiency increases to a maximum, and then decreases again. Finally, when Rp_0 has become large enough to reduce $\langle u_z \rangle$ to zero (cf. Fig. 7-12), the mechanical power output and the efficiency also drop to zero. Further increase in Rp_0 causes $\langle u_z \rangle$ to become negative, with the result that mechanical as well as electrical power again comes into the flow--the flow has entered the second region of brake or flow damper operation.

The effect on the efficiency curves of an increase in R_m/α is essentially the same as it was on the flow rate curves (Fig. 7-12). As R_m/α is increased, the effect of the electro-magnetic forces is lessened with the result that less pressure force is required to produce the same change in flow rate or efficiency.

In order to give an indication of the variation of the efficiency with the parameters α and M, the maximum efficiencies for several values of α and M are shown in Figs. 7-14 and 7-15 (in all of the efficiency curves that were

obtained, the maximum efficiencies in the pump and generator modes of operation were very nearly equal). There are relatively few points shown in Figs. 7-14 and 7-15 because of the relatively large amount of computer time required to produce a set of efficiency curves. For the same reason, most of the calculations were made concerning even excitation, because for the few points at which the efficiency was obtained for odd excitation, it was much lower than for even excitation (see Figs. 7-14 and 7-15).

Figure 7-14 shows a plot of the maximum obtainable efficiency as a function of the Hartmann number M for $\alpha = 1.0$. As in the conduction-driven flow situation, the efficiency increases monotonically with increasing M (cf. Ch. IV, particularly Fig. 4-6). Figure 7-15 shows a plot of the maximum obtainable efficiency as a function of α for $M = 10.0$. For even excitation, the efficiency decreases monotonically with increasing α; while for odd excitation it also decreases, but not as rapidly (the two forms of excitation are becoming more nearly equally effective).

7.6 Relation to Existing Experiments

To the author's knowledge, there have been no detailed, scientific, experimental investigations of induction driven magnetohydrodynamic channel flow. There has been considerable interest in the use of induction pumps for liquid metals,[*]

---

[*] See, for example, Blake.[10]

Fig. 7-14

Maximum Efficiency
as a Function of M

$\alpha = 1.0$

Fig. 7-15

Maximum Efficiency
as a function of α

M = 10.0
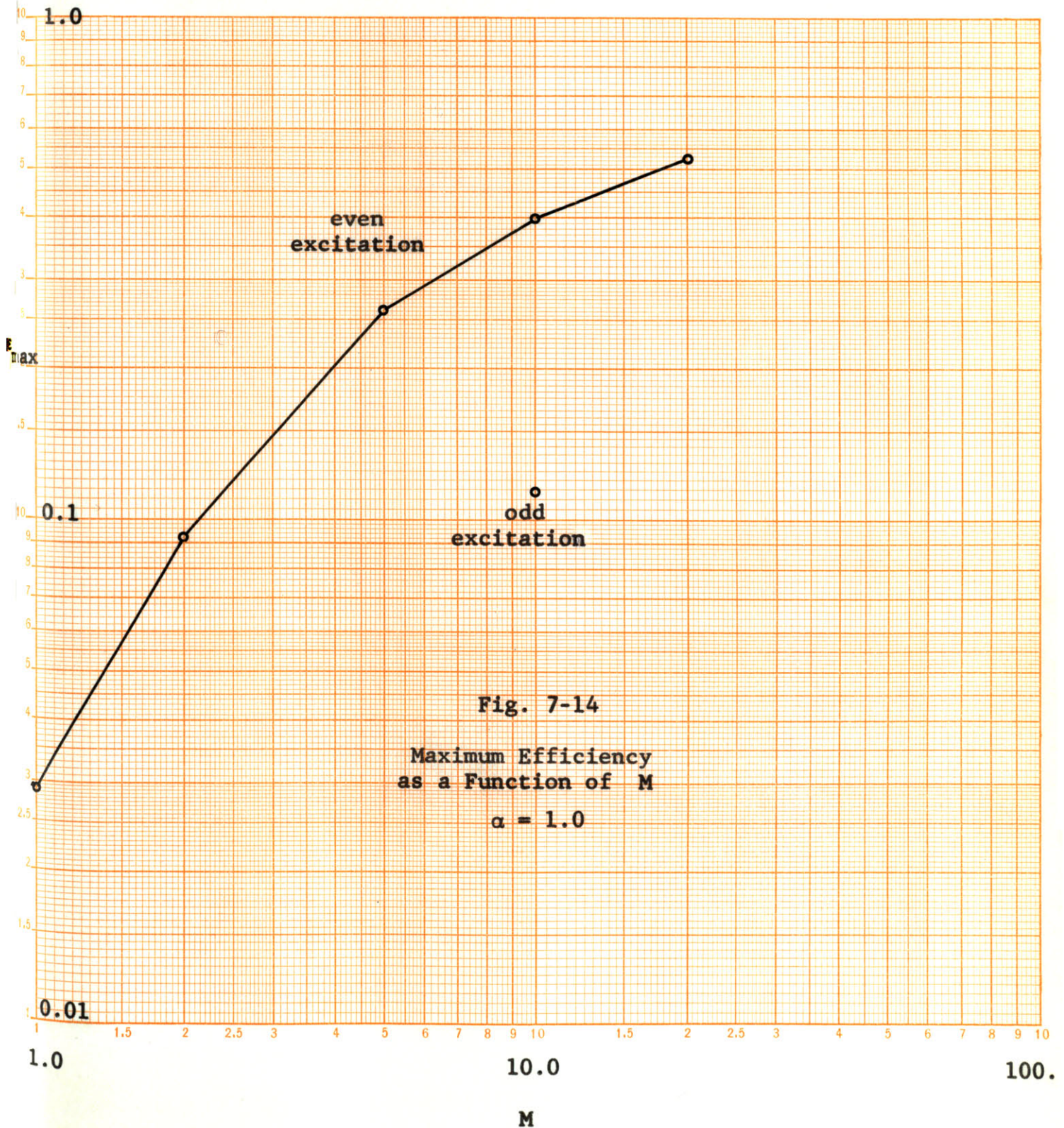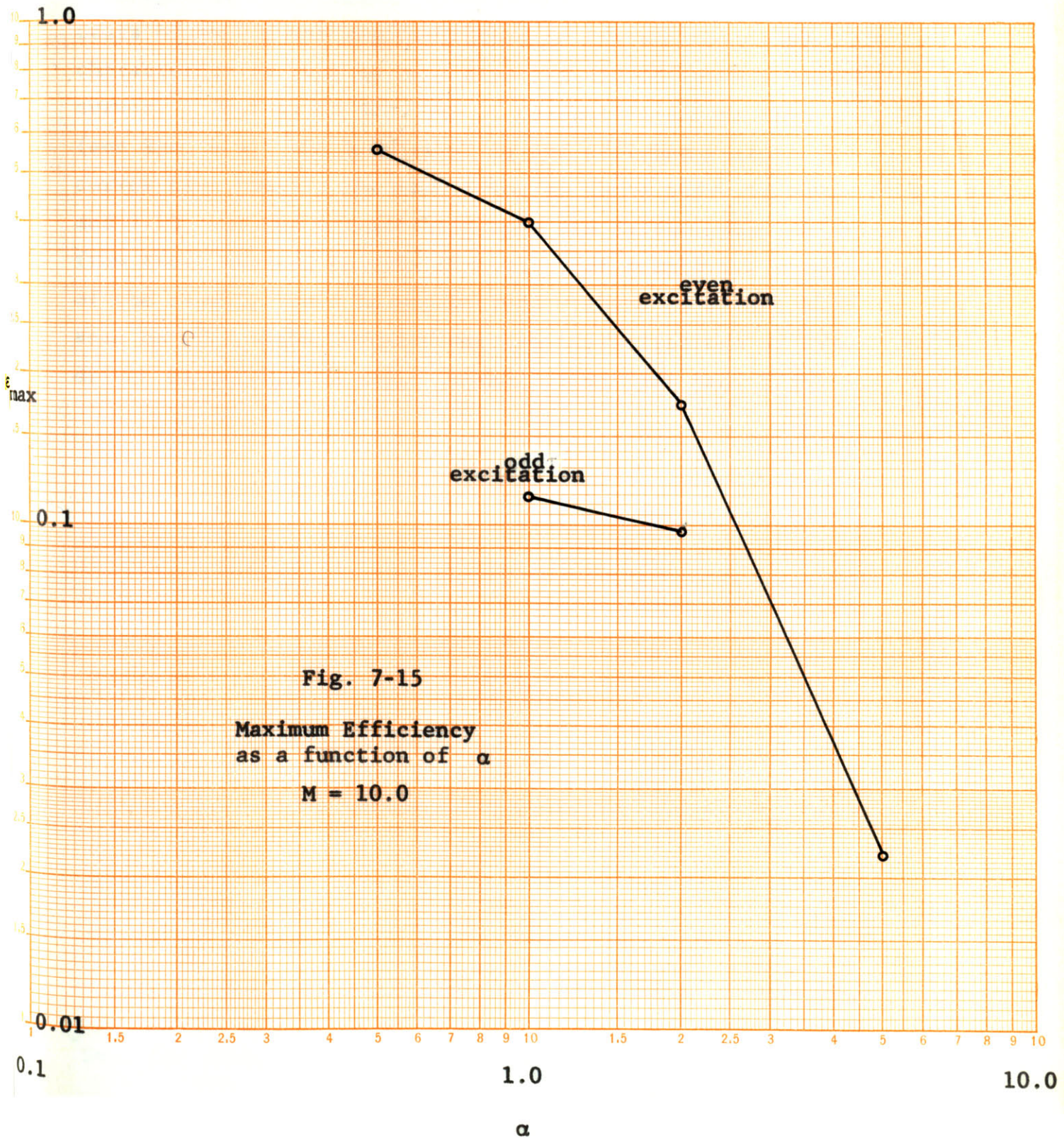
although the experimental results that are published concerning tests of such pumps are restricted to overall operating characteristics such as head-capacity and efficiency-capacity curves.* Just as in the case of conduction-driven flow (see Sec. 4.4), the head-capacity and efficiency-capacity curves have roughly the same forms as those shown in Figs. 7-12 and 7-13, but the actual conditions are sufficiently different from those assumed in this analysis that quantative correlation of the results would be unjustified. There is a real need for some careful, detailed experimental investigations of induction-driven magnetohydrodynamic channel flows (see Sec. 9.3).

---

*See, for example, Barnard and Collins.[42]

Chapter VIII

TIME VARIATIONS IN THE FLUID VELOCITY

Section 5.2 describes the formidable difficulties that are encountered in attempting to find solutions to the induction-driven flow equations in the general case in which the fluid velocity varies with time. With respect to this problem the present chapter has two purposes: first, to develop a quantitative understanding of the relative responses of a viscous fluid to time-varying and steady forces through the analysis of a simplified, but exactly soluble problem; and second, to develop and discuss the equation that governs the second-harmonic components of the fluid velocity, under the assumption that these components are small in comparison with the mean velocity.

8.1 The Relative A-C to D-C Response in Parallel Flow

In order to obtain a quantitative understanding of the response of a viscous fluid that is subjected to both steady and time-varying forces, the following simple hydrodynamic situation is considered. A fluid characterized by a mass density ρ and an absolute viscosity η flows in the z-direction between infinite parallel planes located at $y = \pm\, a$, as shown in Fig. 8-1. Furthermore, the fluid is subjected to a uniform (with respect to space) body force in the z-direction that consists of a constant plus a sinusoid of frequency ω. (Note that this is quite similar to the force that is applied to the fluid by the traveling magnetic field
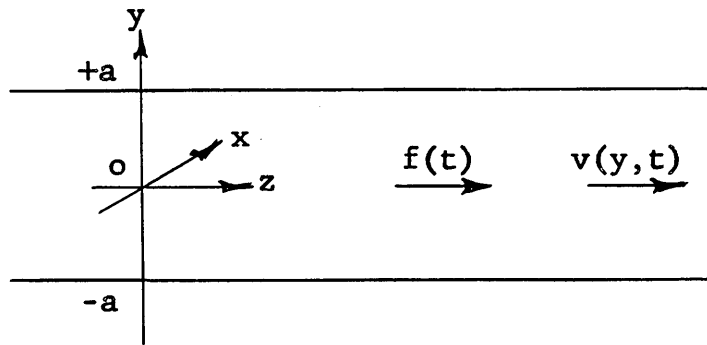
Fig. 8-1   A Time-Varying Viscous Flow
Between Parallel Planes

in induction driven magnetohydrodynamic flow [cf. Eq. (5.3.9)].
If the applied body force   f(t)   is given by

$$f(t) = f_o(1 + \sin \omega t) \; , \tag{8.1.1}$$

the fluid velocity   v(y,t)   must satisfy the diffusion equation

$$\frac{\partial^2 v}{\partial y^2} - \frac{\rho}{\eta} \frac{\partial v}{\partial t} = - \frac{f_o}{\eta} (1 + \sin \omega t) \; , \tag{8.1.2}$$

the symmetry condition

$$v(-y) = v(y) \; , \tag{8.1.3}$$

and the boundary condition

$$v(\pm\, a) = 0 \; . \tag{8.1.4}$$

Because Eq. (8.1.2) is linear, it may be solved separately
for the d-c and a-c components of the fluid velocity, which are
due respectively to the d-c and a-c terms in the applied force.

The solution for the d-c driving term is the familiar

$$v_{dc} = \frac{f_o}{2\eta} (a^2 - y^2) , \qquad (8.1.5)$$

the average of which, with respect to y, is

$$\langle v_{dc} \rangle = \frac{f_o a^2}{3\eta} . \qquad (8.1.6)$$

By analogy with a problem in the conduction of heat in a solid, the a-c velocity is found to be

$$v_{ac} = \frac{4}{\pi\rho} \sum_{n=0}^{\infty} \frac{(-1)^n}{(2n + 1)} \cos[\frac{(2n + 1)\pi y}{2a}]$$

$$\cdot \int_0^t \sin \omega\tau \, e^{-\alpha_n(t - \tau)} d\tau , \qquad (8.1.7)*$$

in which

$$\alpha_n = \frac{\eta}{\rho} (2n + 1)^2 \pi^2/4a^2 , \qquad (8.1.8)$$

if the sinusoidal force commences at $t = 0$. When the integral in Eq. (8.1.7) is performed, and the portion of the result that corresponds to the transient solution is dropped, the desired steady-state solution is found to be

---

*See Carslaw and Jaeger,[43] p. 131, Eq. (9). (Note that there is a misprint in this equation in that ℓ^2 should be replaced by $4\ell^2$ in the denominator of the exponential.)

$$v_{ac} = \frac{4f_o}{\pi\rho} \sum_{n=0}^{\infty} \frac{(-1)^n}{(2n + 1)} \cos[\frac{(2n + 1)\pi y}{2a}]$$

$$\cdot \frac{(\alpha_n \sin \omega t - \omega \cos \omega t)}{\alpha_n^2 + \omega^2} . \tag{8.1.9}$$

Because the time-average value of the a-c velocity is zero, the root-mean-square value is used as a measure of the a-c response. If the root-mean-square value of Eq. (8.1.9) with respect to time is taken, the result is

$$(v_{ac})_{rms} = \frac{2\sqrt{2} f_o}{\pi\rho} \sum_{n=0}^{\infty} \frac{(-1)^n \cos[\frac{(2n + 1)\pi y}{2a}]}{(2n + 1)(\alpha_n^2 + \omega^2)^{1/2}} . \tag{8.1.10}$$

Finally, the average of Eq. (8.1.10) with respect to y is given by

$$\langle(v_{ac})_{rms}\rangle = \frac{4\sqrt{2} f_o}{\pi^2\rho} \sum_{n=0}^{\infty} (2n + 1)^{-2}(\alpha_n^2 + \omega^2)^{-1/2} . \tag{8.1.11}$$

The ratio ξ of the a-c to the d-c response of the fluid may now be defined as

$$\xi = \frac{\langle(v_{ac})_{rms}\rangle}{\langle v_{dc}\rangle} = \frac{12\sqrt{2}}{\pi^2} \cdot \frac{\eta}{\rho a^2} \sum_{n=0}^{\infty} (2n + 1)^{-2}(\alpha_n^2 + \omega^2)^{-1/2} . \tag{8.1.12}$$

Equation (8.1.12) can be put in dimensionless form by introducing the dimensionless parameter

$$R = \rho a^2 \omega / \eta \, ,$$

(8.1.13)

which resembles a hydraulic Reynolds number. If Eq. (8.1.13) and the definition of α_n [Eq. (8.1.8)] are substituted in Eq. (8.1.12), the result is the final expression for ξ

$$\xi = \frac{12\sqrt{2}}{\pi^2} \frac{1}{R} \sum_{n=0}^{\infty} (2n+1)^{-2} [\frac{(2n+1)^4 \pi^4}{16R^2} + 1]^{-1/2} .$$

(8.1.14)

Equation (8.1.14) shows that the ratio ξ of the a-c to the d-c response depends only on the dimensionless parameter R (a fact that could have been conjectured from dimensional analysis at the start).

The nature of the behavior of ξ as a function of R can be quite well understood by considering its behavior for very small and very large values of R. When R is sufficiently small, the first term will dominate the second term in the square brackets in Eq. (8.1.14), with the result that, with the aid of the identity

$$\sum_{n=0}^{\infty} \frac{1}{(2n+1)^4} = \frac{\pi^4}{96} \, ,$$

(8.1.15)*

ξ is found to be given by

$$\xi \to \frac{1}{\sqrt{2}} \, , \quad \text{as} \quad R \to 0 \, .$$

(8.1.16)

---

*Identities such as these are most easily established from their connection with Fourier series. See, for example, Rogosinski,[44] p. 15.

On the other hand, when R is sufficiently large, the second
term will dominate the first term in the square brackets in
Eq. (8.1.14) up to an n that is so large that the size of
$(2n + 1)^2$ makes further terms in the series so small as to
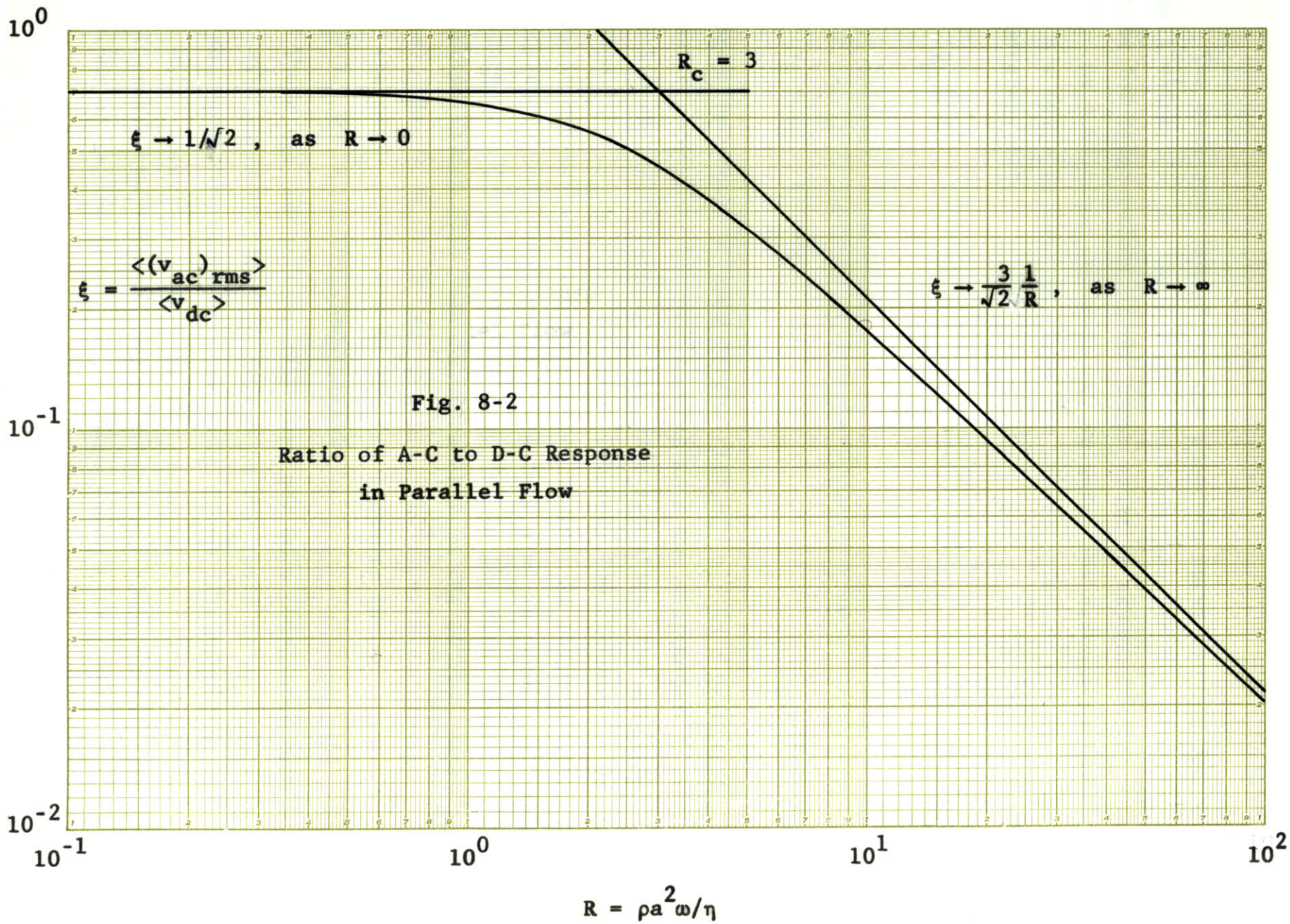be negligible. This reasoning, combined with the identity

$$\sum_{n=0}^{\infty} \frac{1}{(2n + 1)^2} = \frac{\pi^2}{8} ,$$

(8.1.17)*

shows that

$$\xi \sim \frac{3}{\sqrt{2}} \frac{1}{R} , \quad \text{as} \quad R \to \infty .$$

(8.1.18)

Figure 8-2 shows the asymptotes that have just been obtained,
together with a plot of the actual function that was obtained by
summing the series in Eq. (8.1.14) numerically for several values
of R. The response curve is similar to that of a simple low-
pass filter; a result that can be anticipated on physical grounds
by considering the mass of the fluid as an energy storage element,
and the viscosity as a source of power dissipation. Note that
the response curve approaches the asymptote $1/\sqrt{2}$ very rapidly,
but approaches the asymptote $3/\sqrt{2}R$ quite slowly. This slow
approach to the high frequency asymptote is due to the fact that
each component in the spatial Fourier series of the a-c fluid
velocity diffuses with a different characteristic time
$(1/\alpha_n)$ [cf. Eq. (8.1.7)].

---

*Identities such as these are most easily established from their
connection with Fourier series. See, for example, Rogosinski,[44]
p. 15.

Fig. 8-2

Ratio of A-C to D-C Response
in Parallel Flow

$R_c = 3$

$\xi \to 1/\sqrt{2}$, as $R \to 0$

$\xi = \dfrac{\langle (v_{ac})_{rms} \rangle}{\langle v_{dc} \rangle}$

$\xi \to \dfrac{3}{\sqrt{2}} \dfrac{1}{R}$, as $R \to \infty$

$R = \rho a^2 \omega / \eta$

129.

The essential feature of the response curve is that for small values of R the a-c and d-c responses are the same, while for large values of R their ratio is asymptotic to 1/R. As a critical value of R, at which the attenuation of the a-c response sets in, take the intersection of the two asymptotes, viz.

$$R_c = 3, \qquad\qquad (8.1.19)$$

or in terms of frequency

$$\nu_c = \frac{\omega_c}{2\pi} = \frac{3}{2\pi} \frac{\eta}{\rho a^2} . \qquad\qquad (8.1.20)$$

In order to obtain an idea of the size of ν_c in a practical situation, consider mercury flowing in a two centimeter (a = 1.0 cm.) slit channel. For this situation, the critical frequency is $\nu_c \sim 5.9 \cdot 10^{-4}$ cps.; a very low frequency. Also, if mercury in a two centimeter channel is subjected to a body force that consists of a d-c term plus an equal amplitude a-c term at a frequency of 120 cps. (as is the case in an induction driven flow that is operated from the 60 cps. power lines), the value of R is $R \sim 6.1 \cdot 10^5$, with the result that the ratio of the a-c to the d-c response is $\xi \sim 3.5 \cdot 10^{-6}$; a very small ratio.

There are two effects that have not been considered here that will increase the dissipation in the fluid in an induction-driven magnetohydrodynamic flow under these circumstances, and that will, therefore, decrease the value of the parameter R and increase the response ratio ξ. First, there is additional dissipation in the fluid due to ohmic power loss. This

additional loss is often accounted for by ascribing to the fluid an additional "magnetic viscosity,"* which is said to be in the ratio M^2 to the absolute viscosity (although the analysis of Sec. 4.1 indicates that at least for brake operation in conduction-driven flow a ratio of M would be a better estimate). Second, the establishment of eddies in the fluid greatly increases the viscous dissipation, and greatly reduces the time required to reach the steady state** (i.e. greatly increases v_c). However, even if a factor of fifty or one-hundred is conceded to each of these effects, the response ratio ξ in the example given above is still only of the order of one percent.

Thus, although the simplified problem that is analyzed above is by no means identical to the question of a-c variations in the fluid velocity in induction-driven flow, it does have many of the same essential features. The importance of the results that are derived above is that they show that the cut-off frequency of common fluids is quite low, that is, that the fluid must oscillate very slowly if viscous forces are to be comparable with inertial forces. These results lend strong support to a theory of laminar induction-driven flow that assumes that a-c variations in the fluid velocity are quite small in comparison with the average d-c flow.

---

* See, for example, Cowling,[45] pp. 10 and 16.

** See, for example, Lamb,[32] Art. 366b. ff.

8.2 The Equation that Governs the Second-Harmonic Time Variation of the Fluid Velocity

The general problem of obtaining in a useful form the equations that govern a particular harmonic component of the fluid velocity is a formidable task (cf. Sec. 5.2). However, under two simplifying assumptions, a single differential equation that governs the second-harmonic time variation can be obtained. The first assumption is that the time variations in the fluid velocity are small in comparison with the mean flow, with the result that linearization may be employed. The practicality of this assumption is supported by the results of Sec. 8.1, where the ratio of the a-c to the d-c response of typical fluids in an idealized situation is shown to be quite small. The second assumption is that the a-c motion of the fluid is entirely due to the a-c electromagnetic force that arises from the interaction of the traveling magnetic field and the mean flow (this should be especially true if R_m is small). Because this primary a-c force is at the second-harmonic frequency [see Eq. (5.3.9)], the time variation of the fluid velocity is assumed to be at the same frequency.

In keeping with the two assumptions discussed above, the fluid velocity is assumed to be of the form

$$\bar{u} = \bar{i}_z u_z(\tilde{y}) + \text{Re}\left\{ [\bar{i}_y \, \hat{\underline{u}}_y(\tilde{y}) + \bar{i}_z \, \hat{\underline{u}}_z(\tilde{y})] \; e^{i2\alpha(\tau - \tilde{z})} \right\},$$

(8.2.1)

in which $u_z(\tilde{y})$ is the mean velocity in the z-direction that has already been determined, and $\hat{\underline{u}}_y(\tilde{y})$ and $\hat{\underline{u}}_z(\tilde{y})$ are the

complex amplitudes of the second-harmonic time variation of the fluid velocity, which must satisfy the restrictions $|\hat{\underline{u}}_y| \ll u_z$ and $|\hat{\underline{u}}_z| \ll u_z$. The incompressibility condition, $\nabla \cdot \bar{u} = 0$, immediately allows $\hat{\underline{u}}_z$ to be eliminated from Eq. (8.2.1) with the result that

$$\bar{u} = \bar{i}_z u_z + \text{Re}\left\{ [\bar{i}_y \hat{\underline{u}}_y + \bar{i}_z \frac{1}{i2\alpha} \hat{\underline{u}}_y{}'] e^{i2\alpha(\tau - \tilde{z})} \right\} . \quad (8.2.2)$$

The procedure for obtaining a single differential equation that governs one of the a-c velocity amplitudes is rather complicated algebraically; therefore, only the method and the result will be described here. First, Eq. (8.2.2), which gives the assumed fluid velocity, and Eq. (5.3.9), which gives the assumed electromagnetic force, are substituted in the non-dimensional magnetohydrodynamic Navier-Stokes equation [Eq. (2.2.13)]. Next, terms involving products of the a-c variable $\hat{\underline{u}}_y$ and/or its derivatives are neglected (the equation is linearized), and the d-c flow equation is subtracted away. Finally, the resulting a-c equation is operated on by the vector operator $[\nabla \times (\nabla \times \ ] \equiv [\nabla(\nabla \cdot \ -\nabla^2 \ ]$, and the y-component of the resulting equation is found to be

$$(1 - u_z)(\hat{\underline{u}}_y'' - 4\alpha^2 \hat{\underline{u}}_y) + u_z'' \hat{\underline{u}}_y$$

$$+ \frac{1}{i2\alpha R} (\hat{\underline{u}}_y^{iv} - 8\alpha^2 \hat{\underline{u}}_y'' + 16\alpha^4 \hat{\underline{u}}_y)$$

$$= - \frac{M^2}{2R} u_z' h_y^2 . \quad (8.2.3)$$

This fourth-order, inhomogeneous, linear differential equation with variable coefficients must be solved subject to two sets

of boundary conditions. First, the existence of the walls
demands that

$$\hat{\underline{u}}_y(\pm 1) = 0 \; . \tag{8.2.4}$$

Second, the walls and the finite viscosity of the fluid
demand that $\bar{u} = 0$ when $\tilde{y} = \pm 1$ for all values of $\tilde{x}$ and
$\tilde{z}$. This in turn requires that $\partial\hat{\underline{u}}_z/\partial z = 0$ for $\tilde{y} = \pm 1$,
which when combined with the incompressibility condition
$\nabla \cdot \bar{u} = 0$, demands that

$$\hat{\underline{u}}_y'(\pm 1) = 0 \; . \tag{8.2.5}$$

Needless to say, the task of solving Eq. (8.2.3) subject to
the boundary conditions given in Eqs. (8.2.4) and (8.2.5) is
far from simple. In fact, the homogeneous part of Eq. (8.2.3)
is similar to that encountered in the study of the linear
stability of plane parallel hydrodynamic and magnetohydro-
dynamic flows.* Some solutions have been obtained in these
cases, both analytically and numerically, after a great deal
of effort.

There is, however, an essential difference between these
linear stability problems and the situation considered here
that may make this problem less difficult. The linear

---

*Specifically, see Lin,[41] p. 28; and Cowling,[45] pp. 60-61.
For a brief discussion of the linear stability of plane
parallel magnetohydrodynamic flows, see Cowling,[45] Ch. 4.
Also, for a complete and detailed study of the linear
stability of hydrodynamic flow, see Lin.[41]

stability problems are characterized by a homogeneous differential equation containing three undetermined constants; the wave number α and the phase velocity c of the disturbance, and the hydraulic Reynolds number R of the mean flow. The classical problem is to determine the minimum value of the hydraulic Reynolds number R at which the imaginary part of c becomes positive for some value of α, and the disturbance grows with time. Thus the characteristic value c must be obtained as a function of the parameters R and α to determine the "neutral stability" curve which separates the region in which the imaginary part of c is negative from that in which it is positive. One of the principal difficulties encountered in these problems is that for the high values of R at which instability occurs, the a-c velocity varies very rapidly with $\tilde{y}$ and is, therefore, difficult to determine.

In contrast, the present problem is governed by an inhomogeneous differential equation [Eq. (8.2.3)] in which the constants M, R and α are known, and from which the a-c velocity $\hat{u}_{-y}$ must be determined. Thus in this problem it is not necessary to search for characteristic values. Furthermore, solutions for smaller values of R would be of interest here, and they should not be as difficult to compute.

Chapter IX

CONCLUDING REMARKS AND SUGGESTIONS
FOR FURTHER INVESTIGATIONS

9.1 Concluding Remarks

The aim of this investigation has been to develop a clear
and detailed understanding of laminar conduction and induction-
driven magnetohydrodynamic channel flows, and of the ways in
which they can operate as energy converters. The development
proceeds from the fundamental equations of incompressible
magnetohydrodynamics to the fundamental solutions for the
fluid velocity and the magnetic field, and thence to the basic
energy conversion properties of the flow.

Although both of the flows considered here have their
counterparts in practical devices (the d-c conduction and the
a-c induction pumps for liquid metals), and are analogous in
some respects to conventional rotating machines (the separately
excited d-c and induction machines), the emphasis here has been
neither on the practical aspects of device design nor on the
similarity of these flows to electric machinery. Rather, the
emphasis has been on considering idealized forms of these
flows as problems in magnetohydrodynamics. However, care has
been taken throughout to avoid any assumptions that cannot
reasonably be realized experimentally. Thus, although the flow
situations that are analyzed here are idealizations in com-
parison with practical liquid metal pumps, they correspond to

flows that can be established in the laboratory and that may well have practical applications.

A brief word is perhaps in order concerning two of the mathematical methods that were employed in the analysis of induction-driven flow. The first is the perturbation expansion technique that was employed in Sec. 6.2 to convert three coupled, non-linear differential equations into an infinite set of linear differential equations that are uncoupled from below. These expansions are only a single example of a variety of very powerful perturbation techniques that have proved to be extremely useful in diverse areas of mathematical physics.* These perturbation methods appear to be suitable to a wide variety of hitherto unsolved non-linear magnetohydrodynamic problems. The second method is the idea of combining analytical and numerical procedures in the search for a solution to a difficult mathematical problem (cf. Sec. 6.3). This approach departs from the time-honored technique of carrying the analysis as far as possible analytically and then of calculating a few terminal numerical results. Rather it seeks to use numerical analysis and high-speed digital computation as integral parts of the mathematical analysis, through the realization that some mathematical operations may now be performed more easily numerically than analytically. The skillful combination of modern analysis and modern high-speed digital computers now makes it possible to obtain solutions to problems formerly thought to be insoluble.

---

*See, for example, Morse and Feshbach,[46] Ch. 9.

9.2 Theoretical Extensions

Several interesting theoretical extensions and generalizations of this investigation suggest themselves. First, the analysis of energy conversion in conduction-driven flow that is presented in Ch. IV can be extended to the case of a finite-aspect-ratio channel, by following the method of Shercliff,[47] for obtaining the velocity profiles. Second, the problems of electric and magnetic end effects at the entrance and exit of an energy conversion section in a magnetohydrodynamic flow configuration appear to be soluble by perturbation expansion techniques that are similar to that of Sec. 6.2 (again the magnetic Reynolds number seems to be a likely choice for the expansion parameter). Third, the results of Ch. IV concerning the operating characteristics of conduction-driven pumps and generators can be combined to predict the operation of a complete magnetohydrodynamic d-c transformer.* Fourth, there is the question of the stability of magnetohydrodynamic velocity profiles such as those shown in Fig. 7-7. This is surely a formidable problem, because even the linear stability of hydrodynamic flows is extremely complex, whereas most actual hydrodynamic and magnetohydrodynamic

---

*Such a device attempts to use a d-c conduction pump coupled to a d-c conduction generator as an electrical to electrical magnetohydrodynamic energy converter. Some experimental models of such devices have been tested (see Pierson[48]), although their performance was rather poor. The author is convinced that careful design can improve the performance of such devices, although their ultimate practicality is perhaps questionable.

instabilities are now generally conceded to be non-linear in character. The work of Poduska[22] in describing the fluid turbulence by the calculus of random functionals appears to be the most promising recent advance in this area. Fifth, numerical calculations concerning Eq. (8.2.3) should provide information as to the amplitude and spatial distribution of the second-harmonic time variations in the fluid velocity in induction driven flow.

The theoretical extensions that are discussed above are not intended to form a complete list (inevitably the most interesting ones will be found to have been omitted); rather they are facets of this investigation in which the author has a continuing interest.

9.3 Experimental Investigations

The field of detailed experimental investigation of magnetohydrodynamic channel flows is wide open. To paraphrase: "Everyone talks about the Hartmann profiles, but no one measures them." The fundamental problem in making a detailed study of a magnetohydrodynamic flow is to find suitable means for measuring the fluid velocity and the magnetic field as functions of time and space with the flowing fluid. For measurements of the fluid velocity, attempts have been made to use an electromagnetic flow meter,* and are currently being made to use a pitot tube.** However, to the author's knowledge,

---

*See Kliman.[36]

**See East.[49]

there are still no detailed, accurate experimental velocity profiles for a magnetohydrodynamic flow. There have apparently been no attempts to measure the magnetic field distribution within a flowing, electrically conducting fluid.

Some of the overall characteristics of a magnetohydrodynamic channel flow that is operating as an energy converter, such as efficiency and volume flow rate, can be measured without probing the flow in detail; and, if such characteristics are measured as functions of the significant parameters under carefully controlled conditions, they should provide significant checks on the results of Chs. IV and VII. (The author intends to embark on such an experimental program.) However, the relation between theory and experiment really will not be resolved satisfactorily until detailed experimental velocity and magnetic field profiles are obtained.

Appendix A

A MODIFIED MATHIEU EQUATION

The purposes of this appendix are: to indicate the relationship of Eqs. (6.3.3) and (6.3.4) to the Mathieu equation; to develop some approximate solutions to these equations; and to indicate the difficulties that are encountered in attempting to apply these solutions to the problems of Sec. 6.3.

For convenience, Eqs. (6.3.3) and (6.3.4) are reproduced below.

$$\varepsilon''_{z0} - \frac{1}{2} M^2 \frac{\cosh^2 \alpha \tilde{y}}{\sinh^2 \alpha} \varepsilon_{z0} = -Rp_o \tag{A.1}$$

$$\varepsilon''_{z0} - \frac{1}{2} M^2 \frac{\sinh^2 \alpha \tilde{y}}{\cosh^2 \alpha} \varepsilon_{z0} = -Rp_o \tag{A.2}$$

Since these equations are quite similar, only Eq. (A.1) is investigated here. Furthermore, only the homogeneous form of the equation is considered, because the complete solution can be obtained from the homogeneous solutions by variation of parameters.

A convenient canonical form of Eq. (A.1) is

$$y'' - (\beta^2 \cosh^2 \alpha x)y = 0, \tag{A.3}$$

in which $\beta = M/(\sqrt{2} \sinh \alpha)$. The substitutions $z = \alpha x$ and $\gamma = \beta/\alpha$ transform Eq. (A.3) to

$$y'' - (\gamma^2 \cosh^2 z)y = 0, \tag{A.4}$$

which is the form of the equation that is considered throughout this appendix.

Relation to the Mathieu Equation

Equation (A.4) can also be written as

$$y'' - \frac{\gamma^2}{2} (1 + \cosh 2z)y = 0,$$
(A.5)

which is readily identified with the canonical form of the modified Mathieu equation

$$v'' - (a - 2q \cosh 2z)v = 0,$$
(A.6)*

by setting $v = y$, $a = \gamma^2/2$, and $q = -\gamma^2/4$. Furthermore, Eq. (A.6) is related to the Mathieu equation

$$v'' + (a - 2q \cos 2z)v = 0,$$
(A.7)

by the transformation $z \rightarrow iz$.

Most of the research concerning Mathieu functions has been concerned with eigenvalue problems in which one of the constants (usually q) in Eq. (A.7) is fixed by the boundary conditions, while the other is a function of the separation constant.**

---

*The two most complete accounts of the theory of Mathieu functions are McLachlan[39] and Campbell;[40] although significant discussions of specific points are given by many others, for example, Ince.[50]

**See, for example, Morse and Feshbach,[46] p. 554 ff. A notable exception to the concentration on eigenvalue problems is the research concerning planetary motion that began with Hill (see McLachlan,[39] Ch. VI).

The problem is to determine whether or not a periodic solution exists for a particular value of q; and if it does, to determine it and the corresponding characteristic value a.

In contrast, the problem presented by Eq. (A.4) is that of obtaining a solution (periodic or not) to the modified Mathieu equation [Eq. (A.6)] for specified values of a and q. Some series developments of such solutions in terms of hyperbolic and Bessel functions have been obtained, but in general these series are difficult to manipulate and the coefficients eventually must be computed numerically.[*] Furthermore, the rate of convergence of these series is often quite slow. For these reasons, the application of existing Mathieu functions to the solution of Eqs. (A.1) and (A.2) does not appear to be very practical.

Solutions Valid Near $z = 0$

Although Eq. (A.4) possesses irregular singular points (in fact, essential singularities) at $z = \pm \infty$, $z = 0$ is an ordinary point, and there are no singular points in the finite z-plane. Therefore, Eq. (A.4) possesses two linearly independent solutions that are regular at $z = 0$, and converge everywhere in the finite z-plane.[**] In the following paragraphs, forms of the even solution of Eq. (A.4)

---

[*] See McLachlan,[39] Ch. VIII.

[**] See, for example, Hildebrand,[51] Sec. 4.3.

that are valid near $z = 0$ are investigated.[*]

For small values of z $(z^2 \ll 1)$, $\cosh^2 z \sim 1$, with the result that Eq. (A.4) takes on the simplified form

$$y'' - \gamma^2 y = 0, \tag{A.8}$$

the even solution of which is

$$y = A \cosh \gamma z, \tag{A.9}$$

in which A is an arbitrary constant.

A natural extension of this simple solution is to attempt to find a solution that is valid over a wider range of z by the WKBJ method.[**] In view of the solution (A.9) that is valid near $z = 0$, the WKBJ method attempts to obtain a solution, which is valid over a wider range of values of z, in the form

$$y = A \cosh [\gamma f(z) z]. \tag{A.10}$$

The substitution of the solution (A.10) in Eq. (A.4) shows that the function $f(z)$ must satisfy the differential equation

$$z^2 f'' - 2f = \cosh z, \tag{A.11}$$

---

[*] Although both even and odd solutions to Eq. (A.4) exist around $z = 0$, for simplicity, only the even solution is discussed here, because even solutions to Eqs. (A.1) and (A.2) are required.

[**] See, for example, Morse and Feshbach,[46] p. 1092 ff.

while the requirement that the solution (A.10) shall reduce to the solution (A.9) when $z \to 0$, demands that

$$f(0) = 1. \tag{A.12}$$

Unfortunately, the solutions of Eq. (A.11) cannot satisfy the restriction (A.12). If, however, the restriction $f(0) = 1$ is ignored, the solution of Eq. (A.11) that is regular at $z = 0$ yields the approximate solution to Eq. (A.4)

$$y = A \cosh \left(\frac{2}{3} \gamma \sinh z\right). \tag{A.13}$$

This solution is clearly incorrect near $z = 0$, and also, in the following section, will be shown to be incorrect asymptotically. However, for a properly chosen value of A, Eq. (A.13) undoubtedly provides a reasonable approximation to the even solution of Eq. (A.4) for a range of values of z.

The solution (A.9) can, however, be extended to a larger range of values of z around $z = 0$ by expanding the even solution of Eq. (A.4) in the following double Taylor series.

$$y(\gamma,z) = \sum_{k=0}^{\infty} \sum_{n=0}^{k} a(n,k) \frac{\gamma^{2n}}{(2n)!} z^{2k} \tag{A.14}$$

If the series solution (A.14) and the series expansion

$$\cosh^2 z = \frac{1}{2} \left[1 + \sum_{k=0}^{\infty} \frac{(2z)^{2k}}{(2k)!} \right] \tag{A.15}$$

are substituted in Eq. (A.4) and terms containing like powers of γ and of z are equated, the following recursion relations are obtained.

$$\alpha(0,k) = 0, \quad k \geq 1 \tag{A.16}$$

$$(2k + 2)(2k + 1) \, \alpha(n, k + 1) - 2n(2n - 1) \, \alpha(n - 1, k)$$

$$-2n(2n - 1) \sum_{j=0}^{k+1-n} \frac{2^{2j}}{(2j)!} \, \alpha(n - 1, k - j) = 0,$$

$$n \geq 1 \tag{A.17}$$

Although the second recursion relation is rather complicated, the initial terms in the series can be worked out without difficulty, and are shown below.

$$y(\gamma,z) = \alpha(0,0) \left\{ \left[1 + \frac{(\gamma z)^2}{2!} + \frac{(\gamma z)^4}{4!} + \frac{(\gamma z)^6}{6!} + \ldots \right] \right.$$

$$+ z^2 \left[\frac{1}{6} \frac{(\gamma z)^2}{2!} + \frac{7}{15} \frac{(\gamma z)^4}{4!} + \frac{11}{14} \frac{(\gamma z)^6}{6!} + \ldots \right]$$

$$+ z^4 \left[\frac{1}{45} \frac{(\gamma z)^2}{2!} + \frac{47}{420} \frac{(\gamma z)^4}{4!} + \frac{383}{1260} \frac{(\gamma z)^6}{6!} + \ldots \right]$$

$$\left. + \ldots \right\} \tag{A.18}$$

The first series in Eq. (A.18) is readily recognized as $\cosh \gamma z$, however, the remaining series have so far escaped identification with known functions, either from the terms that are written out or from their general recursion relations.

Asymptotic Solutions

The task of obtaining solutions to Eq. (A.4) that are valid for large values of $|z|$ is simplified by the substitution $\xi = \sinh z$, which transforms Eq. (A.4) to

$$(1 + \xi^2)y'' + \xi y' - \gamma^2(1 + \xi^2)y = 0 . \tag{A.19}$$

If $\xi^2 \gg 1$ (say $\xi > \sim 3.2$ or $z > \sim 1.9$), Eq. (A.19) can be rewritten approximately as

$$\xi^2 y'' + \xi y' - \gamma^2 \xi^2 y = 0, \qquad (A.20)$$

which is a form of the Bessel equation.[*] The general solution of Eq. (A.20) is

$$y = c_1 I_0(\gamma \xi) + c_2 K_0(\gamma \xi), \qquad (A.21)$$

in which I_0 and K_0 are the modified Bessel functions of the first and second kinds of order zero, and c_1 and c_2 are arbitrary constants. Thus, for $z > \sim 2$, the even solution to Eq. (A.4) can be written approximately as

$$y = c_1 I_0(\gamma \sinh|z|) + c_2 K_0(\gamma \sinh|z|). \qquad (A.22)$$

The function $I_0(x)$ is equal to one for $x = 0$ and increases rapidly with increasing x, while the function $K_0(x)$ has a logarithmic singularity at $x = 0$ and decreases rapidly with increasing x. For large values of x, these functions have the asymptotic behaviors

$$I_0(x) \sim \frac{e^x}{\sqrt{2\pi x}}, \quad x \to \infty; \qquad (A.23)$$

---

[*] See Hildebrand,[51] Sec. 4.8.

and

$$K_0(x) \sim \frac{e^{-x}}{\sqrt{\frac{2}{\pi} x}} \,, \quad x \to \infty \,. \tag{A.24}$$

For $x = 5.0$, the value of $I_0(x)$ obtained from Eq. (A.23) is in error by about 3%, while for $x = 10.0$ the value of K_0 obtained from Eq. (A.24) is in error by about 4%. Therefore, for $\gamma \sinh |z| > \sim 10.0$, the even solution to Eq. (A.4) can be written as .

$$y = \frac{c_1 e^{\gamma \sinh |z|} + c_2 e^{-\gamma \sinh |z|}}{\sqrt{\gamma \sinh |z|}} \,. \tag{A.25}$$

A comparison of Eqs. (A.25) and (A.13) shows that in detail the solution (A.13) does not have the correct asymptotic behavior, although it does possess the proper characteristic form $\exp [\gamma \exp (z)]$.

Difficulties in Applications

Considerable difficulty is encountered in attempting to apply the approximate solutions of Eq. (A.4) that have been developed here to the specific problem of obtaining solutions to equations like Eqs. (A.1) and (A.2). In general, a series solution such as Eq. (A.18) must be employed for small values of z; an intermediate solution such as Eq. (A.13) is best for moderate values of z; while an asymptotic solution such as Eq. (A.22) is required for large values of z. These solutions must be matched at points where their errors are comparable, and then the arbitrary coefficients must be determined so that the complete solution satisfies the prescribed boundary conditions. Furthermore, the solutions that must be employed and the points of matching may change with changes in γ and the range of z.

To carry through such a process analytically is a complicated and not particularly rewarding task.

The process of employing these approximate solutions and the method of variation of parameters to obtain solutions to the inhomogeneous form of Eq. (A.4) is even more involved. Thus, although approximate analytical solutions to equations like Eqs. (A.1) and (A.2) can be obtained by the methods described in this appendix, the form of such solutions is so complicated that they are of limited use in a complicated physical problem.

Appendix B

NUMERICAL METHODS

This appendix describes the principal numerical methods that were employed in performing the numerical calculations concerning induction driven flow. Because all the functions involved in the basic calculations (e.g., u_{z00}, h_{y010}, etc.) are functions of the single space coordinate $\tilde{y}$ that varies from zero to one, the numerical work was standardized by considering each of these functions at fifty-one evenly spaced points between zero and one. The spacing between points ($h = 0.02$) was chosen so as to provide a sufficient number of points for the plotting of accurate profiles, and to provide a balance between round-off and truncation errors in the numerical calculations.

Differential Equation Integration

The fundamental numerical problem involved in the calculations relating to Sec. 6.3 is the integration of an even or an odd solution to the second-order linear differential equation,

$$y'' - A(x)y = B(x),\qquad\qquad\qquad (B.1)$$

as x varies from zero to one. In either case, $A(x)$ must be even; in addition, if an even solution is desired, $B(x)$ must be even and $y(0)$ must be specified; while if an odd solution is desired, $B(x)$ must be odd and $y'(0)$ must be specified.

The numerical integration was performed by the use of the sixth-order integration formula

$$y_{n+1} = 2y_n - y_{n-1} + \frac{h^2}{12}(y''_{n+1} + 10y''_n + y''_{n-1}) - \frac{h^6}{240}y^{vi}(\xi),$$
$$(B.2)*$$

---

*See Hildebrand,[52] p.223.

in which the point $x = \xi$ lies between x_n and x_{n+1}. Because Eq. (B.1) is linear, its integration using Eq. (B.2) is straightforward, viz.

$$y_{n+1} \simeq [2y_n(1 + \frac{5}{12} h^2 A_n) - y_{n-1}(1 - \frac{h^2}{12} A_{n-1})$$

$$+ \frac{h^2}{12} (B_{n-1} + 10B_n + B_{n+1})]/(1 - \frac{h^2}{12} A_{n+1}) \qquad (B.3)$$

This formula is self starting under the restrictions specified above.

With $h = 0.02$, the truncation error in Eq. (B.3) is about $3 \cdot 10^{-13} \cdot y^{vi}(\xi)$. Checks of the functions that were computed using this integration formula showed that $y^{vi}(\xi)$ was never large enough to make the relative truncation error greater than about 10^{-8}, and that it was usually much smaller. To prevent round-off error from adding to this truncation error, the calculations involved in these integrations were performed double-precision, which on the IBM 709 means accuracy to about seventeen decimal digits.

Averaging

In order to find the average value of any of the functions involved in the calculations (e.g., velocity profiles), the definite integral of such a function from zero to one must be evaluated. This was accomplished by applying the six-point, seventh-order Newton-Cotes integration formula

$$\int_{x_n}^{x_{n+5}} f(x)\,dx = \frac{5h}{288} \, (19f_n + 75f_{n+1} + 50f_{n+2}$$

$$+ 50f_{n+3} + 75f_{n+4} + 19f_{n+5})$$

$$- \frac{275}{12096} \, h^7 f^{vi}(\xi) \, , \qquad\qquad (B.4)*$$

ten times to cover the interval from zero to one.

With $h = 0.05$, the truncation error in Eq. (B.4) is about $3 \cdot 10^{-14}$, and again the relative truncation error is never greater than about 10^{-8}.

Differentiation

Numerical differentiation is required in two different places in the calculations relating to Sec. 6.3. First, the z-component of the magnetic field can be obtained from the y-component by differentiation, because the divergence restriction demands that $h_y' - i\alpha h_z = 0$. Second, the derivatives at $\tilde{y} = 1$ of the particular solutions to the various magnetic field equations [cf. Eqs. (6.3.) and (6.3.)] must be calculated in order to form the total higher-order magnetic field solutions so that they have zero slope at $\tilde{y} = 1$.

The first situation requires the differentiation of a function over the entire interval from zero to one; however, extreme accuracy is not necessary, because the profiles of the z-component of the

---

*See Hildebrand,[52] p. 73.

magnetic field that are so produced are terminal results that are not used in further calculations. The following seven-point, sixth-order Lagrangian differentiation formulas are reasonably accurate and yet simple to apply. In the interior of the interval, the symmetrical formula

$$f'_n = \frac{1}{60h} (-f_{n-3} + 9f_{n-2} - 45f_{n-1} + 0f_n + 45f_{n+1}$$

$$-9f_{n+2} + f_{n+3}) - \frac{h^6}{140} f^{vii}(\xi) \qquad (B.5)*$$

may be employed, but near the ends of the interval, non-symmetrical formulas, such as

$$f'_n = \frac{1}{60h} (-147f_n + 360f_{n+1} - 450f_{n+2} + 400f_{n+3}$$

$$-225f_{n+4} + 72f_{n+5} - 10f_{n+6}) + \frac{h^6}{7} f^{vii}(\xi) \qquad (B.6)$$

must be used.

The second situation requires that the derivative of a function be calculated quite accurately at the single point $\tilde{y} = 1$. For this purpose, the following eight-point, seventh-order Lagrangian differentiation formula was employed.

$$f'_n = \frac{1}{420h} (-60f_{n-7} + 490f_{n-6} - 1764f_{n-5}$$

$$+ 3675f_{n-4} - 4900f_{n-3} + 4410f_{n-2}$$

$$- 2940f_{n-1} + 1089f_n) + \frac{h^7}{8} f^{viii}(\xi) \qquad (B.7)$$

---

*The coefficients for a large number of Lagrangian differentiation formulas are tabulated by Lowan, Salzer, and Hillman.[53]

Although numerical differentiation is often a dangerous procedure,[*] the system of differentiation formulas described above has worked out quite well. For example, the higher-order longitudinal magnetic field profiles, which depend on the accuracy of both types of differentiation for their values at $\tilde{y} = 1$ to be zero, have values there that are from 10^{-3} to 10^{-5} of the average value of the field over the interval.

---

[*] See Hildebrand,[52] Sec. 3.8.

Appendix C

THE DIGITAL COMPUTATION

The numerical calculations involved in this investigation were performed by the IBM 709 Data Processing System at the Computation Center of the Massachusetts Institute of Technology.[*] The computer programs were written by the author in the FAP[**] and FORTRAN[***] programming languages, and were run on the computer under the FORTRAN MONITOR SYSTEM.[****] A total of about three and one-half hours of computer time was used in debugging and testing the programs and producing the final results.

---

[*] For a description of the IBM 709, see IBM,[54] while for a description of the facilities of the Computation Center at M.I.T., see Computation Center.[55]

[**] For a description of the FORTRAN ASSEMBLY PROGRAM (FAP), see IBM.[56]

[***] For a description of the FORTRAN programming system, see IBM.[57]

[****] For a description of the FORTRAN MONITOR SYSTEM, see Computation Center,[55] and IBM.[56]

Appendix D

FURTHER SETS OF VELOCITY PROFILES

The purpose of this appendix is to provide a more complete
set of velocity profiles to augment those that were discussed in
Sec. 7.2. The sets of profiles that are presented were chosen in
an attempt to make the variation of the velocity profile with the
type of excitation (even or odd) and changes in the parameters
α and M as clear as possible, without presenting an excessive
number of plots.

Sets of velocity profiles are presented for both even and
odd excitations, with α = 0.5, 1.0 and 2.0, and M = 2.0, 5.0,
and 10.0. Figures D-1 through D-6 show the profiles for even
and odd excitations, with M = 2.0, and α = 0.5, 1.0, and 2.0;
while Figs. D-7 through D-12 show the profiles for both excita-
tions, with M = 5.0, and α = 0.5, 1.0, and 2.0. The profiles
for both excitations, with M = 10.0, and α = 0.5 and 1.0 are
shown in Ch. VII (Figs. 7-3 through 7-6), and this group is
completed in Figs. D-13 and D-14, which show the profiles for
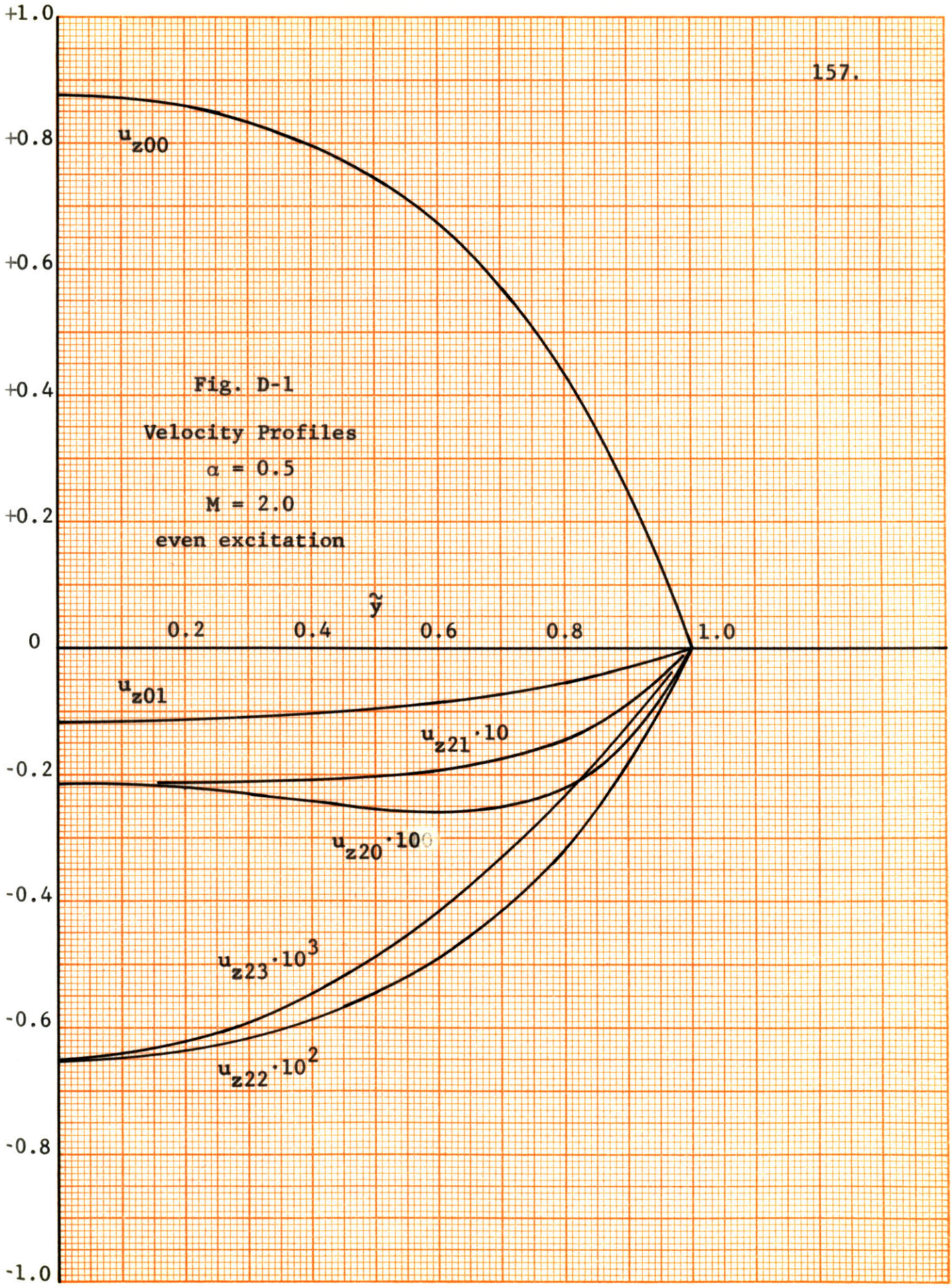both excitations, with M = 10.0 and α = 2.0.

Fig. D-1

Velocity Profiles

$\alpha = 0.5$

$M = 2.0$

even excitation

Fig. D-2

Velocity Profiles

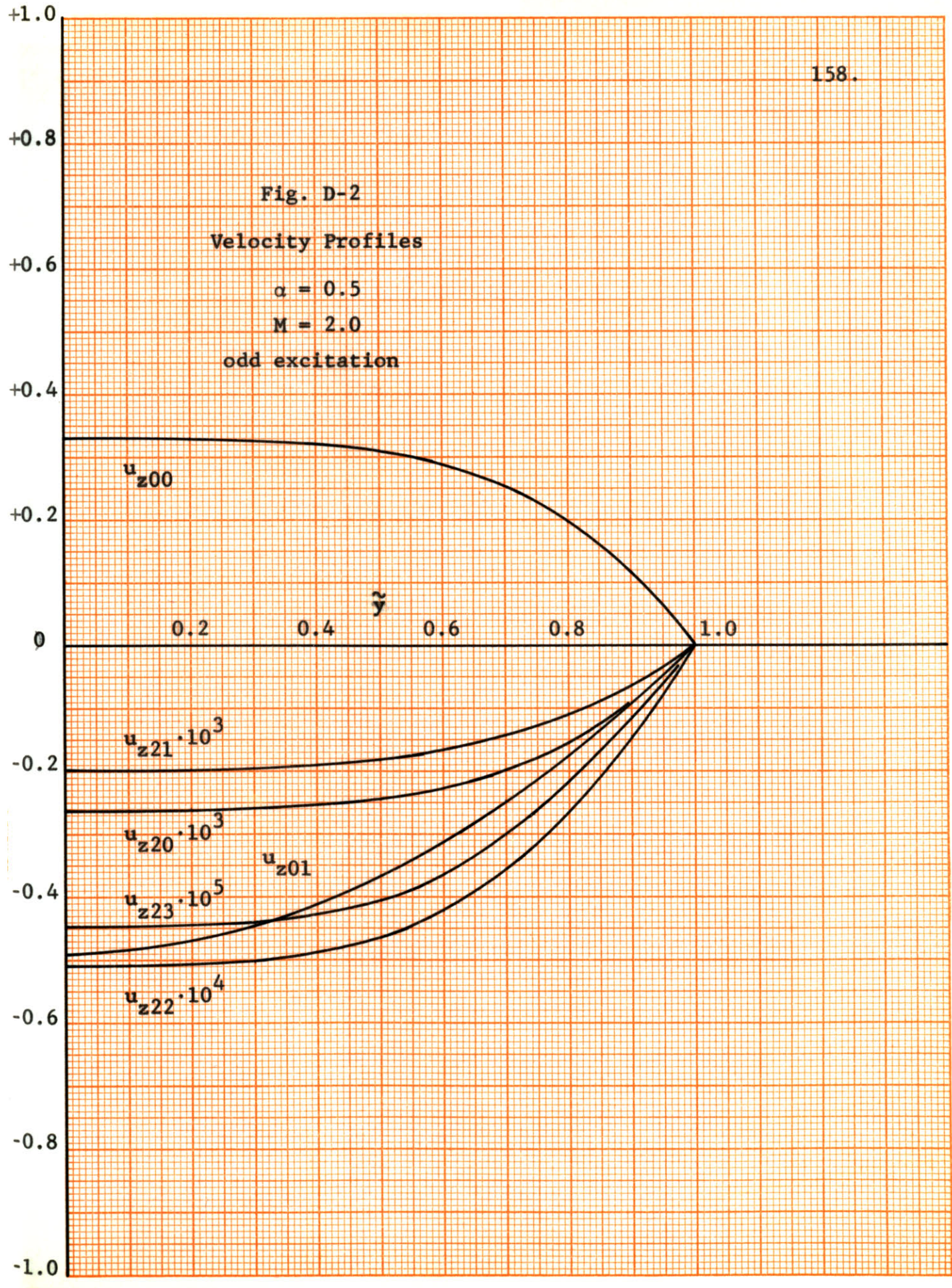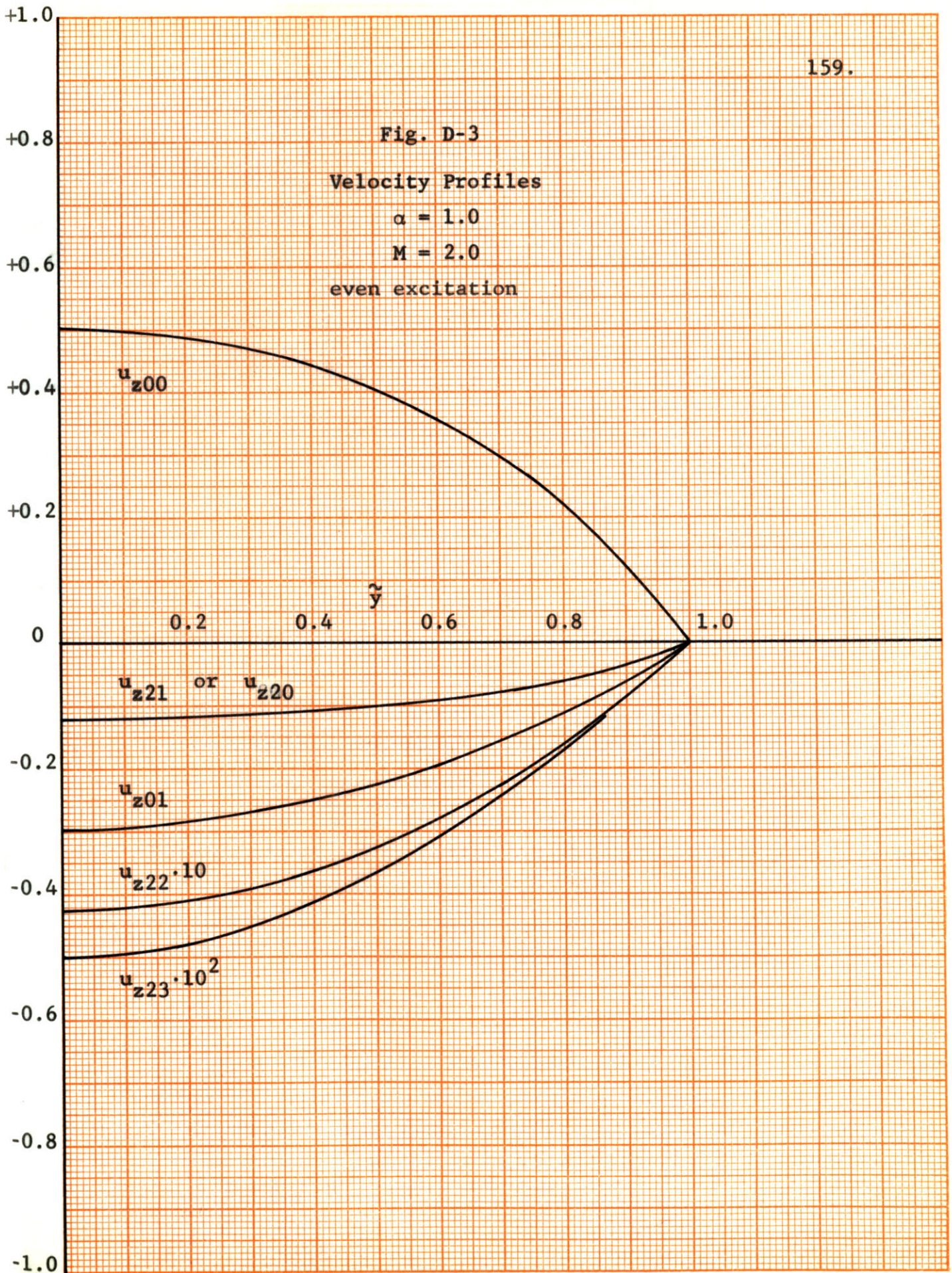$\alpha = 0.5$

$M = 2.0$

odd excitation

158.

Fig. D-3

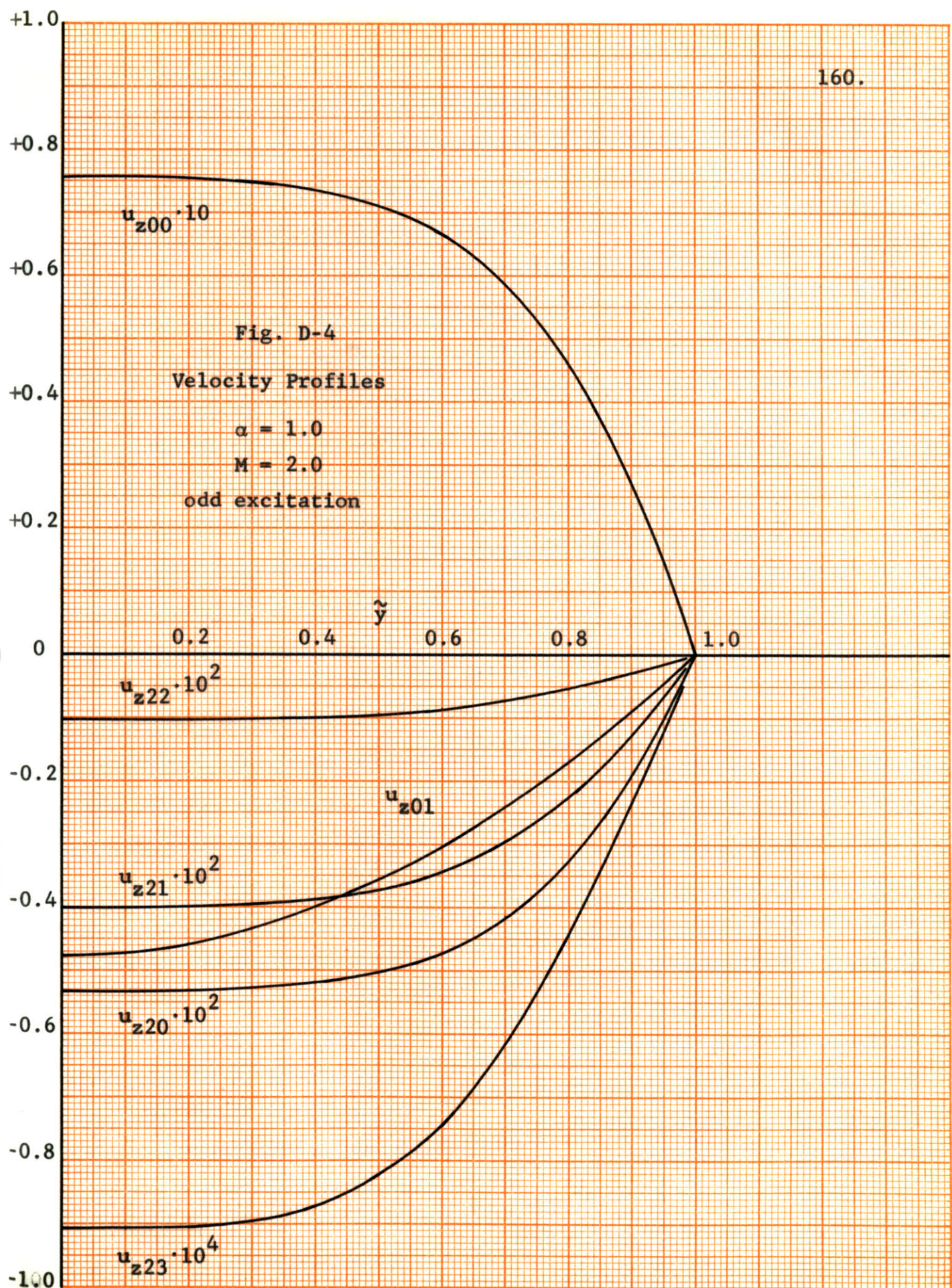Velocity Profiles
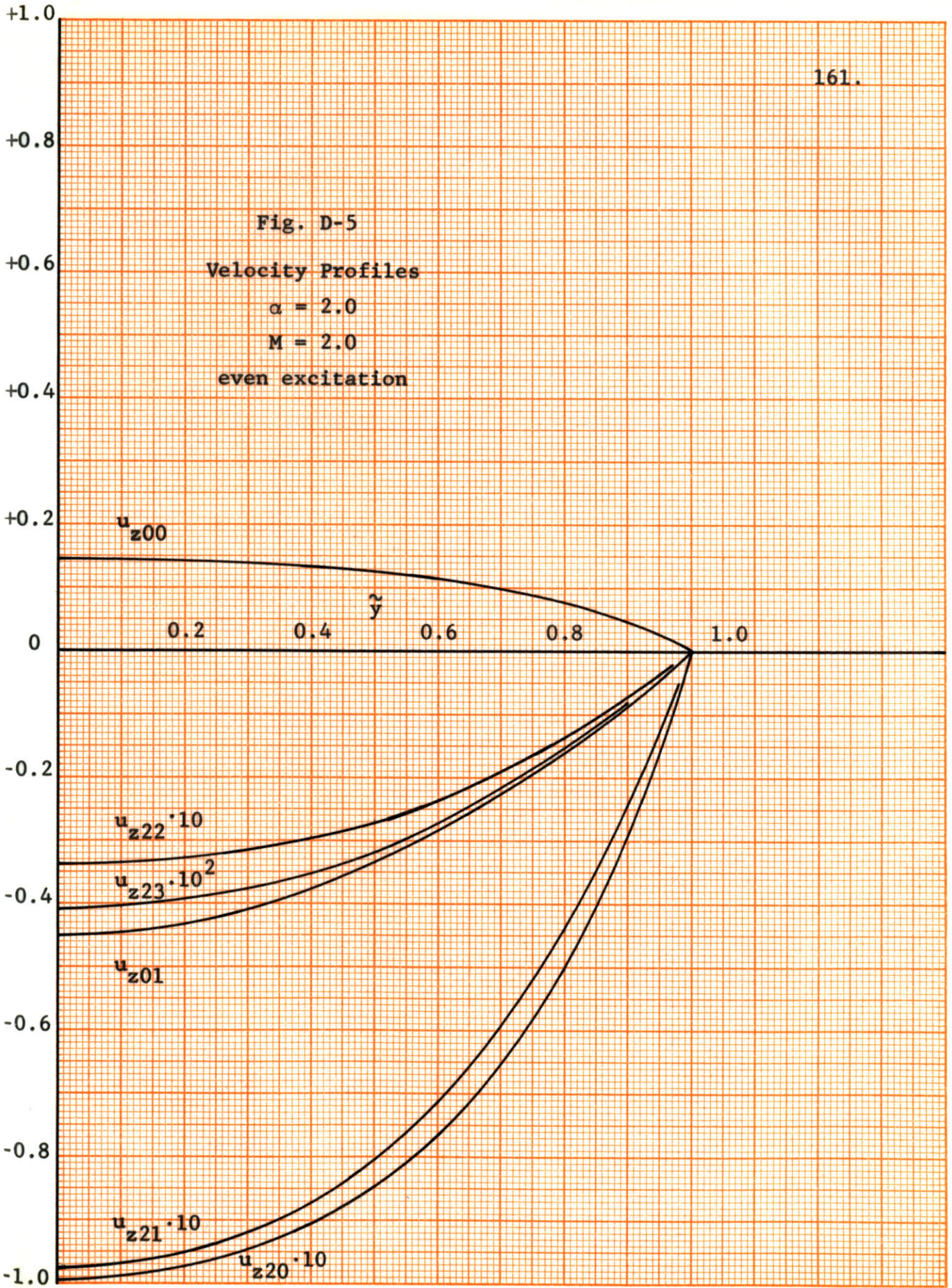
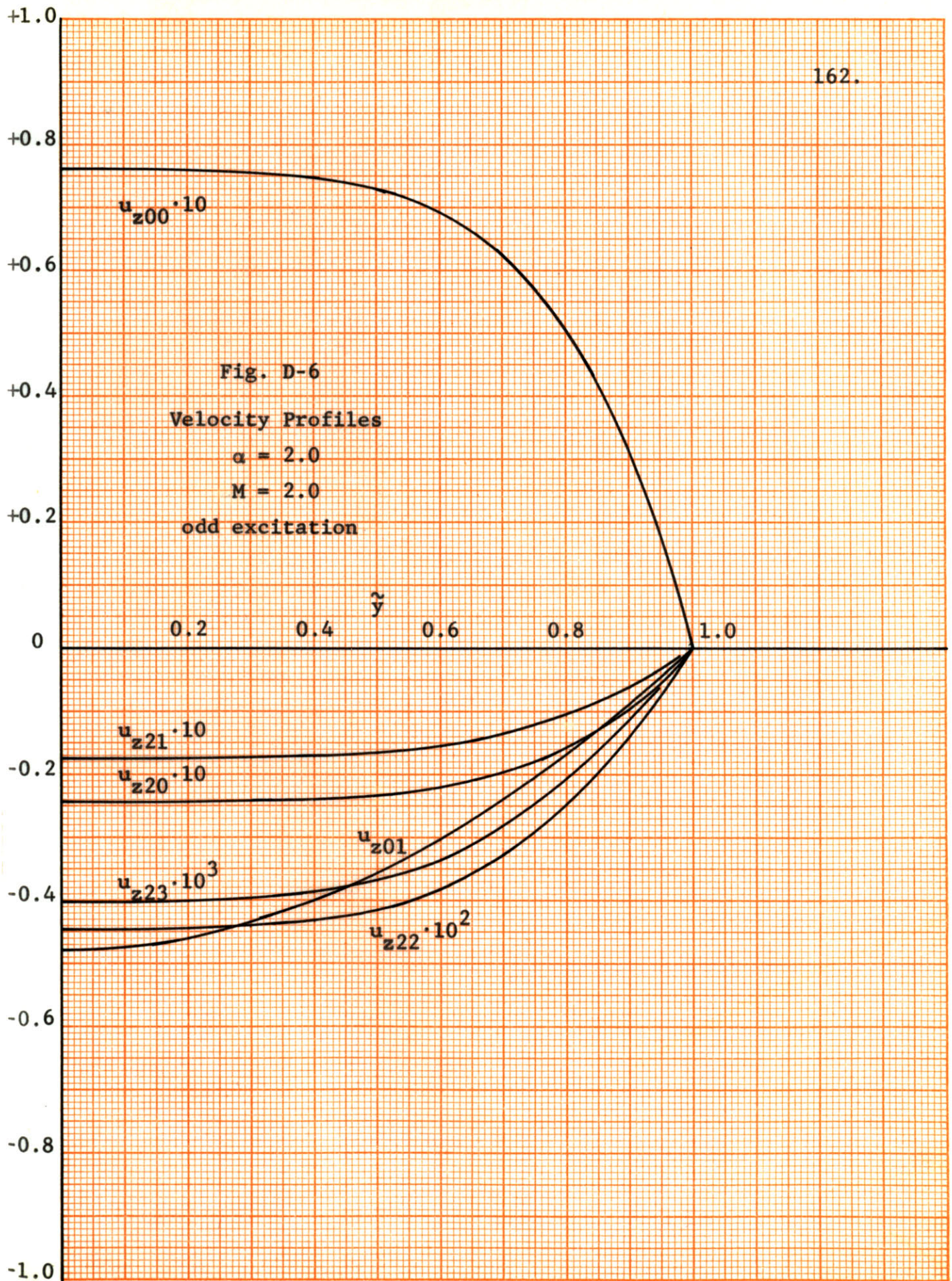$\alpha = 1.0$

$M = 2.0$

even excitation

Fig. D-4

Velocity Profiles

$\alpha = 1.0$

$M = 2.0$

odd excitation

160.

$u_{z00} \cdot 10$

$u_{z22} \cdot 10^2$

u_{z01}

$u_{z21} \cdot 10^2$

$u_{z20} \cdot 10^2$

$u_{z23} \cdot 10^4$

$\tilde{y}$

Fig. D-5

Velocity Profiles

$\alpha = 2.0$

$M = 2.0$

even excitation

162.

Fig. D-6

Velocity Profiles

$\alpha = 2.0$

$M = 2.0$

odd excitation

$u_{z00} \cdot 10$

$u_{z21} \cdot 10$

$u_{z20} \cdot 10$

u_{z01}

$u_{z23} \cdot 10^3$

$u_{z22} \cdot 10^2$

$\tilde{y}$

Fig. D-7

Velocity Profiles

$\alpha = 0.5$

$M = 5.0$

even excitation

u_{z00}

$u_{z21} \cdot 10^3$

$u_{z22} \cdot 10^4$

$u_{z01} \cdot 10$

$u_{z20} \cdot 10^2$

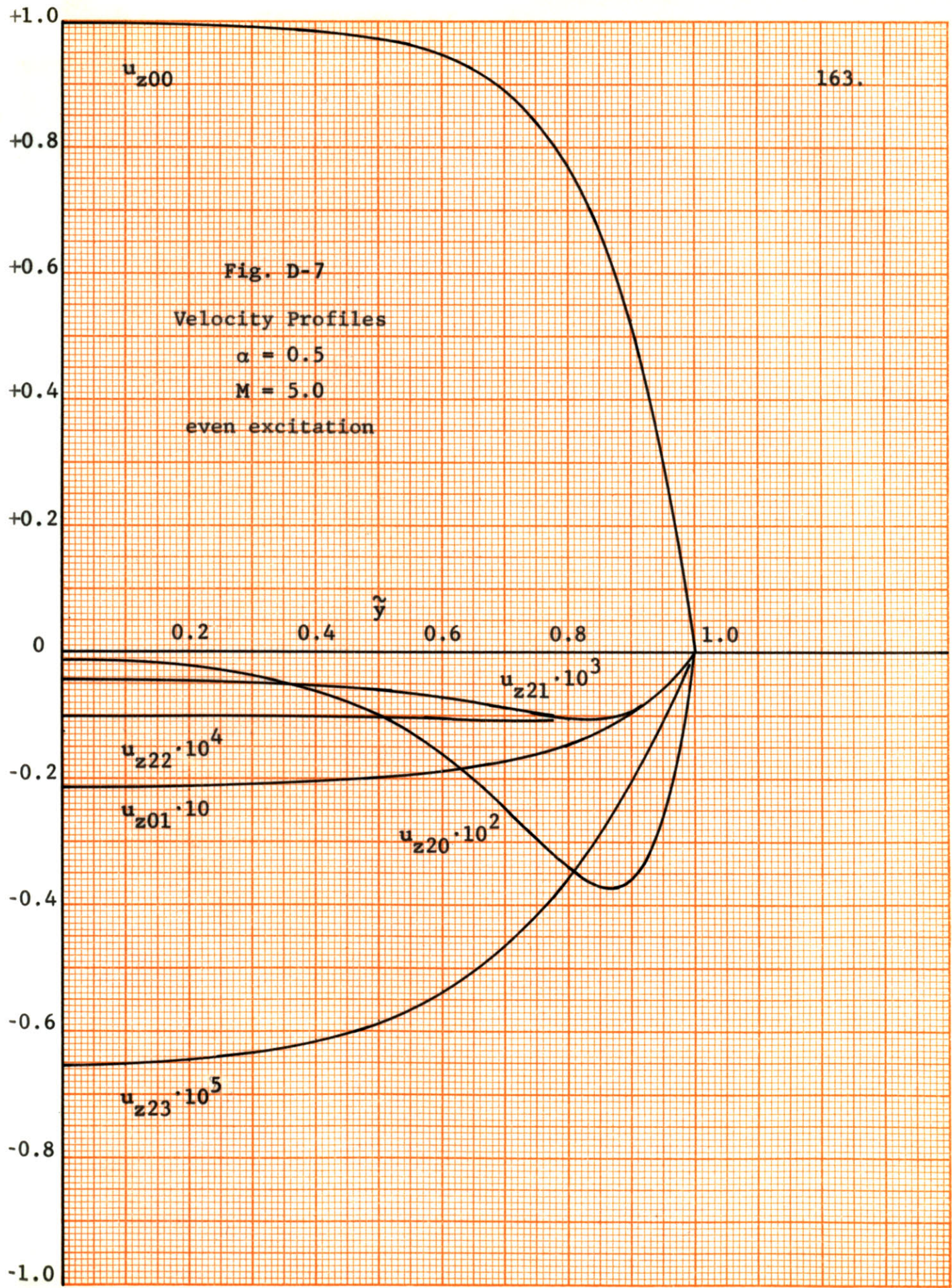$u_{z23} \cdot 10^5$

163.

Fig. D-8

Velocity Profiles

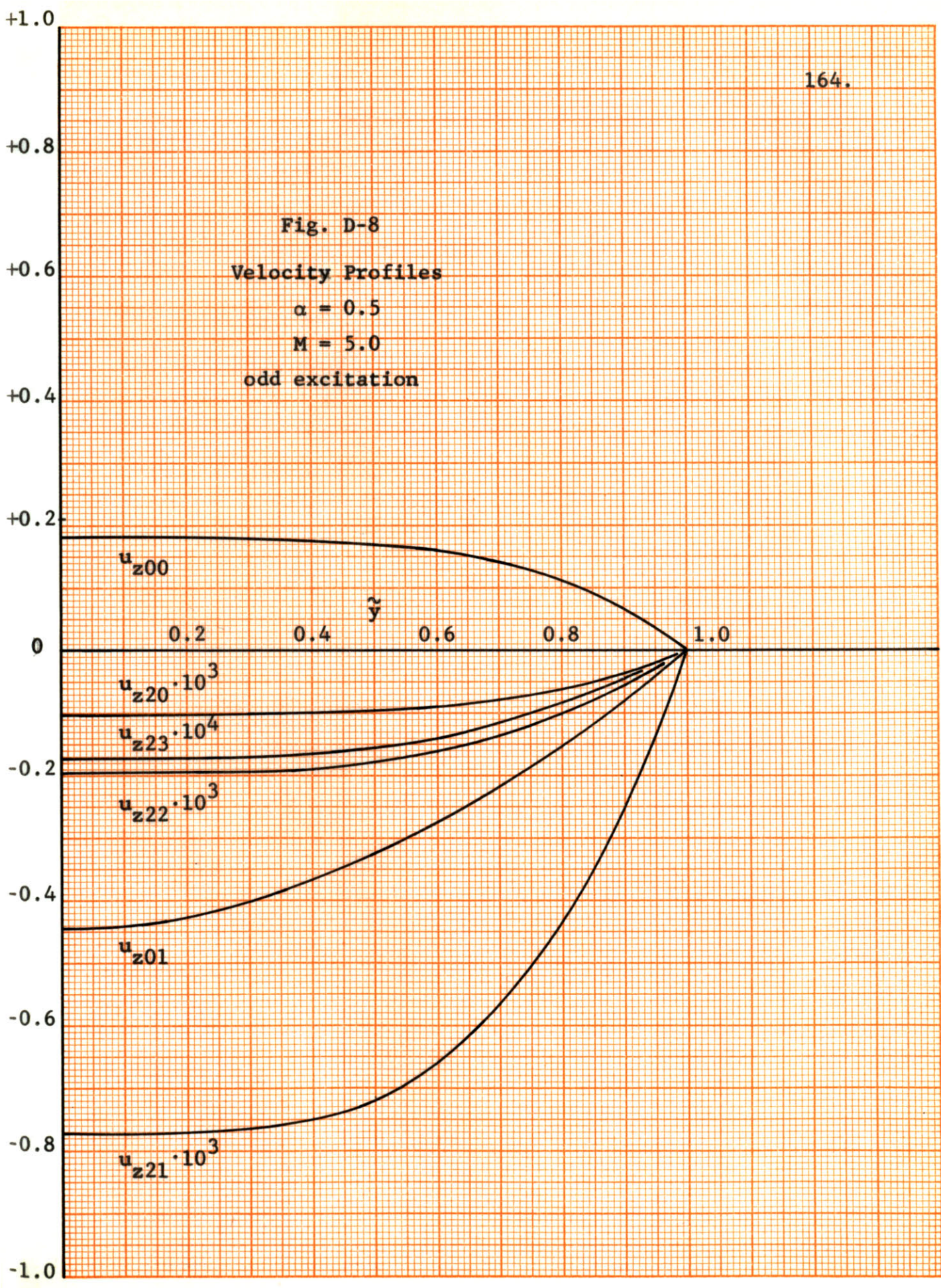$\alpha = 0.5$

$M = 5.0$

odd excitation

164.

Fig. D-9

Velocity Profiles

$\alpha = 1.0$

$M = 5.0$

even excitation
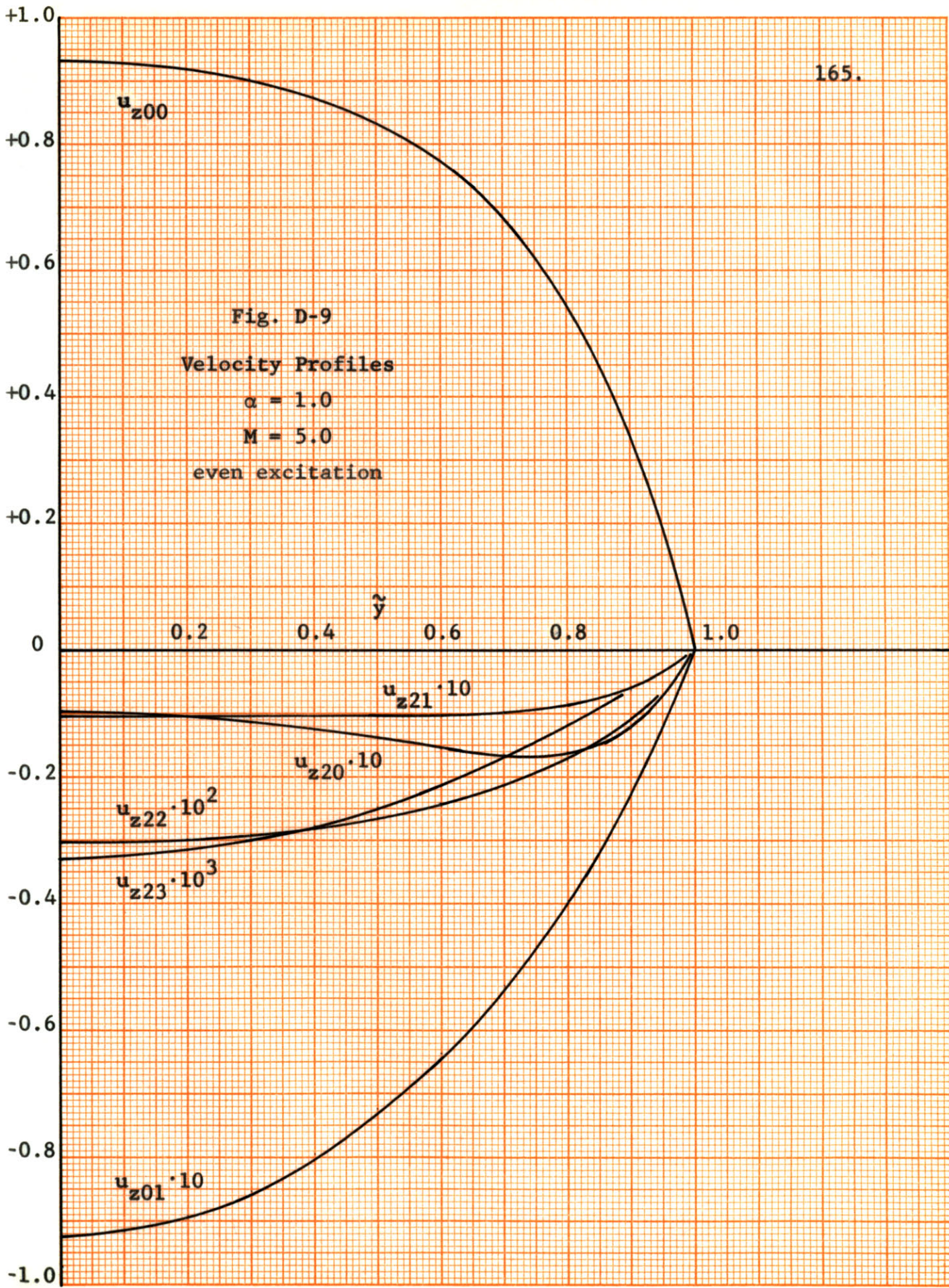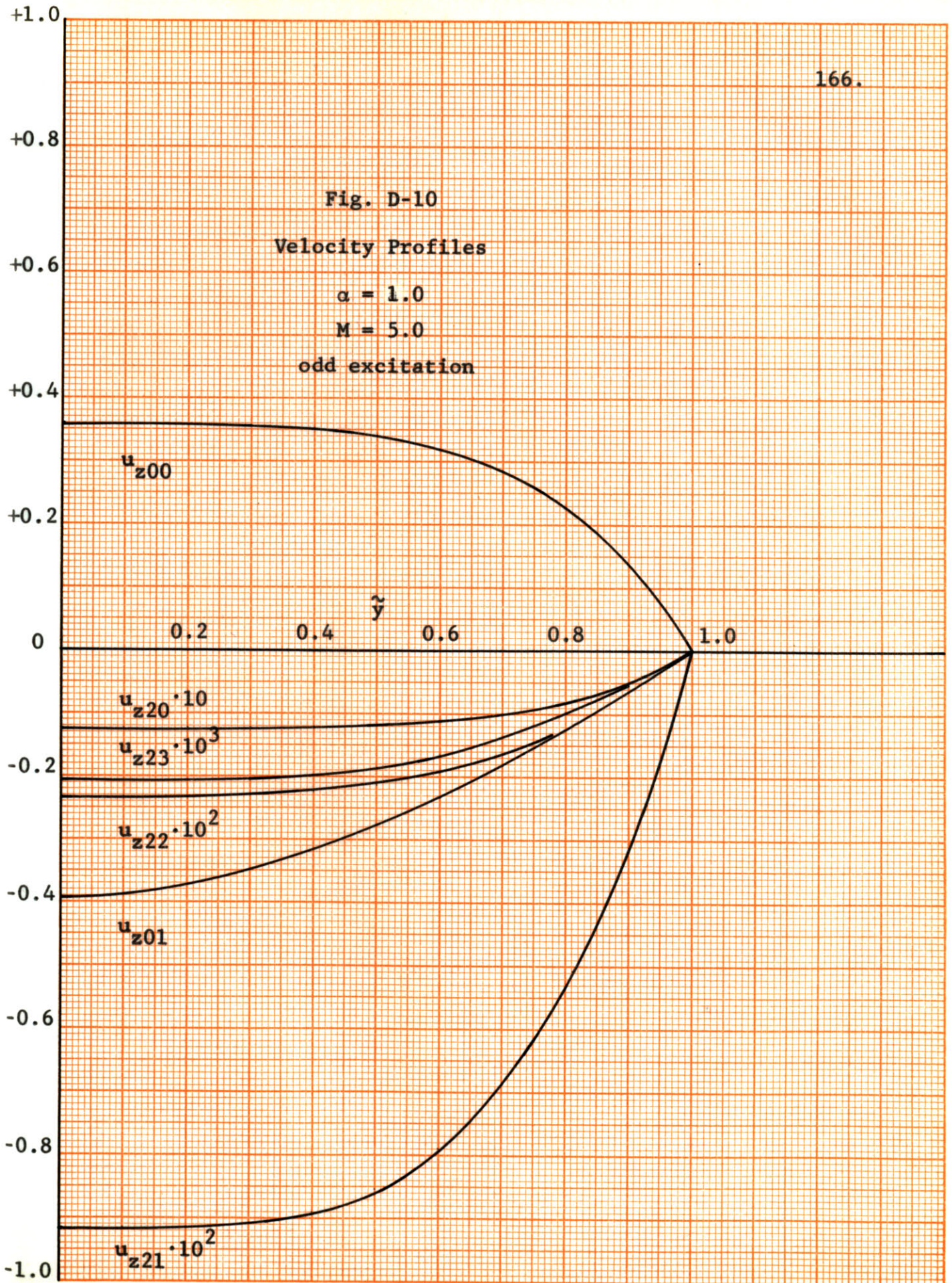
Fig. D-10

Velocity Profiles

$\alpha = 1.0$

$M = 5.0$

odd excitation

u_{z00}

$u_{z20} \cdot 10$

$u_{z23} \cdot 10^3$

$u_{z22} \cdot 10^2$

u_{z01}

$u_{z21} \cdot 10^2$

$\tilde{y}$

166.

Fig. D-11

Velocity Profiles

$\alpha = 2.0$

$M = 500$

even excitation

$\tilde{y}$

u_{z00}

u_{z01}

$u_{z22} \cdot 10$

$u_{z23} \cdot 10^2$

$u_{z21} \cdot 10$

$u_{z20} \cdot 10$

167.
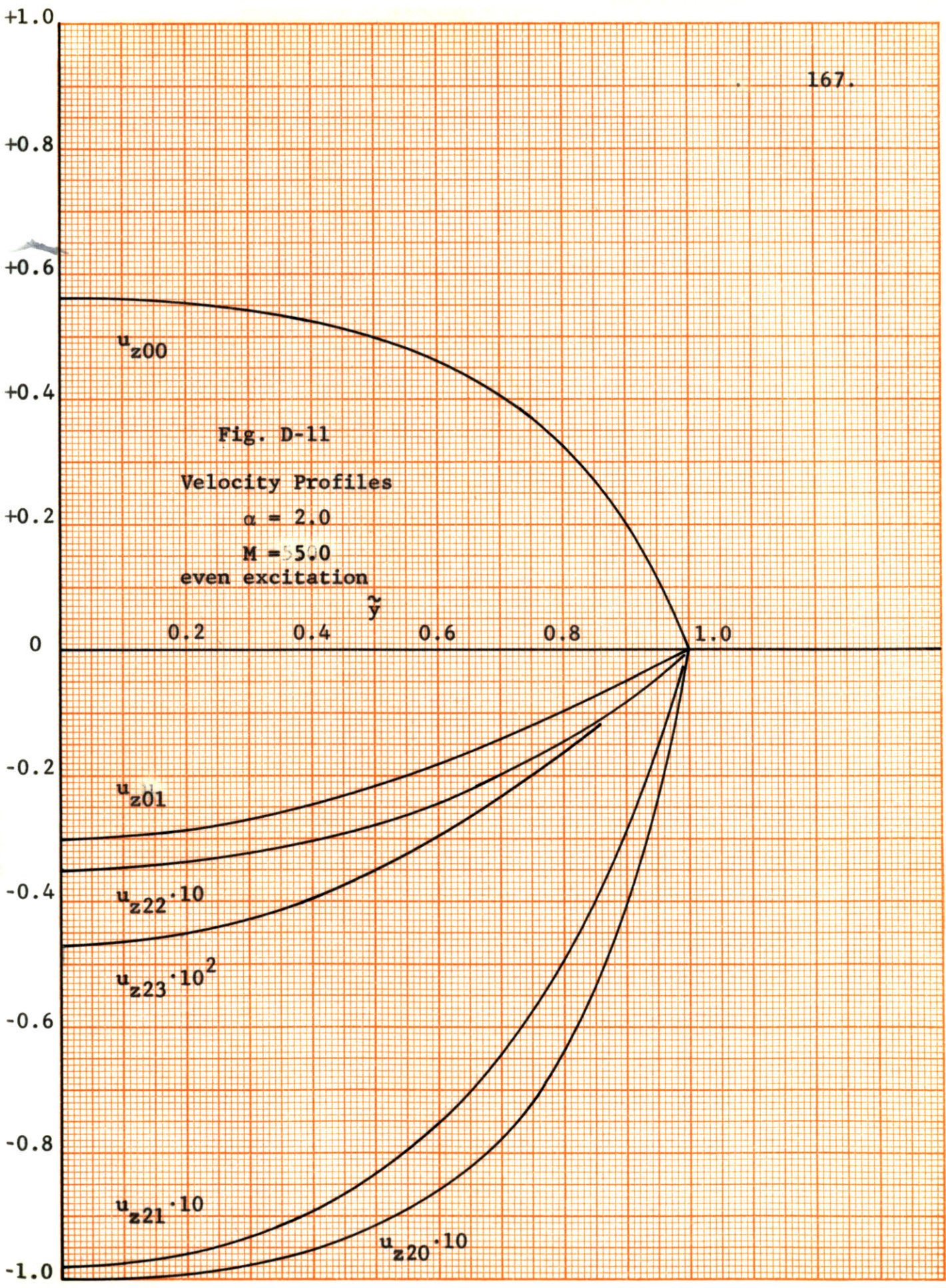
Fig. D-12

Velocity Profiles

$\alpha = 2.0$

$M = 5.0$

odd excitation

u_{z00}

$u_{z22} \cdot 10$

u_{z01}

$u_{z21} \cdot 10$

$u_{z20} \cdot 10$

$u_{z23} \cdot 10^3$

$\tilde{y}$

168.
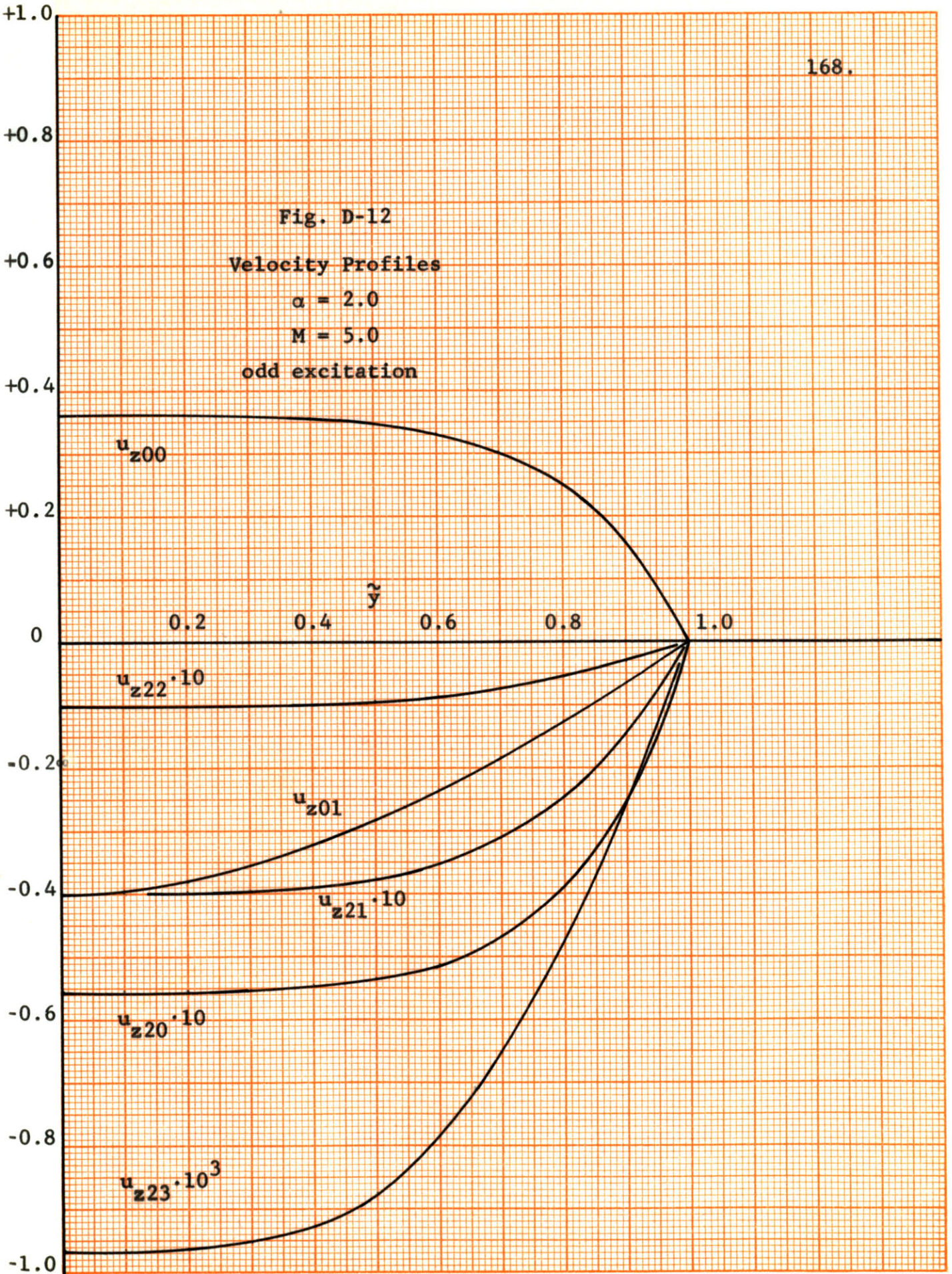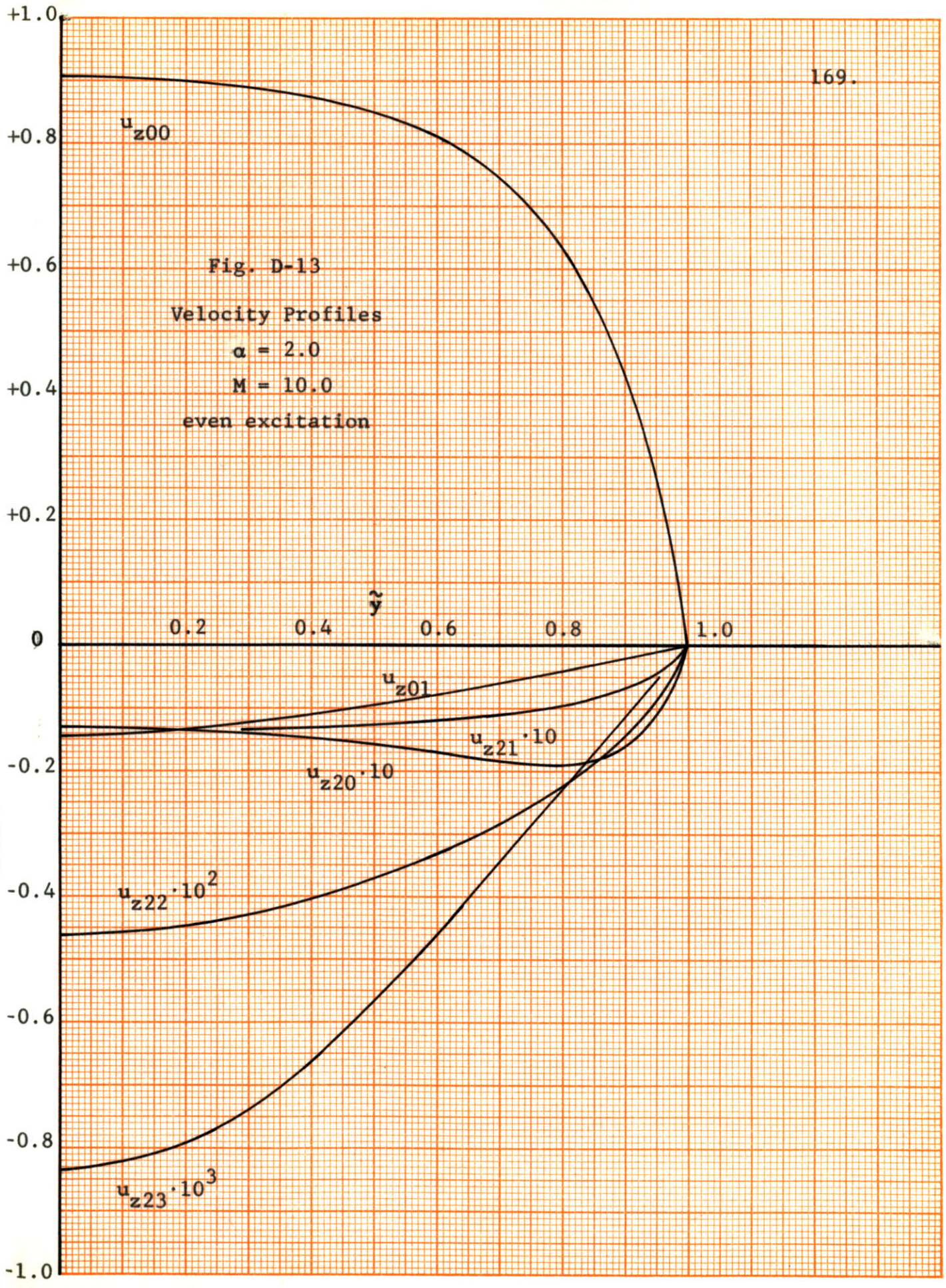
Fig. D-13

Velocity Profiles

$\alpha = 2.0$

$M = 10.0$

even excitation

u_{z00}

u_{z01}

$u_{z21} \cdot 10$

$u_{z20} \cdot 10$

$u_{z22} \cdot 10^2$

$u_{z23} \cdot 10^3$

$\tilde{y}$

169.

Fig. D-14

Velocity Profiles

$\alpha = 2.0$

$M = 1000$

odd excitation

$\tilde{y}$

u_{z00}

$u_{z21} \cdot 10$

$u_{z20} \cdot 100$

u_{z01} $u_{z22} \cdot 10^2$

$u_{z23} \cdot 10^3$

169a.
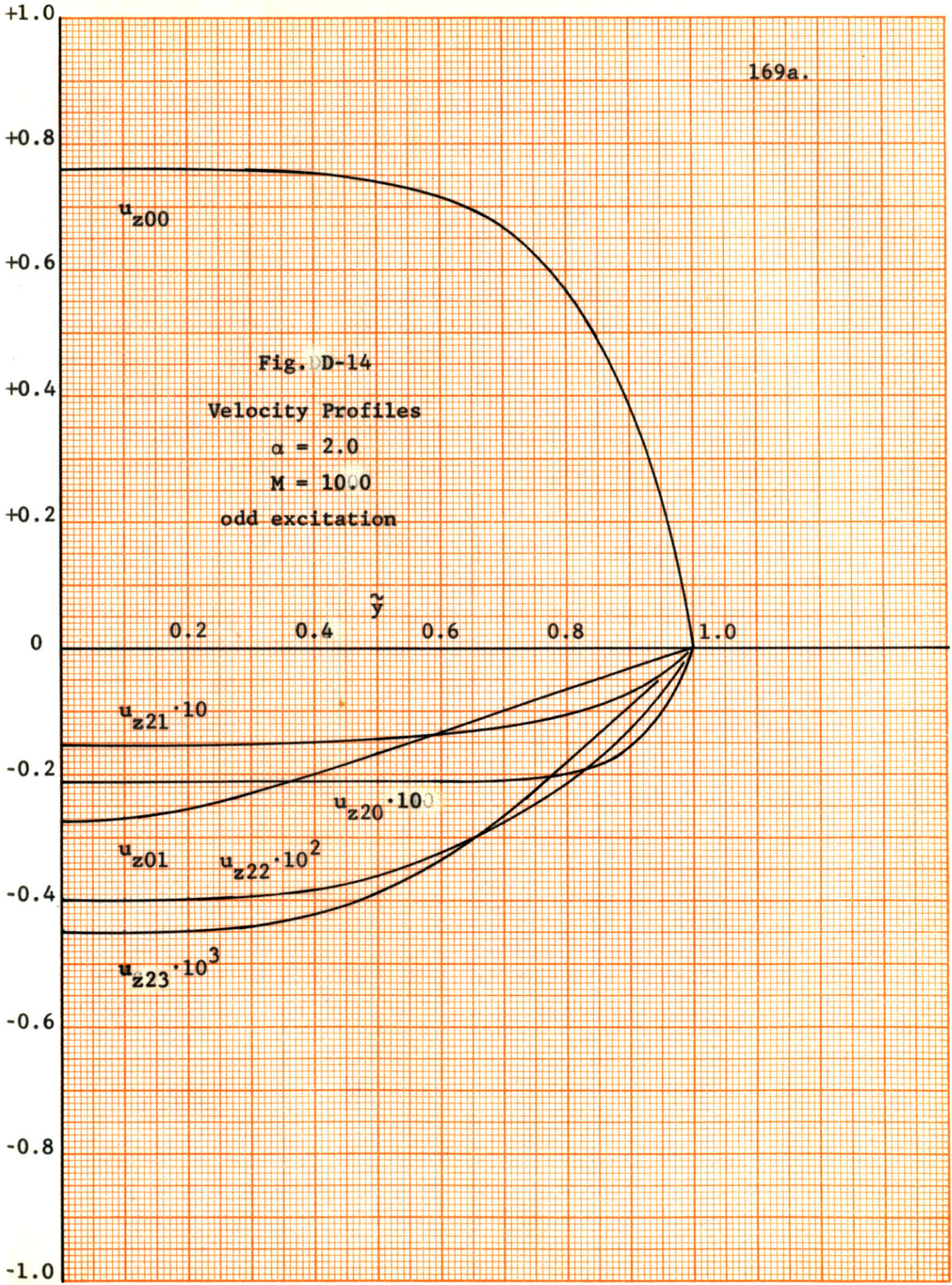
Appendix E

A BIOGRAPHICAL NOTE

John Paul Penhune was born in Flushing, New York on
February 13, 1936, and grew up in eastern New Jersey and on
Long Island. He was graduated from Great Neck High School in
1953, and entered M.I.T. in the same year with a four-year,
full-tuition scholarship from the Grumman Aircraft Engineering
Corporation. He worked in a variety of positions at Grumman
during the summers of his undergraduate years, and received a
B.S. degree in Electrical Engineering and a commission in the
Signal Corps in 1957. In the same year he entered the Graduate
School at M.I.T. in Electrical Engineering, as a teaching assistant;
and in September, 1958 he married Nancy Lee Peabody of Houlton, Maine.
During his graduate years, he taught courses in electromechanical
energy conversion and electromagnetic field theory, and was given
a Special Electrical Engineering Award for excellence in teaching
in 1959. He began research in magnetohydrodynamics with the Energy
Conversion Group at M.I.T. in 1958, and attended the Summer School
in Theoretical Physics of the University of Grenoble, France during
the summer of 1959. In 1960, he became an Instructor in Electrical
Engineering. He is a coauthor of Case Studies in Electromagnetism,
and is a member of Eta Kappa Nu, Tau Beta Pi, Sigma Xi, The American
Physical Society, and the Institute of Radio Engineers.

Bibliography

1. Hartmann, J., "Hg.-Dynamics I," Kgl. Danske Videnskab. Selskab, Math.-fys. Medd. 15, No. 6(1937).

2. Martin, T., Faraday's Diary, G. Bell and Son, London, 1932, Vol. I, p. 409 ff.

3. Northrup, E.F., "Some Newly Observed Manifestations of Forces in the Interior of an Electric Conductor," Phys. Rev. 24, 474(1907).

4. Hartmann, J. and Lazarus, F., "Hg.-Dynamics II," Kgl. Danske Videnskab. Selskab, Math.-fys. Medd. 15, No. 7(1937).

5. Penhune, J.P., "Energy Conversion in Laminar Flow," WADD TR 60-148, H.H. Woodson and W.D. Jackson, Eds., 1960, pp. 17-34.

6. Cage, J.F., Jr., "Electromagnetic Pumps for High-Temperature Liquid Metal," Mech. Eng. 75, 467(1953).

7. Barnes, A.H., "Pumping of Liquid Metals," Proc. UN Int. Conf. on the Peaceful Uses of Atomic Energy 9, 259(1955).

8. Watt, D.A., "Electromagnetic Pumps for Liquid Metals," Engineering 181, 264(1956).

9. Blake, L.R., "A-C and D-C Conduction Pumps for Liquid Metals," Engineer 202, 541(1956).

10. Blake, L.R., "Conduction and Induction Pumps for Liquid Metals," Proc. I.E.E. 104A, 49(1957).

11. Watt, D.A., "A Study in Design of Traveling Field Electromagnetic Pumps for Liquid Metals," A.E.R.E. ED/R 1696, 1956.

12. Harris, L.P., Hydromagnetic Channel Flows, Tech. Press of the Mass. Inst. of Tech., Cambridge, Mass., and John Wiley and Sons, New York, 1960.

13. Sporn, P. and Kantrowitz, A., "Large-Scale Generation of Electric Power by Application of the Magnetohydrodynamic Concept," Power 103, No. 11, 62(1959).

14. Steg, L. and Sutton, G.W., "The Prospects of MHD Power Generation," Astronautics 5, No. 8, 22(1960).

15. Way, S. et al., "Experiments with MHD Power Generation,"
ASME 60-WA-328, 1960.

16. Rosa, R.J., "Experimental Magnetohydrodynamic Power Generation,"
Appl. Phys. 31, 735(1960).

17. Marshall, J., "Acceleration of Plasma into Vacuum," Proc. Sec.
UN Int. Conf. on the Peaceful Uses of Atomic Energy 31,
341(1958).

18. Meyer, R.X., "Magnetic Plasma Propulsion by Means of a
Traveling Sinusoidal Field," AD-240 965, 1960.

19. Covert, E.E. and Haldemann, C.W., "The Traveling Wave Pump,"
ARS 1460-60, 1960.

20. Shapiro, A.H., The Dynamics and Thermodynamics of Compressible
Fluid Flow, Ronald Press, New York, 1953, Vol. I.

21. Hunsaker, J.C. and Rightmire, B.G., Engineering Applications of
Fluid Mechanics, McGraw-Hill Book Company, New York, 1947.

22. Poduska, J.W., "Random Theory of Turbulence," Master's Thesis
at the Mass. Inst. of Tech., Cambridge, Mass., 1960.

23. Pai, S.-I., Viscous Flow Theory, I - Laminar Flow,
D. Van Nostrand Company, Princeton, New Jersey, 1956.

24. Pai, S.-I., Viscous Flow Theory, II - Turbulent Flow,
D. Van Nostrand Company, Princeton, New Jersey, 1957.

25. Murgatroyd, W., "Experiments on Magneto-Hydrodynamic Channel
Flow," Phil. Mag. 44, 1348(1953).

26. Lundquist, S., "Studies in Magneto-Hydrodynamics,"
Arkiv Fysik 5, 297(1952).

27. Lock, R.C., "The Stability of the Flow of an Electrically
Conducting Fluid Between Parallel Planes Under a Transverse
Magnetic Field," Proc. Roy. Soc. (London) A233, 105(1955).

28. Globe, S., "The Effect of a Longitudinal Magnetic Field on
Pipe Flow of Mercury," ASME 60-WA-192, 1960.

29. Prandtl, L. and Tietjens, O.G., _Applied Hydro- and Aeromechanics_, Dover Publications, New York, 1957.

30. Stuart, J.T., "On the Stability of Viscous Flow Between Parallel Planes in the Presence of a Co-Planar Magnetic Field," _Proc. Roy. Soc._ (London) _A221_, 189(1954).

31. Fano, R.M., Chu, L.J., and Adler, R.B., _Electromagnetic Fields, Energy, and Forces_, John Wiley and Sons, New York, 1960.

32. Lamb, Sir H., _Hydrodynamics_, Dover Publications, New York, 1945.

33. Pai, S.-I., "Energy Equation of Magneto-Gas Dynamics," _Phys. Rev._ _103_, 1424(1957).

34. Hildebrand, F.B., _Methods of Applied Mathematics_, Prentice-Hall, Englewood Cliffs, New Jersey, 1952.

35. White, D.C., and Woodson, H.H., _Electromechanical Energy Conversion_, John Wiley and Sons, New York, 1959.

36. Kliman, G.B., "Velocity Profiles in Hydromagnetic Channel Flow," Master's Thesis at the Mass. Inst. of Tech., Cambridge, Mass., 1959.

37. Barnes, A.H., "Direct-Current Electromagnetic Pumps," _Nucleonics_ _11_, No. 1, 16(1953).

38. Erdélyi, A., _Asymptotic Expansions_, Dover Publications, New York, 1956.

39. McLachlan, N.W., _Theory and Application of Mathieu Functions_, Oxford at the Clarendon Press, 1947.

40. Campbell, R., _Théorie Générale de l'Equation de Mathieu_, Masson, Paris, 1955.

41. Lin, C.C., _The Theory of Hydrodynamic Stability_, Cambridge at the University Press, 1955.

42. Barnard, J. and Collins, G.D., "Test of a 1200-gpm Linear A-C Electromagnetic Pump," _AECD-3460_, 1951.

43. Carslaw, H.S. and Jaeger, J.C., Conduction of Heat in Solids, Oxford at the Clarendon Press, 1959.

44. Rogosinski, W., Fourier Series, Chelsea Publishing Company, New York, 1959.

45. Cowling, T.G., Magnetohydrodynamics, Interscience Publishers, London, 1957.

46. Morse, P.M. and Feshbach, H., Methods of Theoretical Physics, McGraw-Hill Book Company, New York, 1953.

47. Shercliff, J.A., "Steady Motion of Conducting Fluids in Pipes Under Transverse Magnetic Fields," Proc. Camb. Phil. Soc. 49, 136(1953).

48. Pierson, E.S., "A Hydromagnetic D-C Converter," Master's Thesis at the Mass. Inst. of Tech., Cambridge, Mass., 1960.

49. East, D.A., Doctoral Thesis research currently in progress at the Mass. Inst. of Tech., Cambridge, Mass.

50. Ince, E.L., Ordinary Differential Equations, Dover Publications, New York, 1956.

51. Hildebrand, F.B., Advanced Calculus for Engineers, Prentice-Hall, New York, 1949.

52. Hildebrand, F.B., Introduction to Numerical Analysis, McGraw-Hill Book Company, New York, 1956.

53. Lowan, A.N., Slazer, H., and Hillman, A., "A Table of Coefficients for Numerical Differentiation," Bull. Am. Math. Soc. 48, 920(1942).

54. IBM, Reference Manual, 709 Data Processing System, International Business Machines Corporation, White Plains, New York, 1959.

55. Computation Center Procedures Handbook, Computation Center, Mass. Inst. of Tech., Cambridge, Mass., 1960.

56. IBM, FORTRAN ASSEMBLY PROGRAM (FAP) for the IBM 709/7090,
     International Business Machines Corporation, White Plains,
     New York, 1960.

57. IBM, Reference Manual, 709/7090 FORTRAN Programming System,
     International Business Machines Corporation, White Plains,
     New York, 1961.